

Figure 6.4- Median Dry Gas and CO₂ Mixture at 100°F

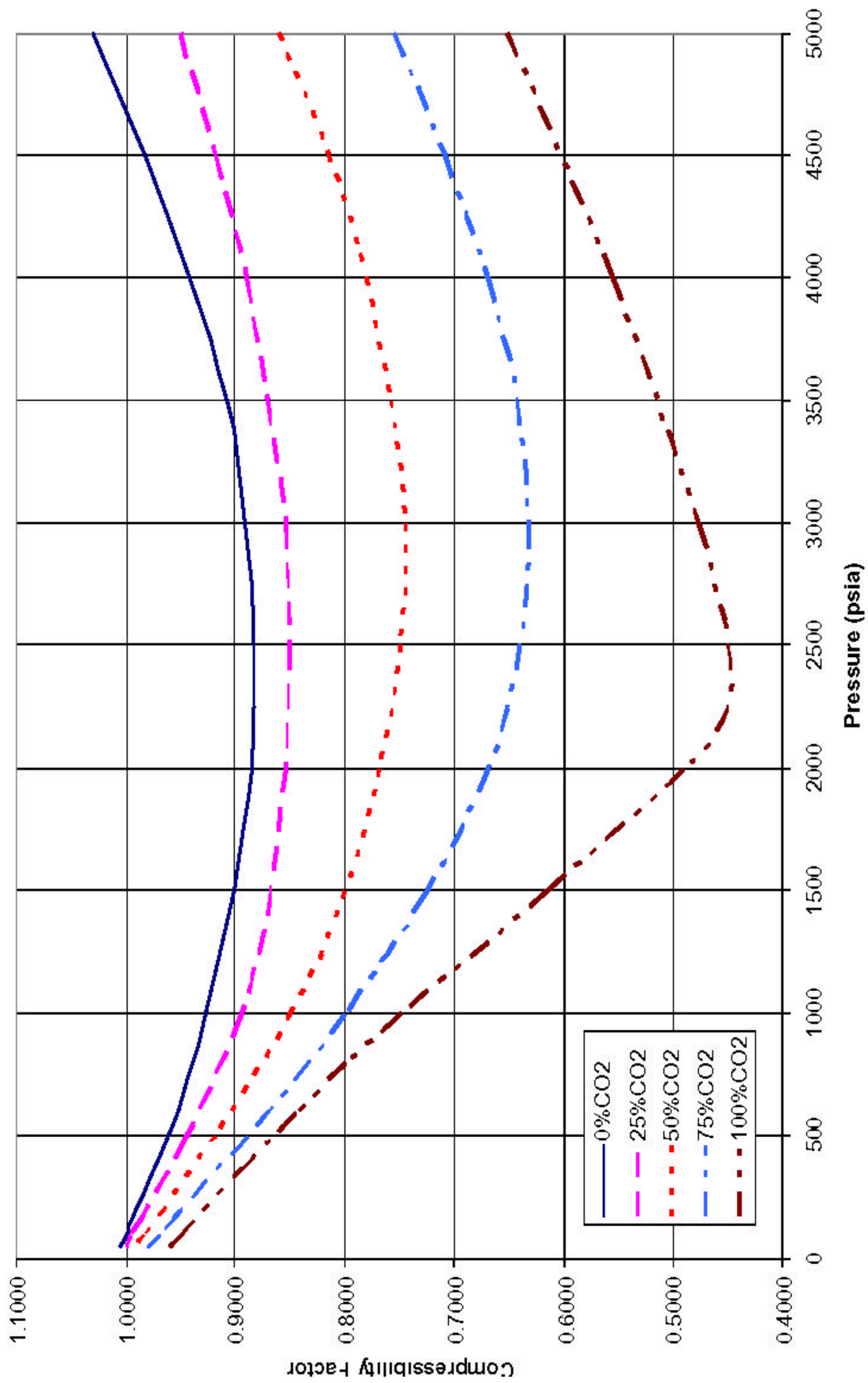


Figure 6.5 - Median Dry Gas and CO₂ Mixture at 160°F

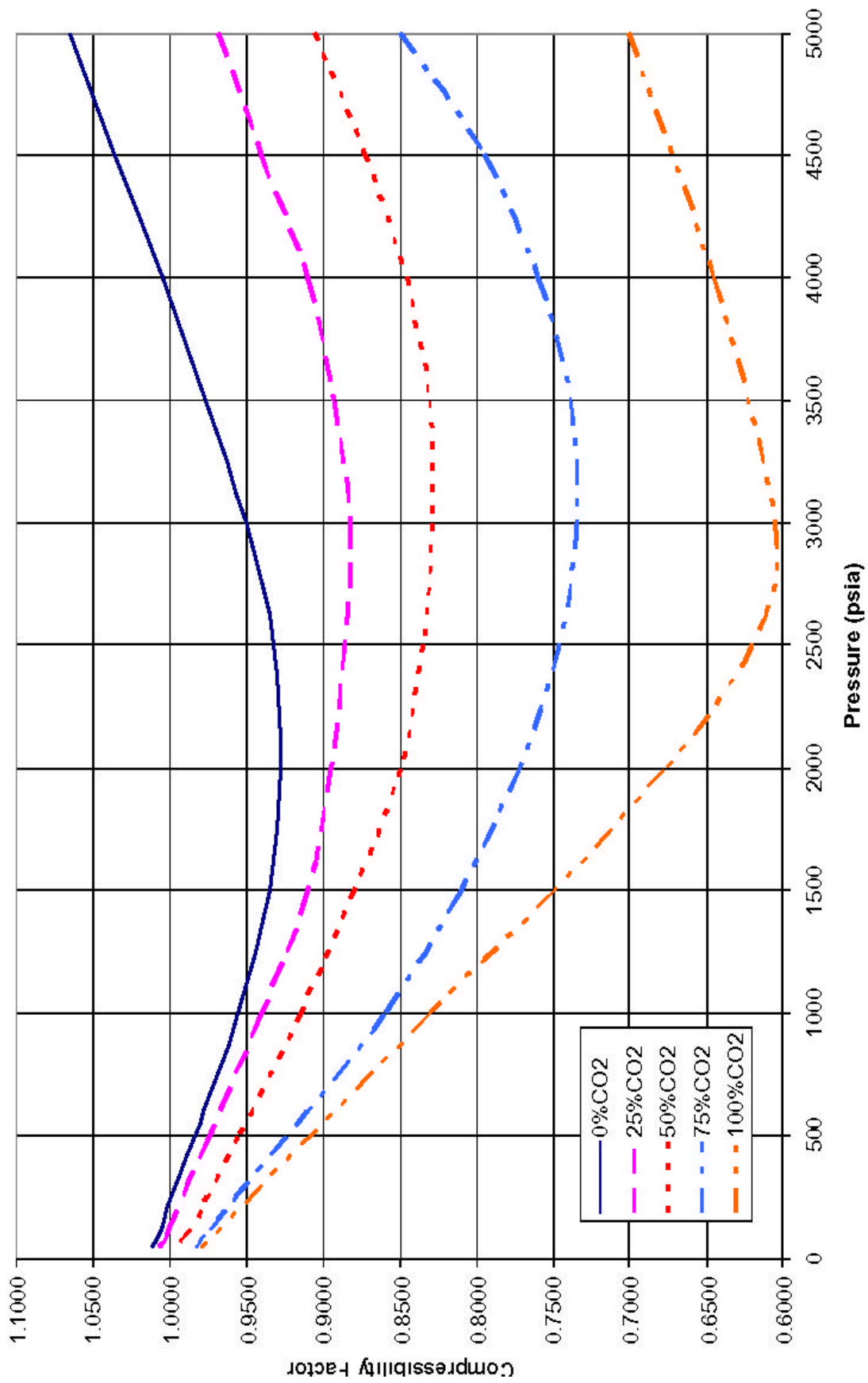


Figure 6.6 - Median Dry Gas and CO₂ Mixture at 220°F

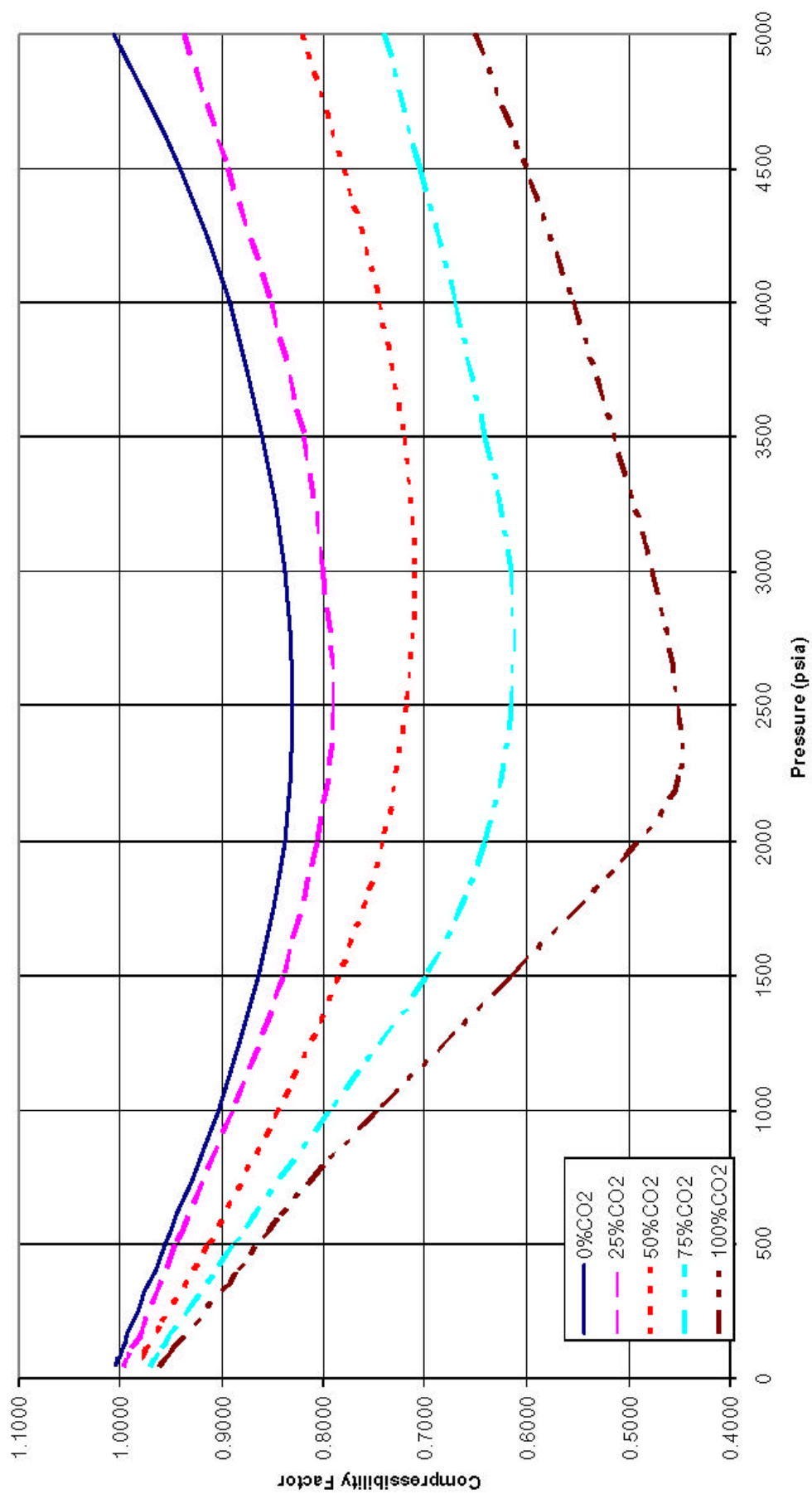


Figure 6.7 - Median Wet Gas and CO₂ Mixture at 160 °F

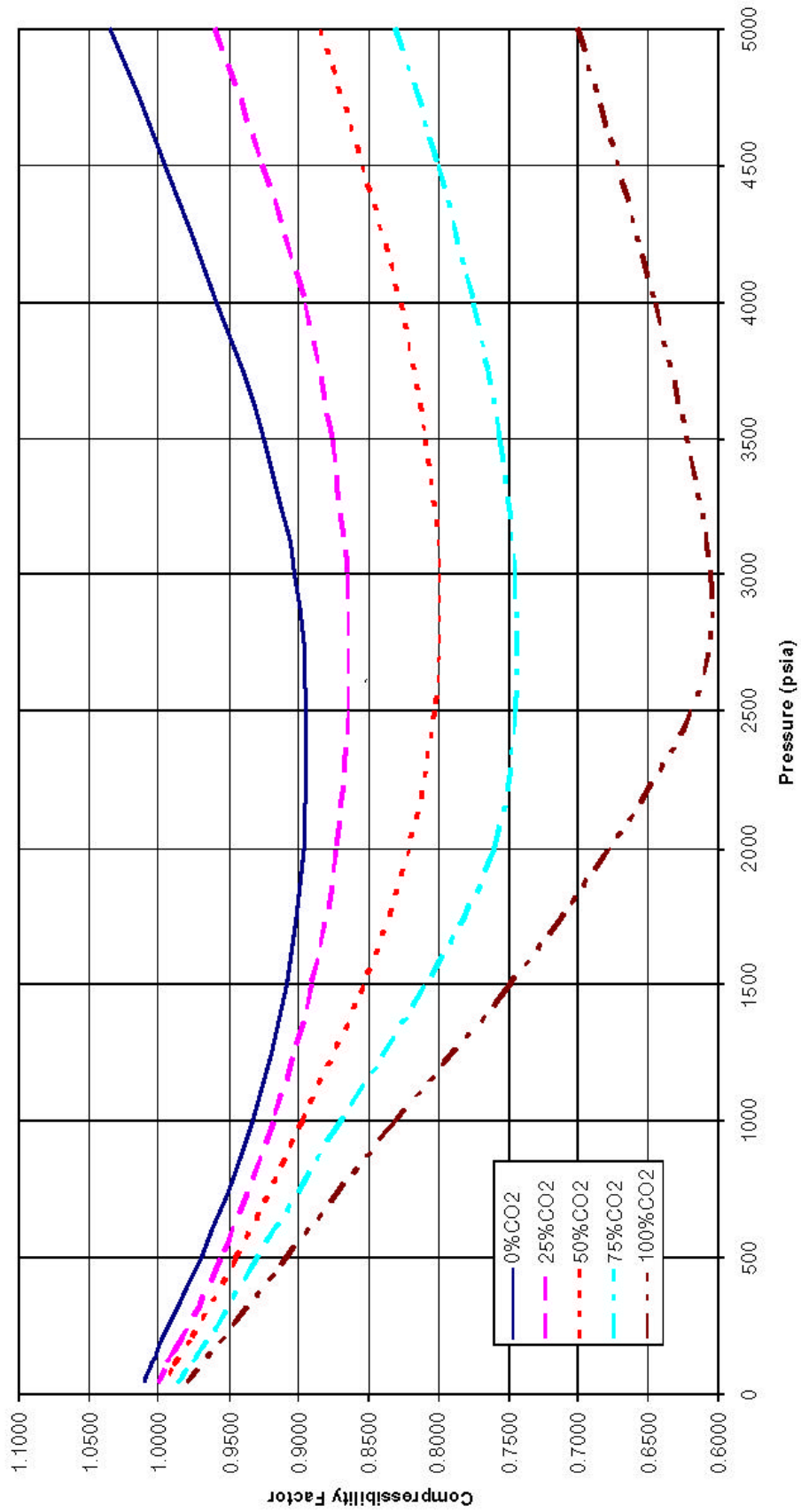


Figure 6.8 - Median Wet Gas and CO₂ Mixture at 220 °F

Table 6.1 - Compressibility Factor of Median Dry Gas and CO₂ Mixture at 100 °F

Pressure	0% CO ₂		25% CO ₂		50% CO ₂		75% CO ₂	
	Smoothed	Lab	Smoothed	Lab	Smoothed	Lab	Smoothed	Lab
5000	0.9950	0.9947	0.9040	0.8981	0.8260	0.8227	0.7000	0.7538
4500	0.9400		0.8550		0.7650		0.6500	
4000	0.8900	0.8918	0.8100	0.8023	0.7150	0.7161	0.6000	0.6584
3500	0.8580		0.7750		0.6750		0.5600	
3000	0.8350	0.8382	0.7550	0.7382	0.6590	0.6452	0.5250	0.5327
2500	0.8300	0.8253	0.7560	0.7297	0.6600	0.6278	0.5090	0.5166
2000	0.8360	0.8596	0.7780	0.8251	0.6850	0.6932	0.5180	0.5045
1500	0.8600	0.8603	0.8150	0.8486	0.7275	0.7293	0.5800	0.5866
1000	0.8950	0.9024	0.8630	0.8985	0.7950	0.8149	0.7050	0.7485
500	0.9450	0.9473	0.9300	0.9325	0.8950	0.9073	0.8500	0.8747
200	0.9800	0.9908	0.9720	0.9807	0.9580	0.9500	0.9350	0.9669
100	0.9910	1.0050	0.9870	0.9937	0.9780	0.9715	0.9620	0.9875
50	0.9970	1.0146	0.9940	0.9958	0.9900	0.9815	0.9750	1.0051

Table 6.2- Compressibility Factor of Median Dry Gas and CO₂ Mixture at 160°F

Pressure	0% CO ₂		25% CO ₂		50% CO ₂		75% CO ₂	
	Smoothed	Lab	Smoothed	Lab	Smoothed	Lab	Smoothed	Lab
5000	1.0300	0.9968	0.9500	0.9449	0.8600	0.8625	0.7550	0.7535
4500	0.9830		0.9175		0.8150		0.7100	
4000	0.9420	0.9309	0.8900	0.8874	0.7800	0.7814	0.6700	0.6737
3500	0.9070		0.8700		0.7580		0.6420	
3000	0.8912	0.8918	0.8550	0.8584	0.7450	0.7487	0.6325	0.6333
2500	0.8828	0.8879	0.8500	0.8532	0.7500	0.7530	0.6400	0.6320
2000	0.8855	0.8830	0.8550	0.8527	0.7680	0.7764	0.6700	0.6787
1500	0.9014	0.8379	0.8680	0.8734	0.8000	0.8093	0.7250	0.7414
1000	0.9275	0.8617	0.8950	0.8942	0.8500	0.8737	0.8000	0.8095
500	0.9609	0.9011	0.9450	0.9439	0.9200	0.9330	0.8900	0.8872
200	0.9900	0.9230	0.9810	0.9785	0.9670	0.9655	0.9500	0.9686
100	0.9996	0.9489	0.9945	1.0226	0.9840	0.9903	0.9700	0.9868
50	1.0050	0.9868	1.0000	1.0189	0.9930	0.9598	0.9800	1.0208

Table 6.3- Compressibility Factor of Median Dry Gas and CO₂ Mixture at 220°F

Pressure	0% CO ₂		25% CO ₂		50% CO ₂		75% CO ₂	
	Smoothed	Lab	Smoothed	Lab	Smoothed	Lab	Smoothed	Lab
5000	1.0650	1.0638	0.9675	0.9648	0.9050	0.9027	0.8500	0.8481
4500	1.0350		0.9400		0.8725		0.7950	
4000	1.0050	1.0152	0.9100	0.9134	0.8450	0.8477	0.7600	0.7517
3500	0.9760		0.8930		0.8300		0.7390	
3000	0.9500	0.9467	0.8825	0.8789	0.8280	0.8249	0.7340	0.7325
2500	0.9320	0.9288	0.8850	0.8883	0.8350	0.8308	0.7460	0.7470
2000	0.9280	0.9148	0.8950	0.8997	0.8500	0.8576	0.7720	0.7715
1500	0.9350	0.9293	0.9100	0.9224	0.8800	0.8862	0.8100	0.8008
1000	0.9550	0.9486	0.9400	0.9425	0.9150	0.9151	0.8600	0.8632
500	0.9840	0.9878	0.9740	0.9683	0.9550	0.9505	0.9250	0.9198
200	1.0013	1.0141	0.9950	0.9894	0.9800	0.9672	0.9640	0.9173
100	1.0075	0.9762	1.0022	0.9669	0.9900	0.9703	0.9770	0.8737
50	1.0110	0.9657	1.0070	0.9768	0.9960	0.9796	0.9840	0.7603

Table 6.4- Compressibility Factor of Median Wet Gas and CO₂ Mixture at 160°F

Pressure	0% CO ₂		25% CO ₂		50% CO ₂		75% CO ₂	
	Smoothed	Lab	Smoothed	Lab	Smoothed	Lab	Smoothed	Lab
5000	1.0050	1.0046	0.9380	0.9368	0.8210	0.8224	0.7400	0.8386
4500	0.9400		0.8950		0.7800		0.7050	
4000	0.8920	0.8928	0.8510	0.8517	0.7450	0.7479	0.6700	0.7296
3500	0.8600		0.8200		0.7200		0.6400	0.7296
3000	0.8380	0.8557	0.8000	0.7938	0.7100	0.7108	0.6150	0.6237
2500	0.8290	0.8284	0.7900	0.7880	0.7180	0.7140	0.6150	0.6041
2000	0.8380	0.8434	0.8070	0.8023	0.7410	0.7375	0.6400	0.6514
1500	0.8650	0.8634	0.8400	0.8388	0.7850	0.7829	0.6980	0.7244
1000	0.9030	0.9050	0.8900	0.8869	0.8450	0.8504	0.7950	0.8952
500	0.9560	0.9608	0.9450	0.9536	0.9150	0.9116	0.8900	0.9439
200	0.9890	0.9849	0.9780	0.9830	0.9610	0.9692	0.9440	1.0891
100	0.9990	0.9891	0.9900	0.9919	0.9760	0.9801	0.9620	1.1870
50	1.0040	0.9896	0.9970	1.1588	0.9830	0.9772	0.9700	1.2069

Table 6.5- Compressibility Factor of Median Wet Gas and CO₂ Mixture at 220°F

Pressure	0% CO ₂		25% CO ₂		50% CO ₂		75% CO ₂	
	Smoothed	Lab	Smoothed	Lab	Smoothed	Lab	Smoothed	Lab
5000	1.0350	1.0365	0.9600	0.9605	0.8840	0.8838	0.8300	0.9190
4500	0.9950		0.9250		0.8540		0.8000	
4000	0.9575	0.9420	0.8950	0.8948	0.8265	0.8336	0.7750	0.8457
3500	0.9240		0.8760		0.8080		0.7550	
3000	0.9030	0.9106	0.8650	0.8632	0.7990	0.7977	0.7450	0.8223
2500	0.8940	0.8913	0.8640	0.8616	0.8030	0.8015	0.7450	0.8194
2000	0.8960	0.8948	0.8725	0.8714	0.8210	0.8261	0.7600	0.8056
1500	0.9090	0.9208	0.8900	0.8817	0.8530	0.8438	0.8100	0.8410
1000	0.9320	0.9211	0.9175	0.9148	0.8975	0.9120	0.8700	0.9863
500	0.9700	0.9688	0.9560	0.9644	0.9450	0.9631	0.9300	1.0686
200	0.9970	0.9753	0.9840	0.9902	0.9770	0.9854	0.9650	0.9701
100	1.0060	0.9855	0.9950	0.9709	0.9900	1.0044	0.9800	0.9680
50	1.0100	0.9864	0.9996	0.9574	0.9950	0.9936	0.9870	0.9983

2.2.1.7 Results and Discussion

The primary goal of this project is to identify depleting gas reservoir (DGR) candidates for geologic storage of sequestered CO₂ based on the projected volume of CO₂ stored, enhanced gas recovery (EGR) and enhanced condensate recovery (ECR). This discussion of results follows the order of the process flow diagram (Figure 4.1) that is presented in the introduction section of this report.

2.2.1.7.1 Median Gas Compositions by Gas Type: Dry, Wet and Retrograde Gases

This section presents the method used to identify the major components of reservoir gas and the range of compositions for each of the categories of the gas reservoir (i.e., dry gas, wet gas, and retrograde gas). The gas compositions were obtained from published SPE papers, Petroleum Engineering Journals, Gas Information System (GASIS) and PVT analyses. The major components of gas reservoir are identified as N₂, CO₂, C₁, C₂, C₃, nC₄, nC₅, C₆, C₇₊. Non-hydrocarbon components were removed and the hydrocarbon components were normalized to 1.0 total mole fraction. These compositions were analyzed to find the *median* composition for each of the categories of gas reservoirs, and a means of identifying the Gas Type from the composition is established. Tables containing the normalized median compositions for each category of gas reservoirs were constructed. The median compositions were calculated from 131 dry gas, 12 wet gas, and 11 retrograde gas samples. A sample of the table constructed is shown in Table 7.1:

Table 7.1: Normalized Median Composition

	C1	C2	C3	C4	C5	C6	C7+	Total Mol %
Dry Gas	96.61	2.67	0.51	0.21	0.00	0.00	0.00	100.00
Wet Gas	90.03	4.75	2.03	1.03	0.42	0.35	1.40	100.00
Retrograde Gas	73.09	8.57	4.53	3.40	1.89	1.64	6.88	100.00

Table 7.1 shows that dry gas reservoir is mainly C₁, whereas wet and retrograde gas reservoirs have appreciable amount of C₇₊. Anticipating sequestration of CO₂ in DGRs to vary based on the phase behavior of the mixture of the CO₂ and the resident hydrocarbon gases and liquids, the development of guidelines and analysis techniques were based on each gas types. The gas compositions of Table 7.1 are the compositions of the initial or discovery gas reservoirs. By definition there are no phase changes in the reservoir for dry and wet gases; consequently, the median dry and wet gas compositions are also the compositions of the respective gases at depleted reservoir conditions. This is not the case for retrograde gas, which undergo a phase change at reservoir conditions. As such, the composition of the retrograde gas' liquid and vapor phases varies with pressure. Three depleted pressures of 50, 250 and 500 psia were used as a range to define the depleted gas reservoir pressure, which is also the initial sequestration pressure. These three gases are labeled as retrograde gases A, B and C for the gases at 50, 250 and 500 psia, respectively, and their compositions are shown in Table 7.2.

Table 7.2: Normalized Median Composition

	C1	C2	C3	C4	C5	C6	C10	Total Mol %
Retrograde Gas A (50 psia)	24.77	5.27	5.41	7.71	6.67	7.34	42.82	100.00
Retrograde Gas B (250 psia)	39.05	6.99	5.82	6.83	5.25	5.49	30.57	100.00
Retrograde Gas C (500 psia)	50.78	7.92	5.64	5.75	4.05	4.07	21.76	100.00

The most noticeable difference in the depleted gas reservoir compositions at the depleted pressure is methane (C_1) and decane (C_{10}). The lowest depleted pressure has less than half the (C_1) mole fraction of the highest depleted pressure, while the lowest depleted pressure has nearly twice the (C_{10}) mole fraction than the highest depleted pressure. This is expected because to achieve the depleted gas reservoir compositions only the vapor phase is produced. Methane is the dominant component in the vapor phase, as such additional depletion of pressure also depletes the mixture of methane. Consequently, the normalized mole fraction of C_{10} is higher due to the decrease of C_1 in the overall mixture.

To avoid finding CO_2 sequestration results that are pertinent to a specific gas reservoir, gas compositions are required for as many sources as possible so that a representative average composition of dry, wet and retrograde gases could be established. Therefore, a specific gas reservoir could be selected or fabricated in the laboratory that was close to the median composition found from data collected for each gas type. But, because general guidelines were required, a specific reservoir study was not mandated. Consequently, a literature review provided 154 gas compositions that were found in the literature and private sources that could be categorized by gas types of dry, wet, and retrograde. Median gas types were calculated for each gas type in order to have guidelines that were not unique to only a specific gas reservoir. A plot was made based on this database that identified regions that could type gases based on their compositions. Several plots were made to find the combination of compositions that would provide the greatest distinction of the gas types for unique gas-type identification. The final plot (Figure 7.1) is the sum of the mole fraction of the butane, propane, pentane, hexane and heptane divided by the mole fraction methane (y-axis) versus mole fraction of ethane divided by mole fraction of methane (x-axis). This is the first step of the depleted reservoir guideline selection process.

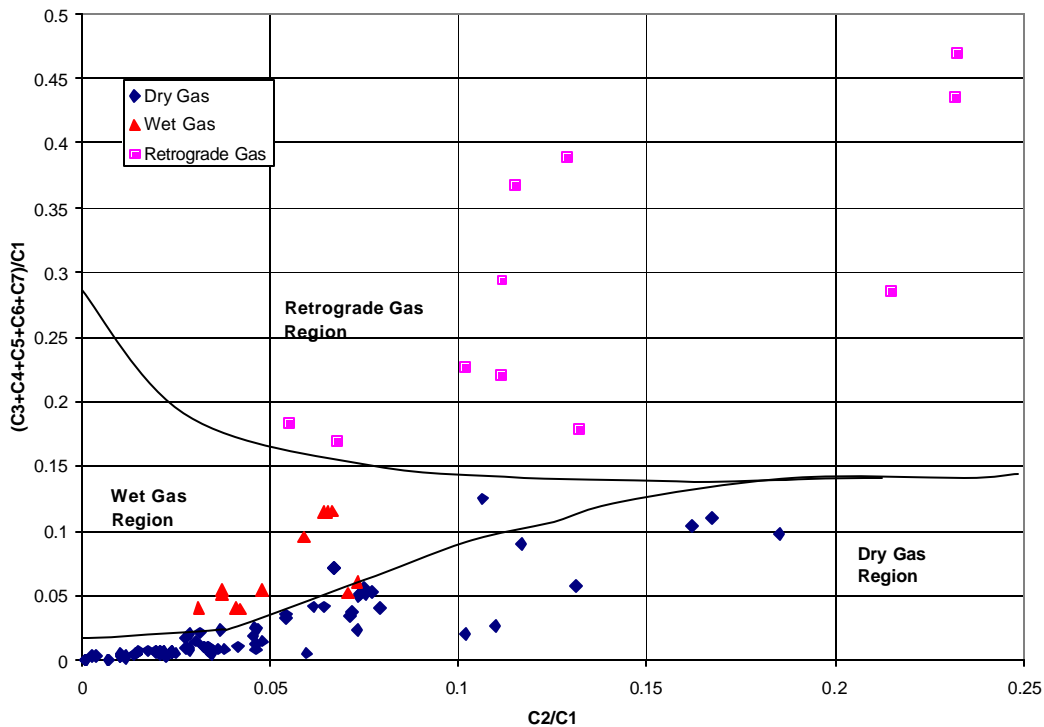


Figure 7.1 – TTU Gas Identification Chart based on hydrocarbon composition of $C_1 - C_{7+}$.

2.2.1.7.2 Analyses of EOS predictions/designs of dry, wet and retrograde for all CO₂ and T

Design of Laboratory Experiments

The Peng Robinson (PR) and Soave-Redlich Kwong (SRK) EOS were used to design the laboratory experiments and make predictions for each of the median compositions for the three gas types (dry, wet, and retrograde) from anticipated lab temperatures (100°F, 160°F, 220°F) and pressures (0-5000 psia). The primary objective of the phase behavior design simulations was to ascertain the occurrence of phase changes while the gas samples are transported from the samples bottles through the charging line and valve assembly to the PVT cell. (Single phase gas transportation from bottle to PVT cell is mandatory.) Temperature specifications of the heaters on the charging line and bottle were designated from these tests by computationally determining the pressure-temperature diagram of the two-phase region (Figures 7.2, 7.3a, 7.4a, 7.5a, 7.6a) and liquid volume-pressure diagrams (Figures 7.3b, 7.4b-d, 7.5b-d, 7.6b-d).

Three important lab designs features were changed as a result of the computational designs:

- * Dry gas: For all laboratory line, bottle, and cell pressures and temperatures the median dry gas compositions remain in the vapor phase. Consequently, no external heaters are required.
- * Wet gas: For the PVT test pressure of 100°F the median wet gas behaves as a retrograde gas because the calculated cricondenthem of the median WG is greater than 100°F and the calculated critical temperature of the median WG is less than 100°F. (The PVT cell temperature of 100°F was not conducted for WG behavior.)
- * Retrograde gases: The calculated cricondenthem of the median RGs exceeded 500°F. Sample bottle pressures were not rated for this temperature; as such RGs could not be moved without phase changes and subsequent undesirable compositional changes in the sample bottle, charging lines and valves. The solution was to separate the C₇ component from the C₁-C₆ components. In other words a mixture of C₁-C₆ was blended and stored as a vapor in a sample bottle, while liquid C₇ was added separately. (This procedure is documented in the 2.2.1.6 Experimental.)

Because of the low volume of percent liquid estimated from EOS calculations, for the retrograde gases, C₇ was replaced with C₁₀ (Table 7.2). This improved the percent liquid volume to reflect more typical retrograde behavior observed from PVT reports of retrograde gases found during the literature search.

Analyses of EOS Predictions

Relative drying and wetting effects of CO₂ on the median dry, wet and retrograde were observed. (Drying and wetting refer to the decrease and increase of hydrocarbon liquids at the surface.) Dry and wet gases by definition are a single vapor phase at reservoir pressure and temperature. As such the critical temperature determined the relative drying and wetting effect. The median dry gas with a critical temperature less than that of CO₂ exhibited a wetting effect for dry gas/CO₂ mixtures, while wet gas with a critical temperature higher than CO₂ showed a drying affect on wet gas/CO₂.

The median dry gas P-T relation on Figure 7.2 is at much lower temperatures than the CO₂ P-T relation (99% CO₂). As CO₂ mole fraction increases from 0% to 100%, the two phase region of the dry gas/ CO₂ mixtures moves to higher temperatures towards the P-T relation of CO₂. This is a wetting effect. In other words the two phase region, in terms of temperature, is moving towards surface temperature and pressure. Except for greater than 95% CO₂ mole fraction, all CO₂ mole fraction mixtures with the median dry gas exhibit dry gas behavior. At greater than 95% CO₂ mole fraction the mixture shows wet gas behavior; however, this liquid is likely to be predominantly CO₂ not hydrocarbons. Specifically, separator conditions of about 1000 psia and surface temperature (65°F-80°F), show that liquid will precipitate (Figure 7.2). The liquid-pressure trends (not shown) showed no liquid present at 100°F, 160°F, 220°F.

The median wet gas P-T relation on Figure 7.3a is at higher temperatures than the CO₂ P-T relation (99% CO₂). As CO₂ mole fraction increases from 0% to 100%, the two-phase region of the wet gas/CO₂ mixtures moves to lower temperatures towards the P-T relation of CO₂. This is a drying effect. In other

words the two phase region, in terms of temperature, is moving towards surface temperature and pressure. For all CO₂ mole fractions at temperatures 160°F and 220°F, the gas has wet behavior. However, at 100°F the gas shows retrograde behavior for CO₂ mole fraction less than 70%. The liquid-pressure trends (not shown) showed no liquid present at 160 and 220 °F. The liquid-pressure trend for 100°F (Figure 7.3b) showed a retrograde behavior with very modest liquid precipitation volume (< 0.5%) for a CO₂ mole fraction less than 60%.

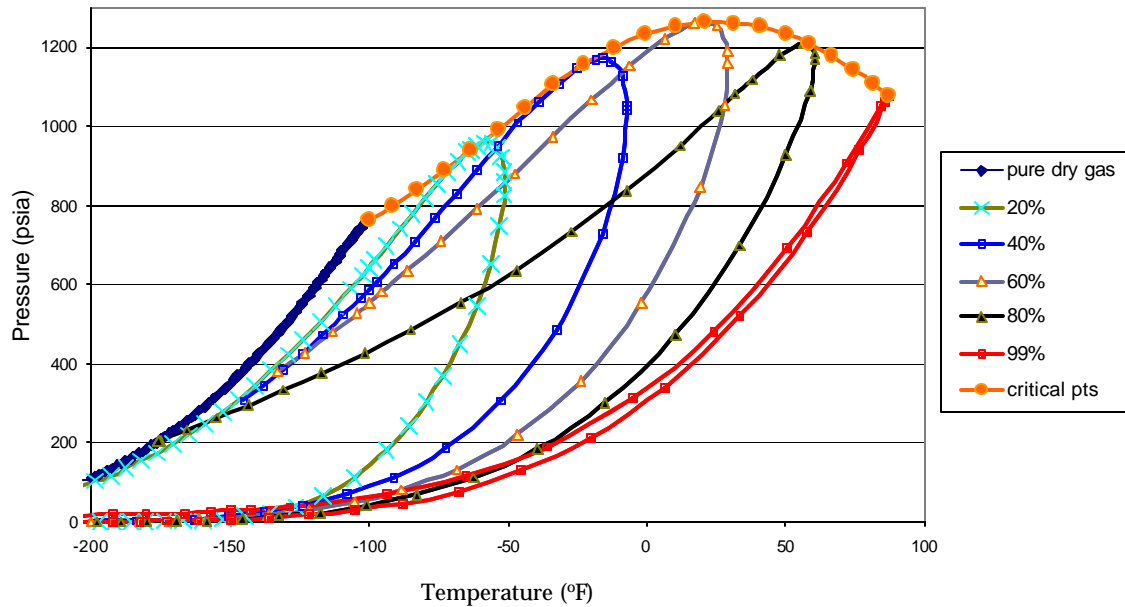


Figure 7.2 – Pressure-temperature diagram of dry gas-carbon dioxide mixtures ranging from 0-99% carbon dioxide

The median retrograde gases' P-T relation on Figures 7.4a, 7.5a and 7.6a for retrograde gases A, B and C, respectively, exhibit a modest degree of retrograde behavior. However, the P-T diagrams for most of the mixtures and all temperatures show indications of volatile and black oil. However, this is a limitation of the application of P-T diagrams to a reservoir in which composition is changing. For example, in the laboratory, the retrograde composition at any of the depleted pressures can be repressurized to form a liquid by decreasing the PVT cell volume. However, in the reservoir for a CO₂ sequestration scenario, there is no means of achieving an increase pressure without changing the composition via increasing CO₂ mole fractions. As such, as pressure and CO₂ mole fraction increases, it is necessary to move from one P-T diagram to another to reflect the path encountered during CO₂ sequestration. A relationship between pressure and CO₂ mole fraction is required to understand the nature of this path (next section).

As CO₂ mole fraction increases from 0% to 100%, the two-phase region of the wet gas/CO₂ mixtures moves to lower temperatures towards the P-T relation of CO₂. In general, the trends are shifting slightly to lower temperatures as CO₂ mole fraction increases, which indicate the drying effect. Unlike the dry and wet gases, the retrograde gases have a noticeable increase of the two-phase region to higher pressures (especially 100°F and 160°F). The liquid-pressure plots for the three depleted retrograde gases at three temperatures is in Figures 7.4b-d, 7.5b-d and 7.6b-d. While specific concentrations vary for each retrograde gas and temperatures, general trends are that retrograde behavior increases with higher CO₂ concentration, higher temperature, and higher depleted pressure.

Because retrograde gases undergo a phase change in the reservoir, the drying/wetting phenomenon is not as obvious from P-T and liquid-pressure diagrams. Additional computational and laboratory tests are in progress; however, preliminary work shows that the retrograde gas continues to act as a retrograde gas and at higher CO₂ concentrations behave like a dry gas; as a result, the hydrocarbon liquid in the reservoir will vaporize as additional CO₂ is stored, and condensate production will be enhanced.

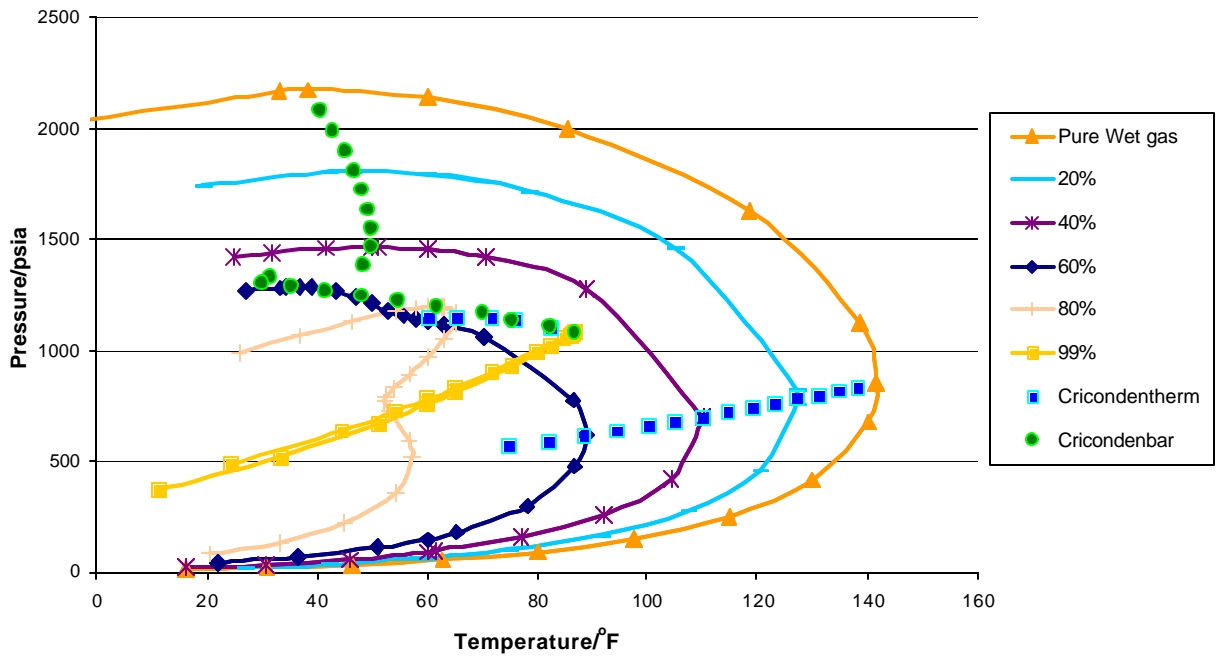


Figure 7.3a– Critical points and Cricondenbar of Wet gas-carbon dioxide mixtures

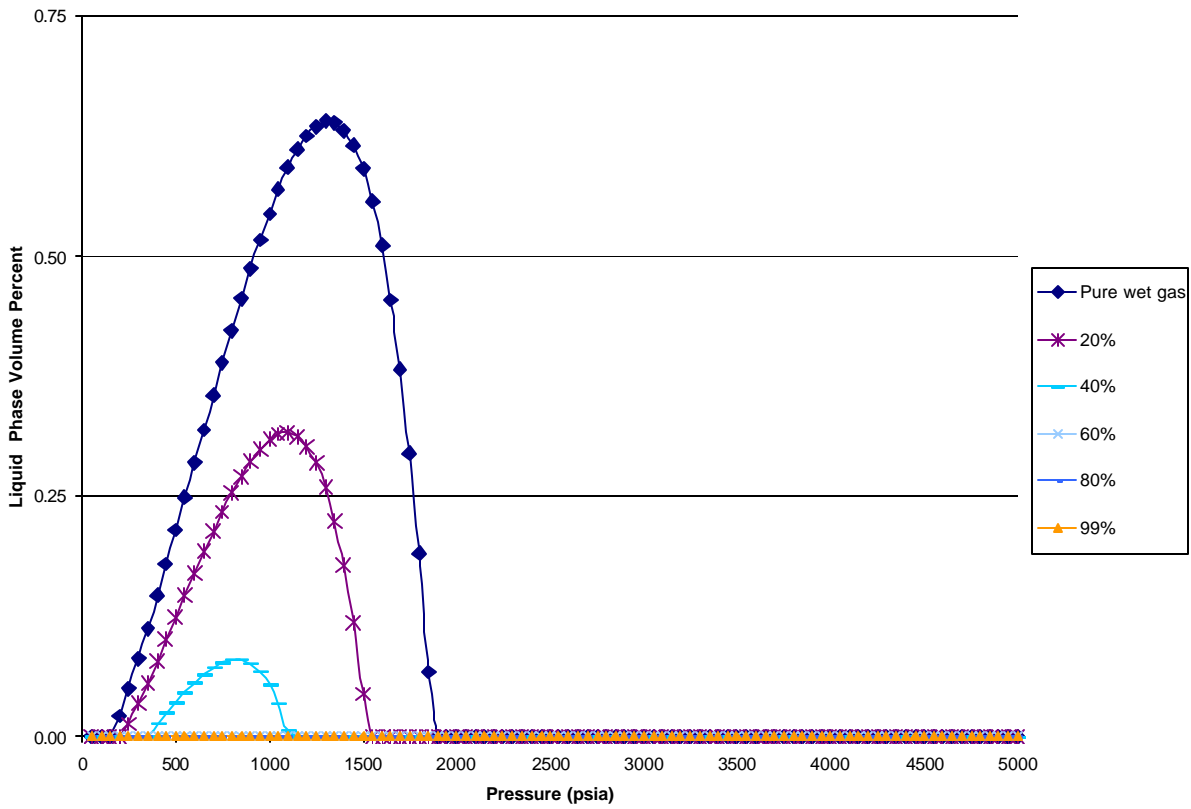


Figure 7.3b - Liquid Volume Percent of Wet Gas-Carbon dioxide Mixtures at 100°F

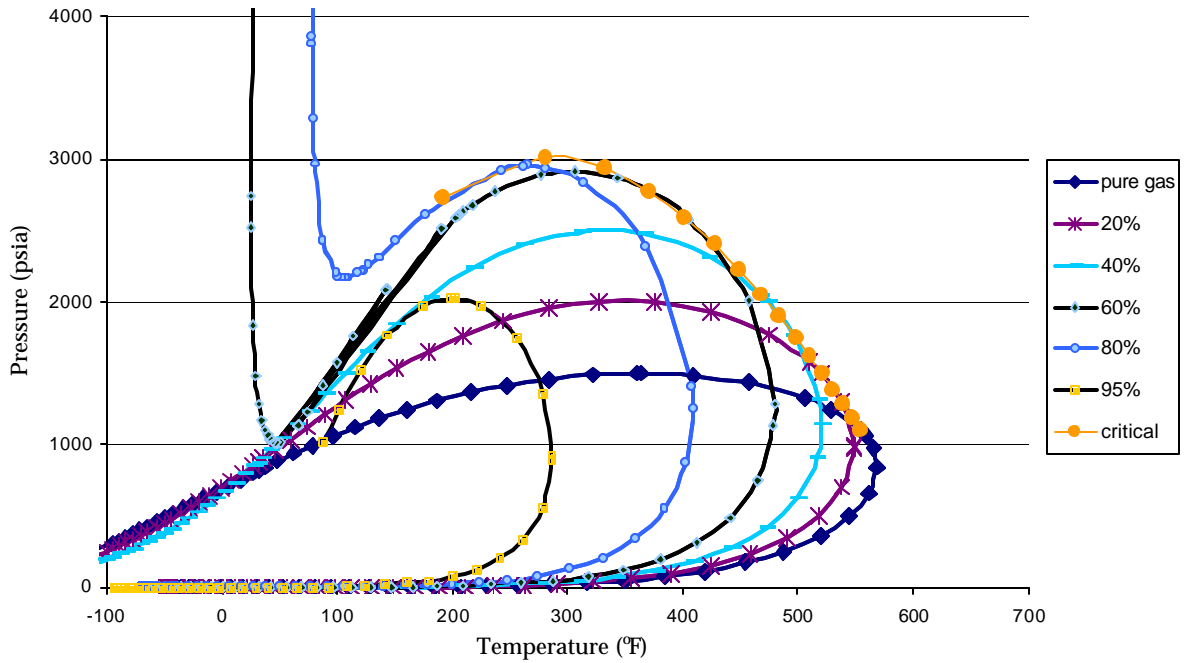


Figure 7.4a - Pressure-temperature diagram of retrograde gas A-carbon dioxide mixtures ranging from 0-95% carbon dioxide

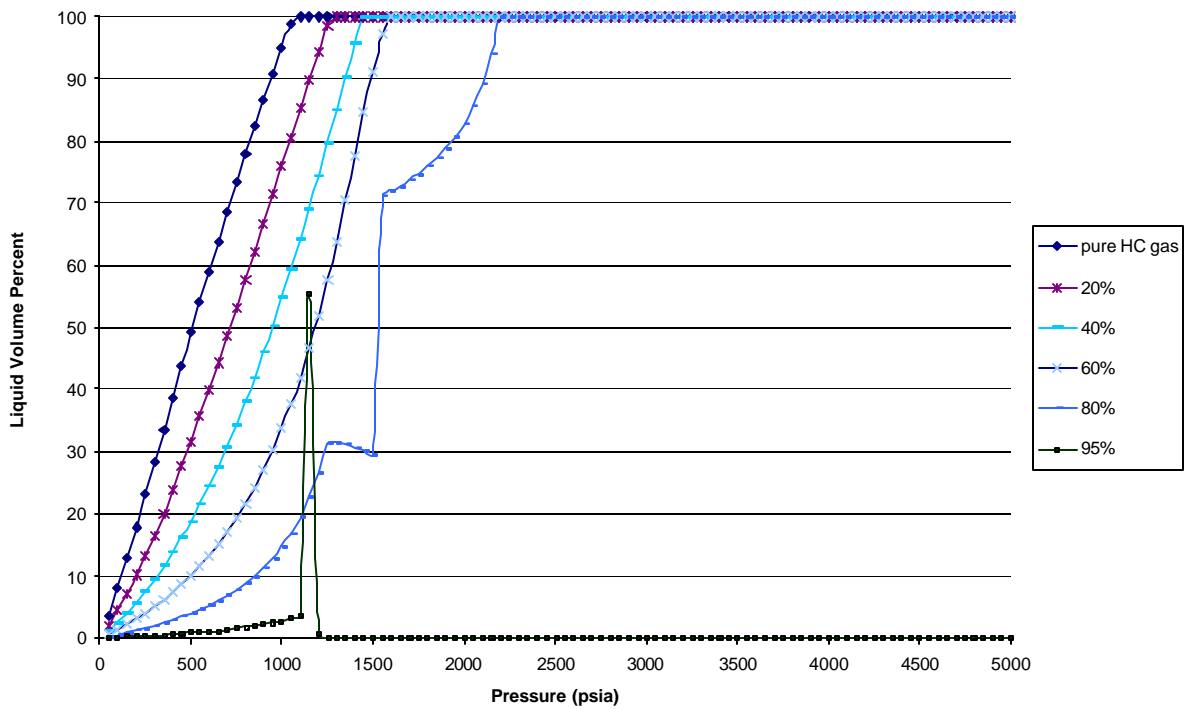


Figure 7.4b – Liquid Volume Percent Retrograde gas A with 0-99% Carbon dioxide at 100°F

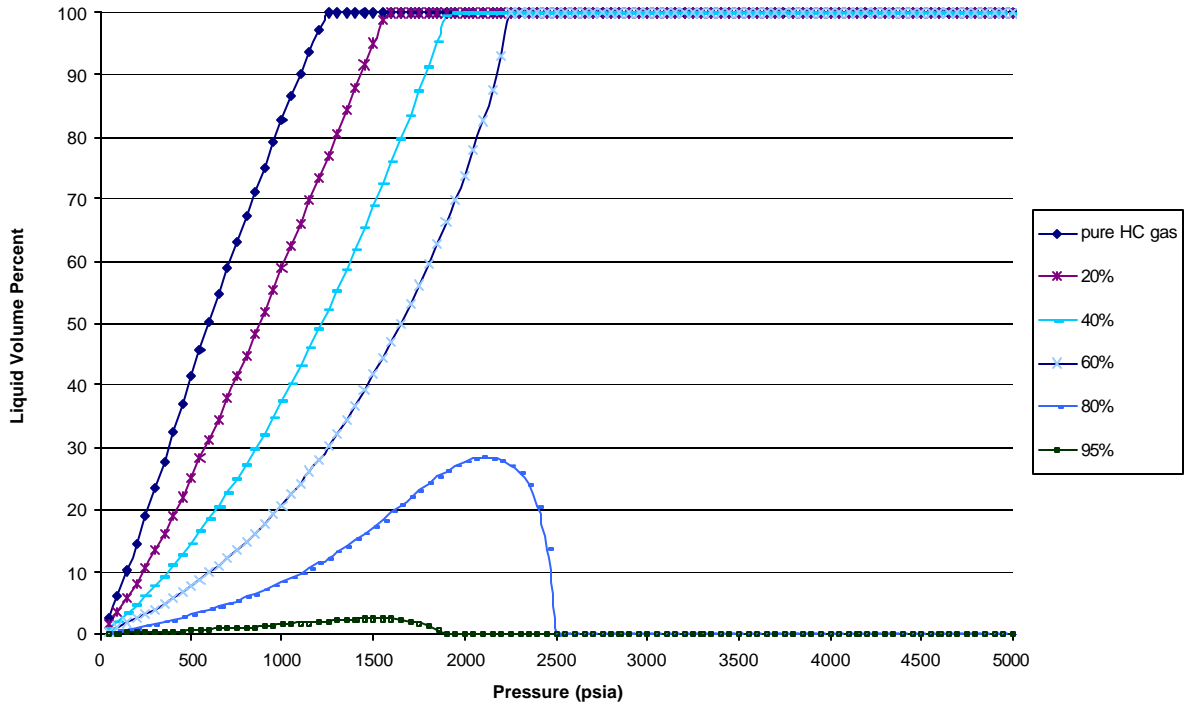


Figure 7.4c – Liquid Volume Percent Retrograde gas A with 0-99% Carbon dioxide at 160°F

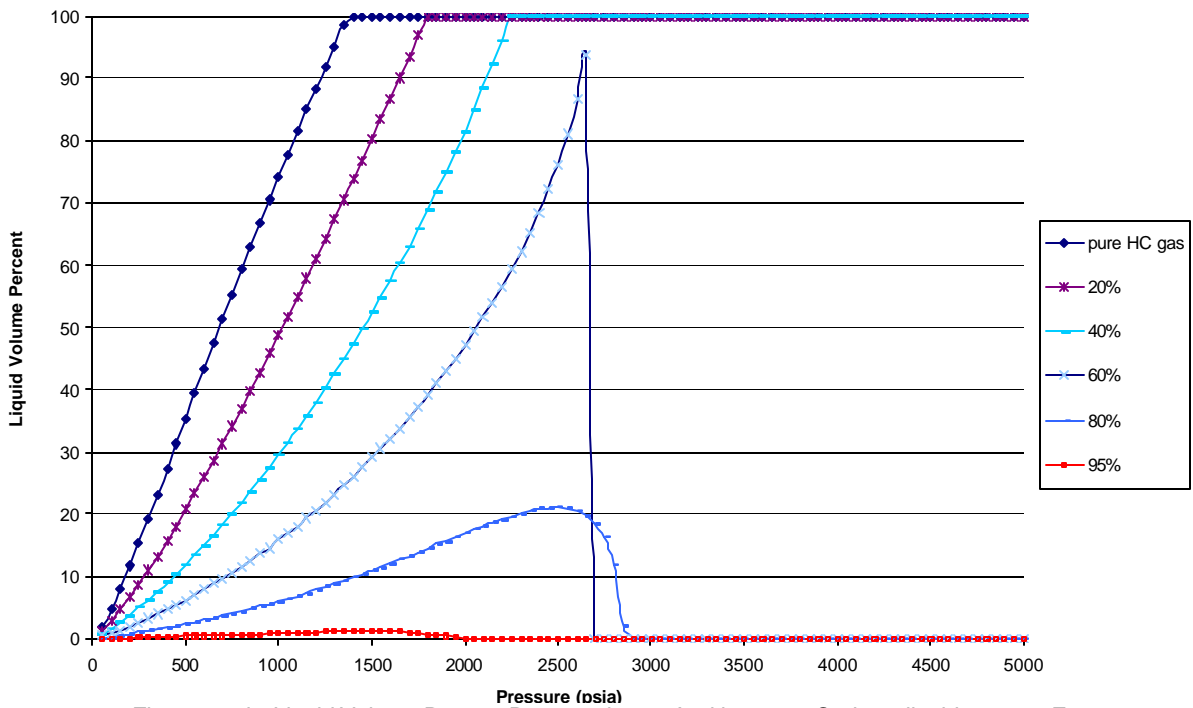


Figure 7.4d – Liquid Volume Percent Retrograde gas A with 0-99% Carbon dioxide at 220°F

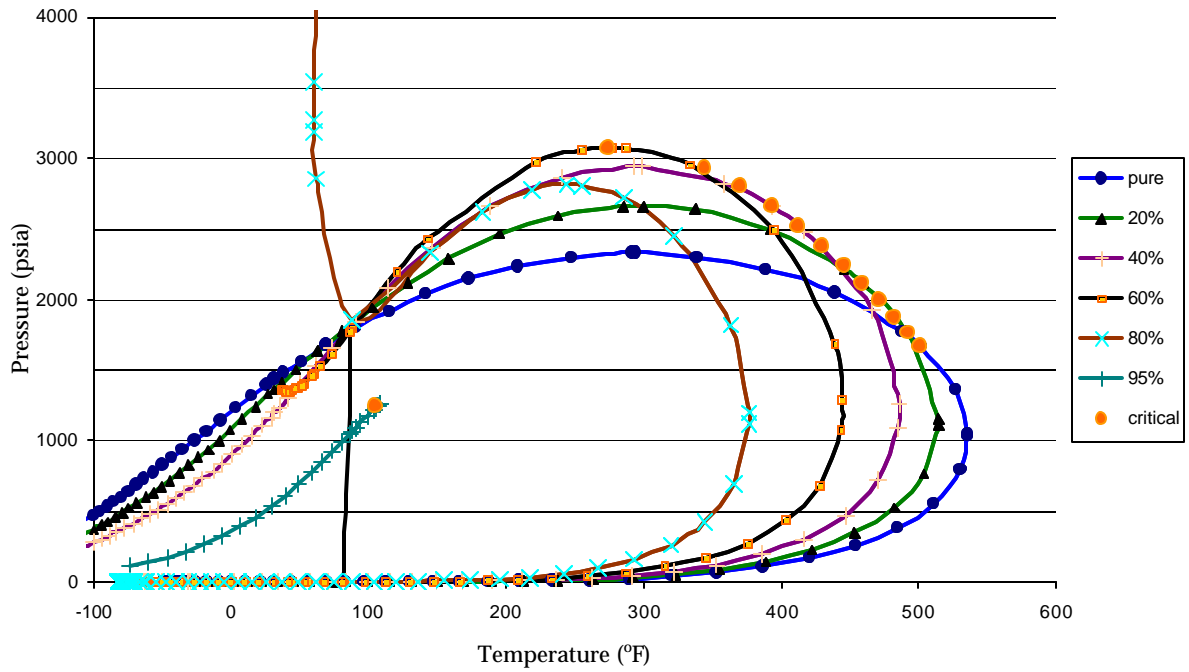


Figure 7.5a - Pressure-temperature diagram of retrograde gas B-carbon dioxide mixtures ranging from 0-95% carbon dioxide

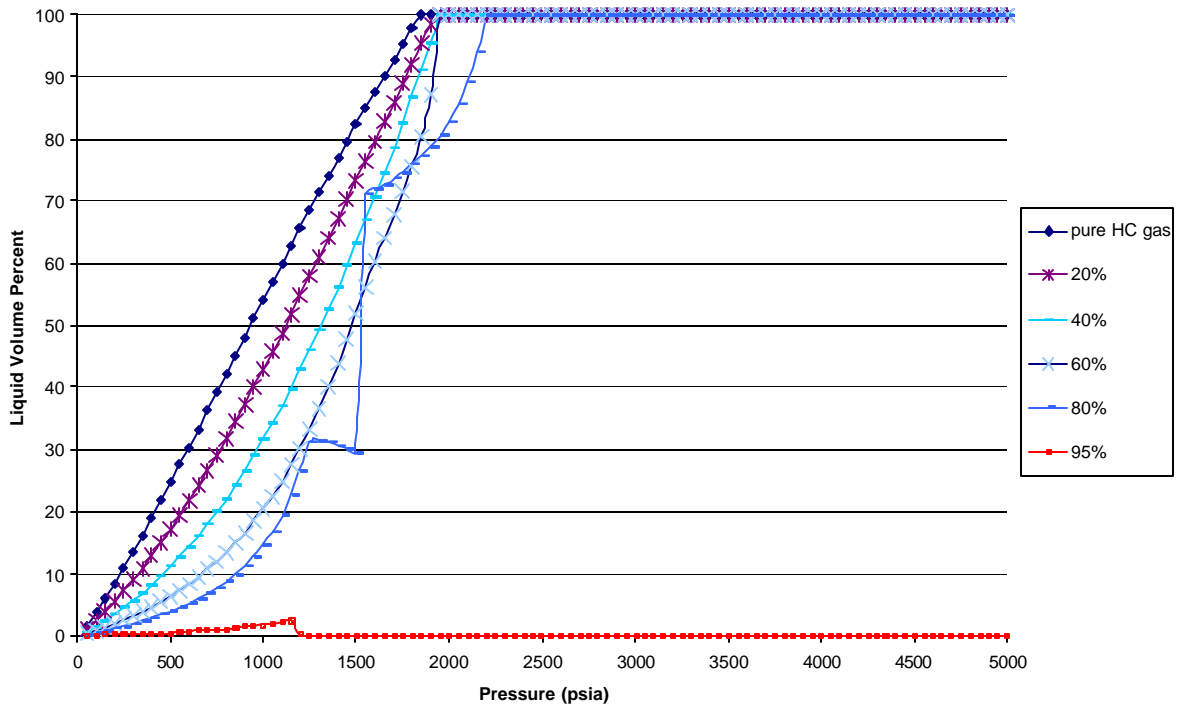


Figure 7.5b – Liquid Volume Percent Retrograde gas B with 0-99% Carbon dioxide at 100°F

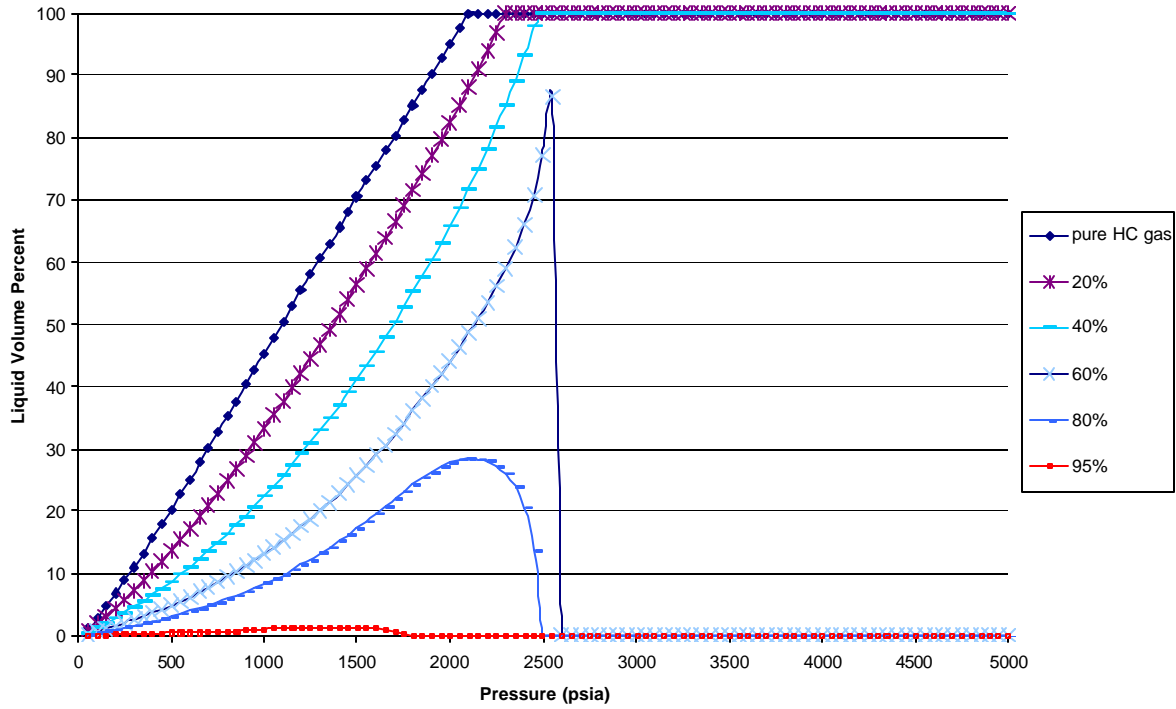


Figure 7.5c – Liquid Volume Percent Retrograde gas B with 0-99% Carbon dioxide at 160°F

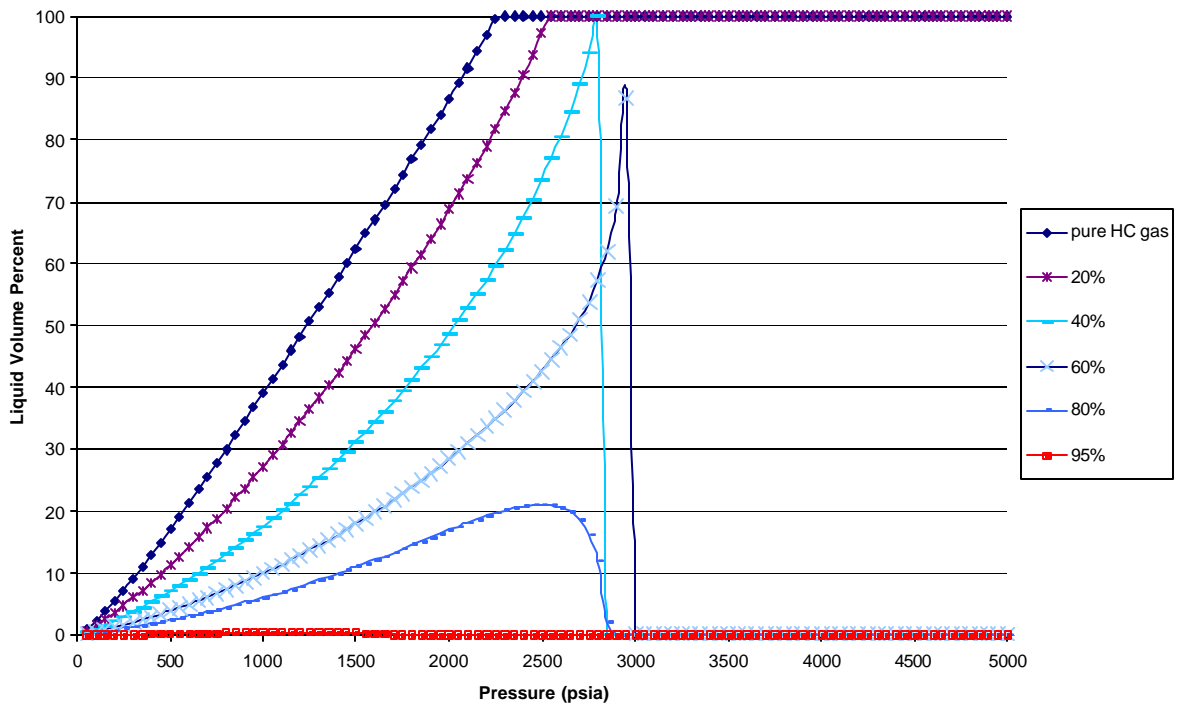


Figure 7.5d – Liquid Volume Percent Retrograde gas B with 0-99% Carbon dioxide at 220°F

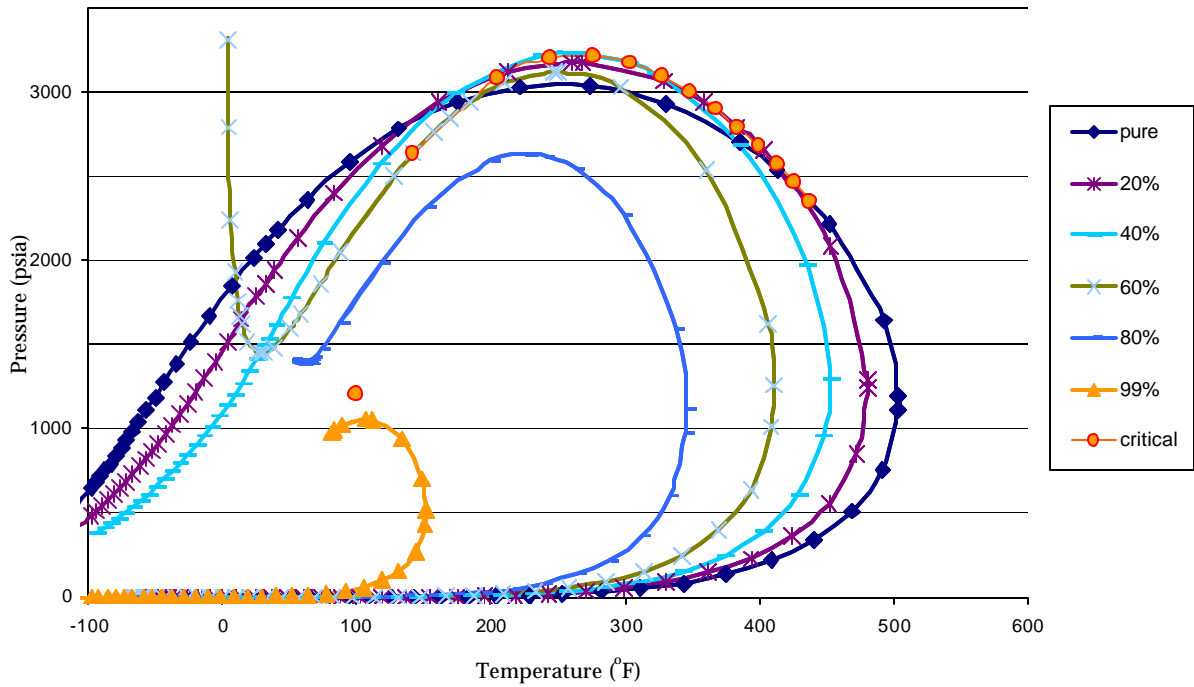


Figure 7.6a - Pressure-temperature diagram of retrograde gas C -carbon dioxide mixtures ranging from 0 -95% carbon dioxide

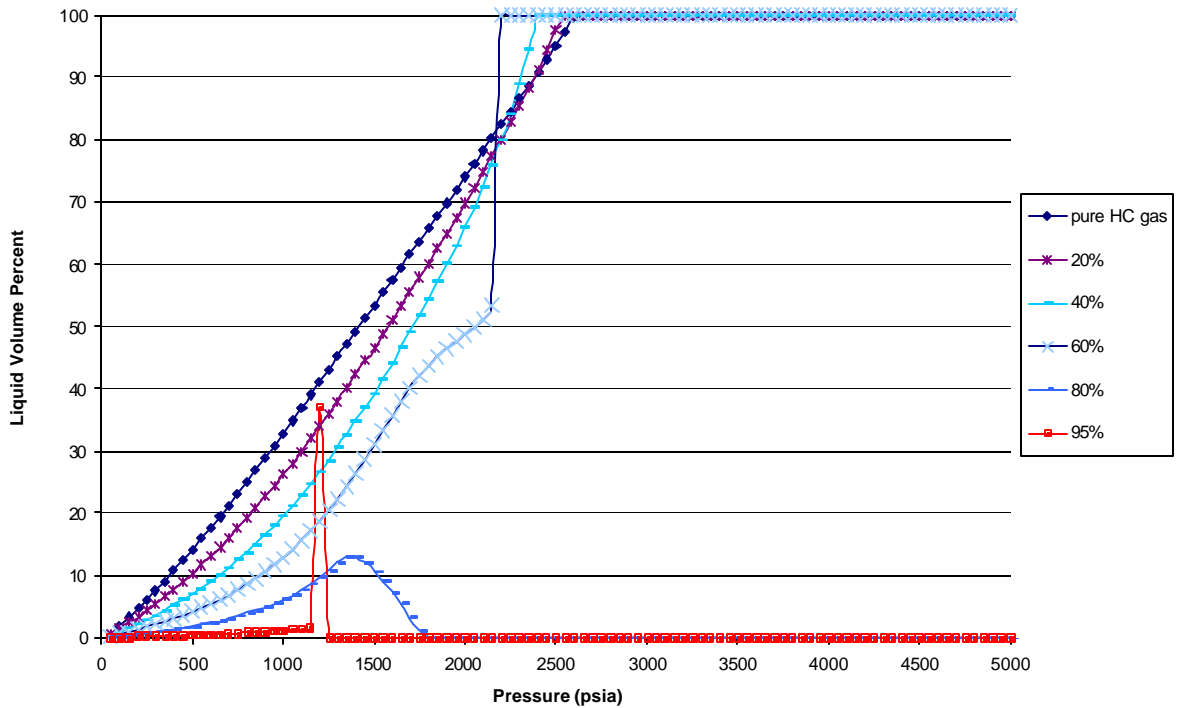


Figure 7.6b – Liquid Volume Percent Retrograde gas C with 0-99% Carbon dioxide at 100°F

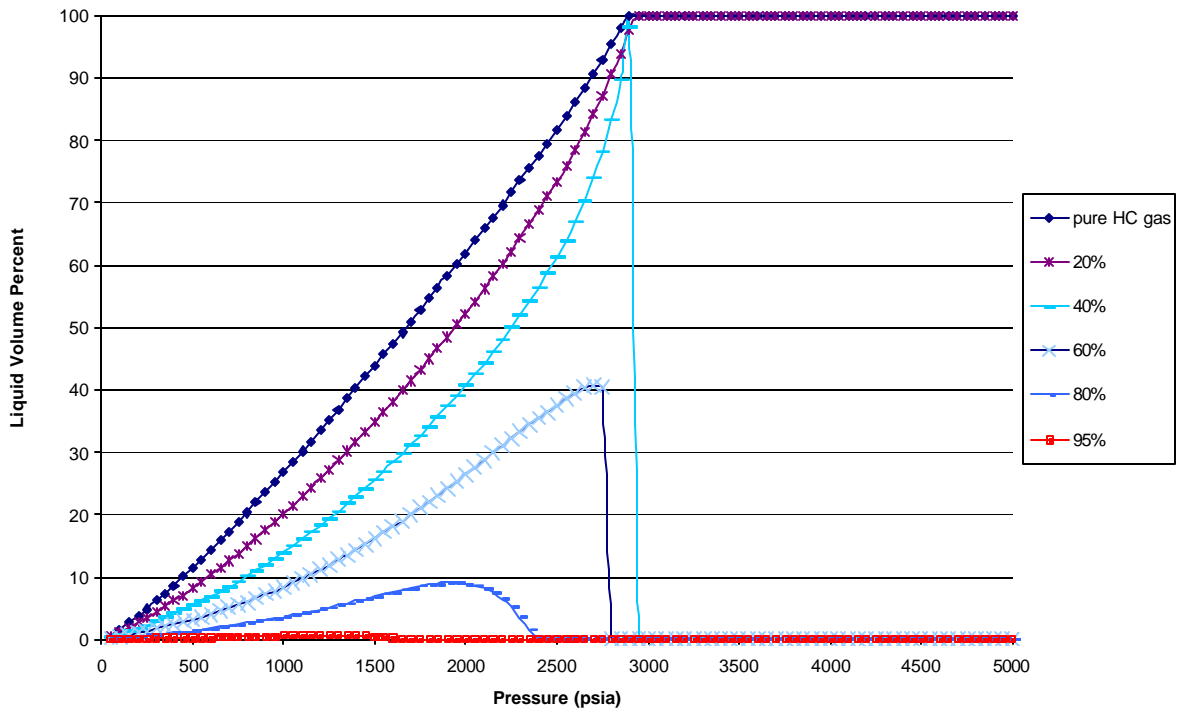


Figure 7.6c – Liquid Volume Percent Retrograde gas C with 0-99% Carbon dioxide at 160°F

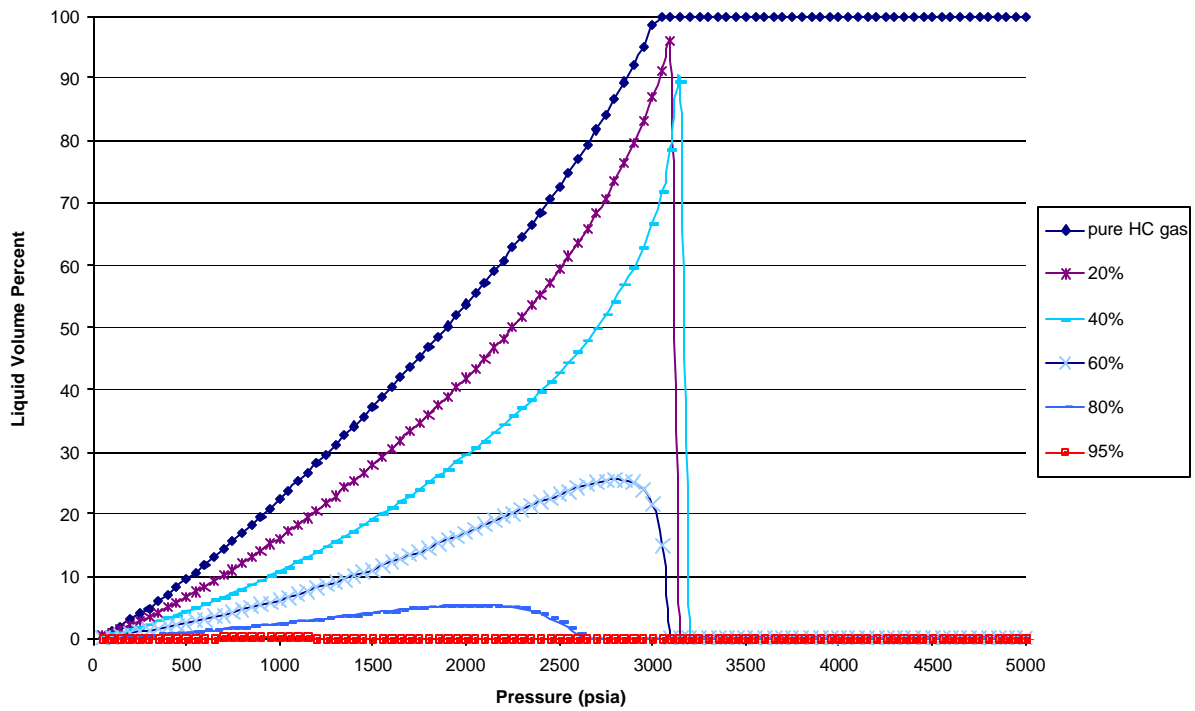


Figure 7.6d – Liquid Volume Percent Retrograde gas C with 0-99% Carbon dioxide at 220°F

2.2.1.7.3 CO₂ mole fraction-pressure relationship (methodology, P/Z vs. P plot)

Discussion and analysis of results ended with the desire for a simple method of estimating the reservoir pressure as a consequence of achieving a certain mole fraction of CO₂ in the DGR (or vice versa). As such a method based on the real gas law, and Z-factor charts as a function of pressure, temperature and Z-factor graphs (Figures 7.7a-c) were made. A unique plot of P/Z vs. P was generated to complement this new method (Figures 7.8a-c). Dry gas is used as an example for illustrating this analysis.

The real gas law can be written for the initial sequestration pressure and temperature of the reservoir and for any pressure and temperature after sequestration begins:

$$P_i V_i = Z_i n_i R T_i \quad (7.1)$$

$$P V = Z n R T \quad (7.2)$$

For dry gas, the reservoir pore volume is constant during sequestration because no phase changes occur. ($V_i = V$). Likewise, reservoir temperature is constant. So that dividing equations 7.1 and 7.2 yields

$$\frac{P V}{P_i V_i} = \frac{Z n}{Z_i n_i} \quad (7.3)$$

Solving for P/Z yields

$$\frac{P}{Z} = \frac{n P_i}{Z_i n_i} \quad (7.4)$$

The number of moles of hydrocarbon gas at sequestration initiation is n_i . For the scenario of dry gas production cessation and only CO₂ sequestration, the total moles (n) is the sum of n_i and the moles of CO₂ injected.

$$n = n_{hc} + n_{CO_2} = n_i + n_{CO_2} \quad (7.5)$$

$$\% CO_2 = \frac{n_{CO_2}}{(n_{hc} + n_{CO_2})} \quad (7.6)$$

so that

$$n = \frac{n_{CO_2}}{\% CO_2} \quad (7.7)$$

and

$$\frac{n_i}{n} = \frac{n_{hc}}{(n_{CO_2} + n_{hc})} = 1 - \% CO_2 \quad (7.8)$$

Substituting into equation 7.1 yields

$$\frac{P}{Z} = \frac{P_i (1 - \% CO_2)}{Z_i} \quad (7.9)$$

Using Equation 7.9, P/Z was calculated as a function of CO₂ mole fraction. To find pressure only, P/Z vs. P plots (Figures 7.8a-c) were calculated from the Z-factor charts (Figures 7.7a-c) so that P/Z is read directly from the y-axis of these plots using the reservoir temperature and the initial depleted reservoir pressure. Initial Pressure is the y-intercept of the three temperature curves because of z-factor being 1.0 at low pressures.

An example of using Figure 7.9, which is generated for a initial pressure of 250 psia shows the pressure doubles to 500 psia following increase in CO₂ mole fraction to 52%-53%. At 78%-83% mole fraction the reservoir pressure required is about 1000 psia. Temperature begins to affect the trends at about 500 psia as evidence from the separation of the three curves at this pressure. The plots can also be used in reverse if mole fraction is known and pressure is desired. If a salable gas exceeds 20 mole % CO₂, an anticipated

reservoir pressure at this CO₂ is 300 psia. This method will likely lead to graphs that can be used to estimate the final volume of CO₂ stored as a function of the hydrocarbon gas in place, initial and final sequestration pressure (ISP and FSP).

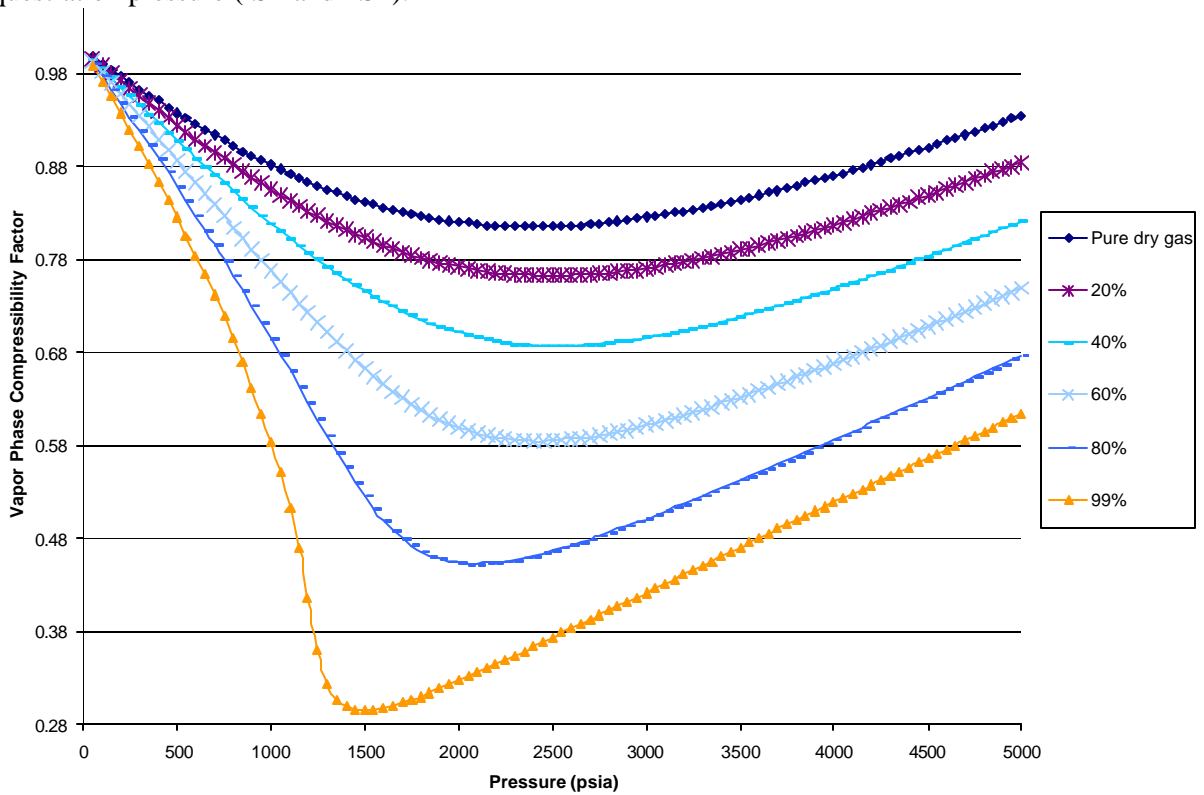


Figure 7.7a– Vapor Phase Compressibility Factor of Dry Gas Carbon Dioxide Mixtures at 100°F

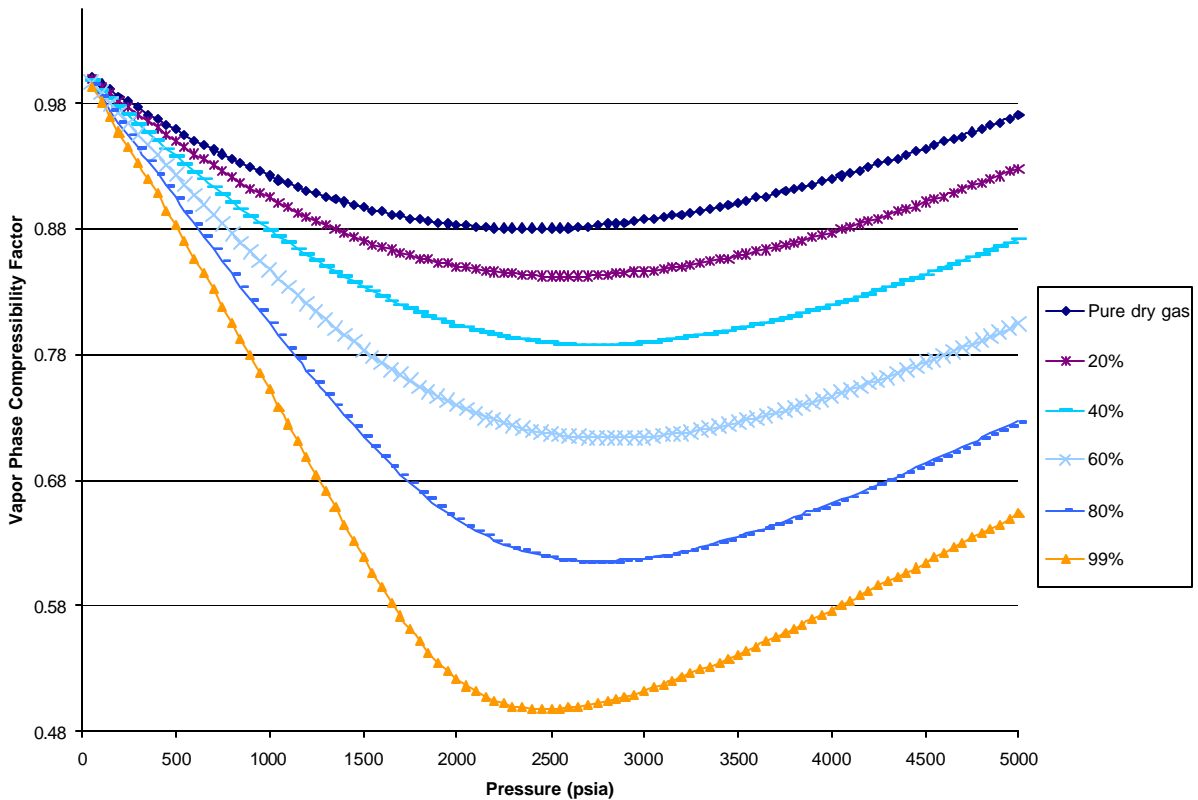


Figure 7.7b – Vapor Phase Compressibility Factor of Dry Gas Carbon Dioxide Mixtures at 160°F

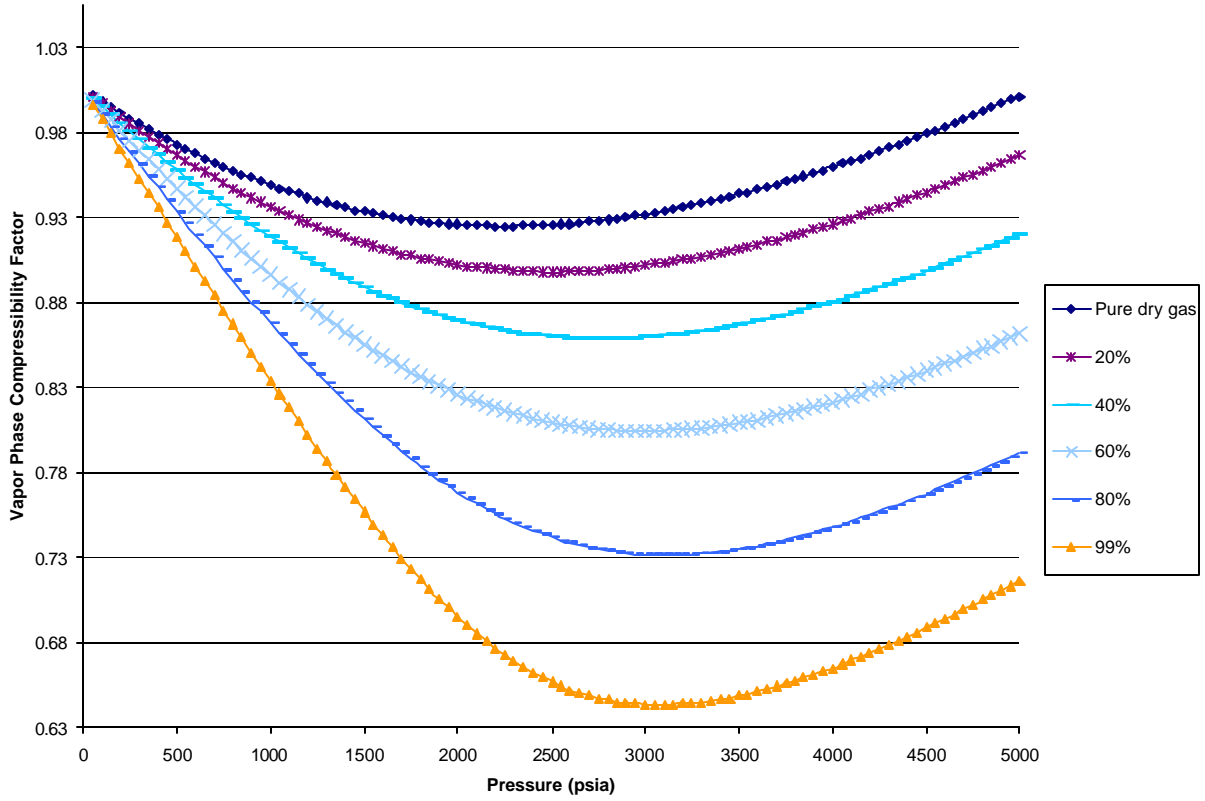


Figure 7.7c – Vapor Phase Compressibility Factor of Dry Gas Carbon Dioxide Mixtures at 220°F

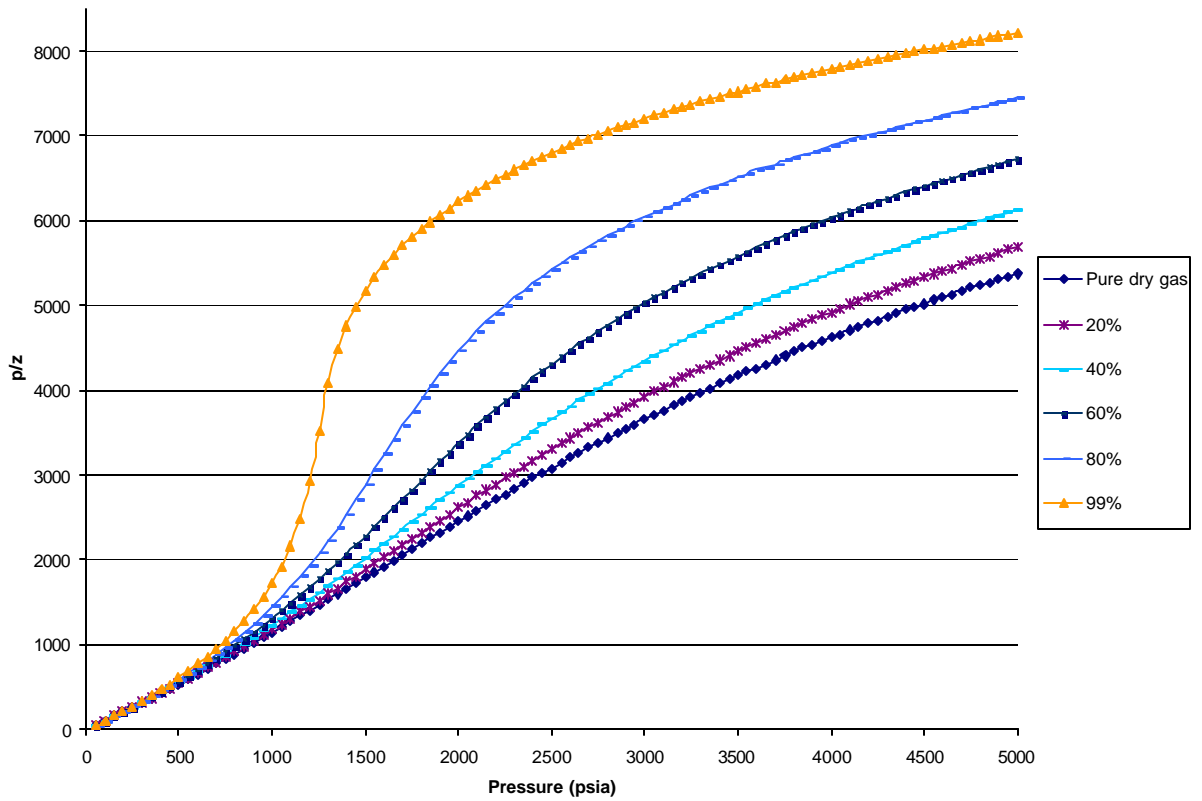


Figure 7.8a – P/Z plot for Dry Gas CO₂ Mixtures at 100°F

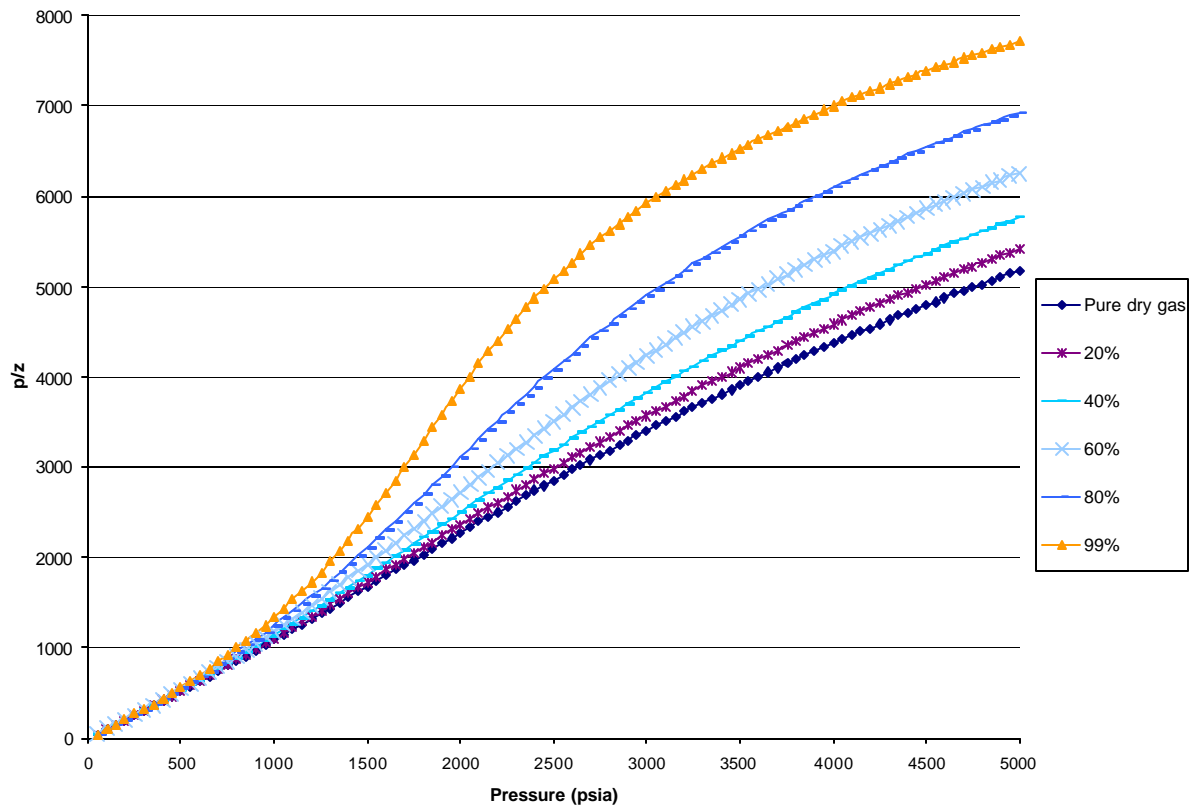


Figure 7.8b – P/Z plot for Dry Gas CO₂ Mixtures at 160°F

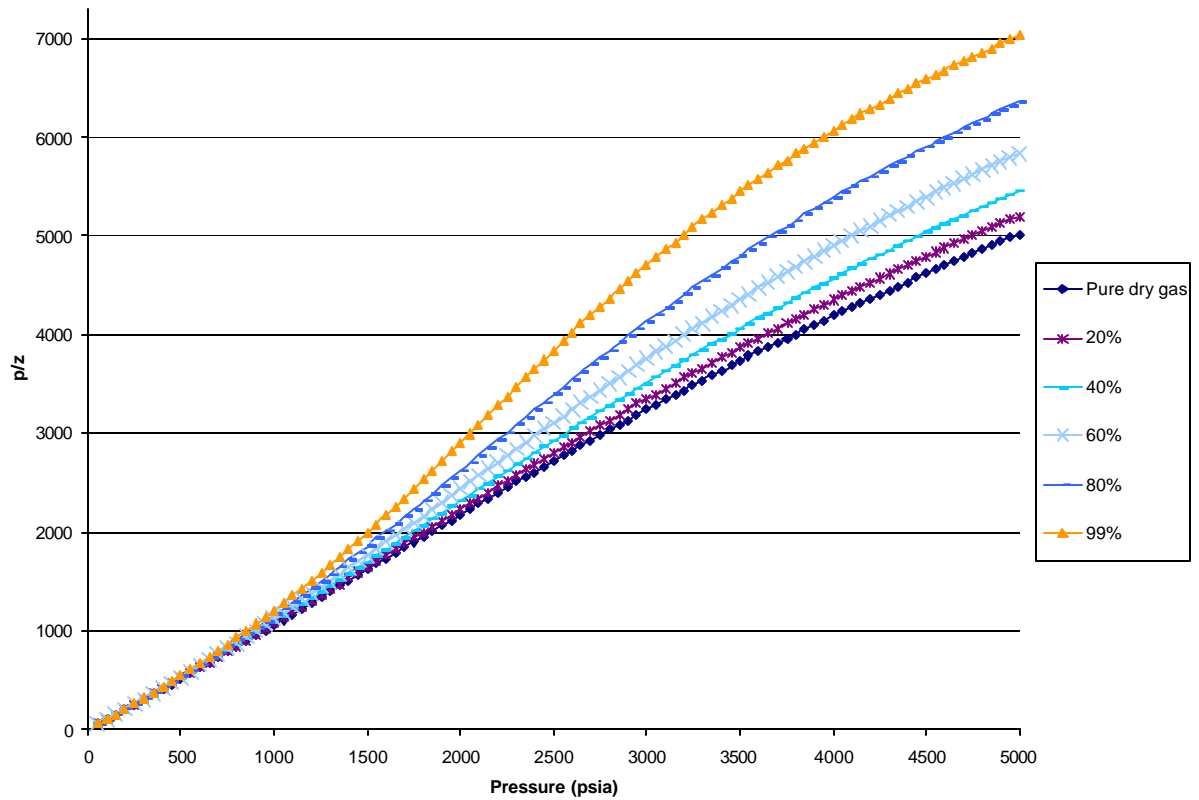


Figure 7.8c – P/Z plot for Dry Gas CO₂ Mixtures at 220°F

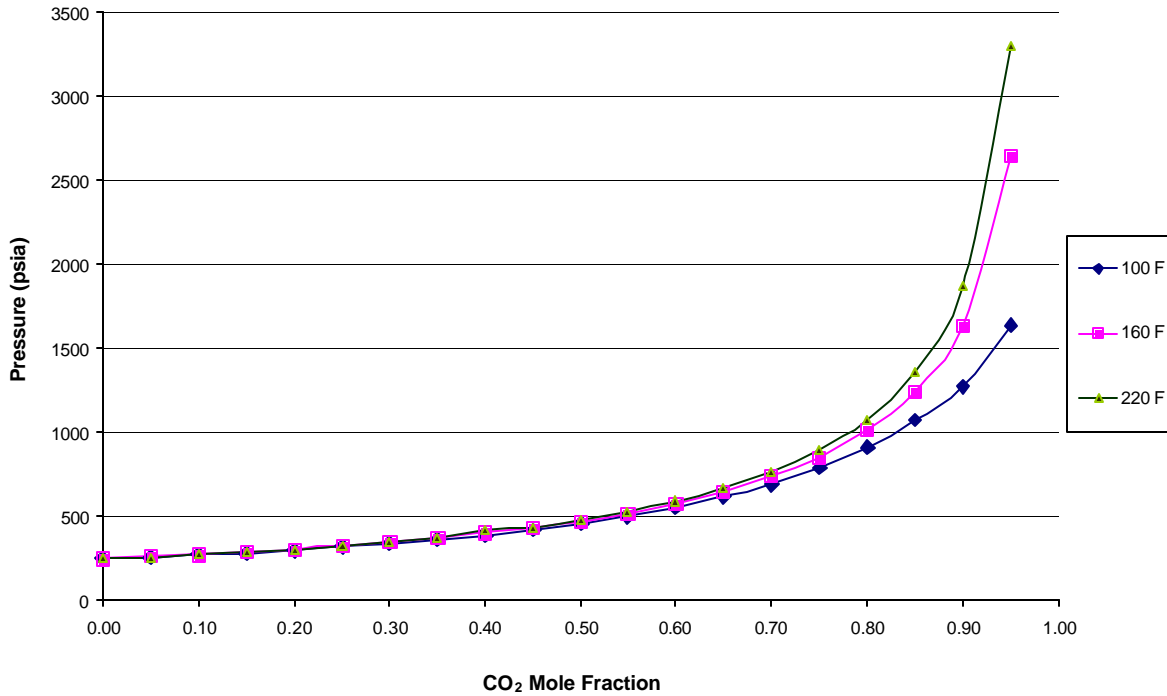


Figure 7.9 - Reservoir Pressure as a function of CO₂ mole fraction for the median dry gas with initial sequestration pressure of 250 psia

2.2.1.7.4 Conceptual View of P/Z for Sequestration Parameter

The current development of a tool for use in designing and monitoring CO₂ sequestration in gas reservoirs is an adaptation to the P/Z plot, a traditionally used analysis technique in the oil and gas industry. Figure 7.1 is a development of this idea. Two trends are established in Figure 7.1: one trend is for the historical production of the gas reservoir and a second trend is for the analogous reservoir as if it were a CO₂ reservoir. The x-axis is the cumulative gas produced (G_p) in standard cubic feet (scf), while the y-axis is the average reservoir pressure (P) in pound-forces per square inch (psia) divided by the Z-factor (Z) of the gas at reservoir pressure and temperature.

The lower line represents the production of a volumetric (closed system) hydrocarbon gas reservoir. The y-intercept is the initial pressure and Z-factor; the x-intercept is the initial gas in place (G). Represented by the following relation:

$$\frac{P}{Z_{hc}} = -\left(\frac{P_i}{Z_{hci}} \frac{1}{G}\right)G_p + \frac{P_i}{Z_{hci}} \quad (7.1)$$

The upper line represents the same gas reservoir if the natural hydrocarbon gas was replaced with CO₂, and mathematical is below:

$$\frac{P}{Z_{co2}} = -\left(\frac{P_i}{Z_{co2i}} \frac{1}{G}\right)G_p + \frac{P_i}{Z_{co2i}} \quad (7.2)$$

The y-intercept for the equivalent CO₂ reservoir is higher only because of the lower Z-factor for CO₂. Likewise, the x-intercept is higher because of the larger magnitude of CO₂ system compressibility compared to hydrocarbon gases. In other words for a given reservoir volume, a larger surface volume

(scf) of CO₂ gas can be contained compared to the surface volume of hydrocarbon gas. Furthermore, a change in Z due to a change in gas composition (in this case from hydrocarbon gas to CO₂) causes the same effect to the x- and y-axes. Consequently, the natural gas and CO₂ lines are parallel to each other.

A modification to the x-axis of the P/Z chart is anticipated to be the cumulative gas produced less the cumulative CO₂ injected ($G_p - G_{inj}$). If a gas with the same Z-factor were injected, the reservoir would respond identically as it did during production except it would be in reverse. So the trend would retrace the natural gas line. However, at the same temperature and pressure, pure CO₂ Z-factors are significantly lower from pure hydrocarbon gases.

During the gas production from a volumetric gas reservoir, the data starts at the initial conditions (figure 7.53, labeled point *a*) and follows the natural gas line, progressing from left to right as gas is produced and pressure is depleted. Under CO₂ sequestration conditions of a depleted gas reservoir, the initial conditions of sequestration are the depleted or near abandonment conditions of a gas reservoir represented by point *b*. With continued CO₂ injection and pressurization of the reservoir, the trend will approach the pure CO₂ line. Three example paths (*c*₁, *c*₂ and *c*₃) are traced on the sketch as dashed lines connecting the two lines.

A sequestration parameter is being investigated that includes reservoir rock and fluid properties that can be used to correlate of SCO₂ volume, EGR and ECR for each of the three gas types. At this time, SCO₂ volume is anticipated to be a function of gas-type, ISP and FSP, formation area, thickness, water saturation and porosity. EGR and ECR are believed to be a function of dispersion of the CO₂ into the natural gas; dispersion is a function of reservoir permeability and gas viscosity. Current studies include introducing reservoir rock properties that can lead to a sequestration parameter that can be used to group compositional reservoir simulation results into a family of curves that can be used to predict the volume of sequestered CO₂ in a depleted gas reservoir. To this end, the volumetric equation

$$G = 43,560Ahf \frac{(1-S_w)}{B_{gi}} \quad (7.3)$$

is likely be substituted in to the slopes of Equations 7.1 and 7.2 to include reservoir pore volume. By substituting Eq. 7.3 into the slope (m_{hc}) of Eq. 7.1, we have

$$m_{hc} = \left(\frac{P_i}{z_{hci}} \frac{B_g}{Ahf(1-S_w)} \right) \quad (7.4)$$

Similarly, by substituting Eq. 7.4 into the slope (m_{co2}) of Eq. 7.2, we have

$$m_{CO_2} = \left(\frac{P_i}{z_{co2i}} \frac{B_g}{Ahf(1-S_w)} \right) \quad (7.5)$$

While the straight lines of Figure 7.1 are believed to be dependent on gas compressibility and the reservoir volume (see Eqs. 7.4-7.5), the path between each is suspected of being dependent on diffusion and/or dispersion of the CO₂ and the natural gas. While diffusion is often considered inconsequential in porous media, dispersion (K_d) can be significant. Permeability (k) and viscosity (μ) are documented as

affecting dispersion. As such, attempts are being made to model the trend between the two lines with permeability and viscosity based-formulas. Hence, by inspection of Equations 7.4-7.5, CO₂ sequestration parameter (CSP) can be functionally expressed as

$$CSP = f(B_g, V_B, k, m, f, K_d) \quad (7.6)$$

Apparently, the formation volume factor, B_g, of Eq. 7.6 appears to be the only term that depends on reservoir temperature and pressure, however, it is conceivable for diffusion-dispersion term, K_d, to be dependent on temperature and pressure as well.

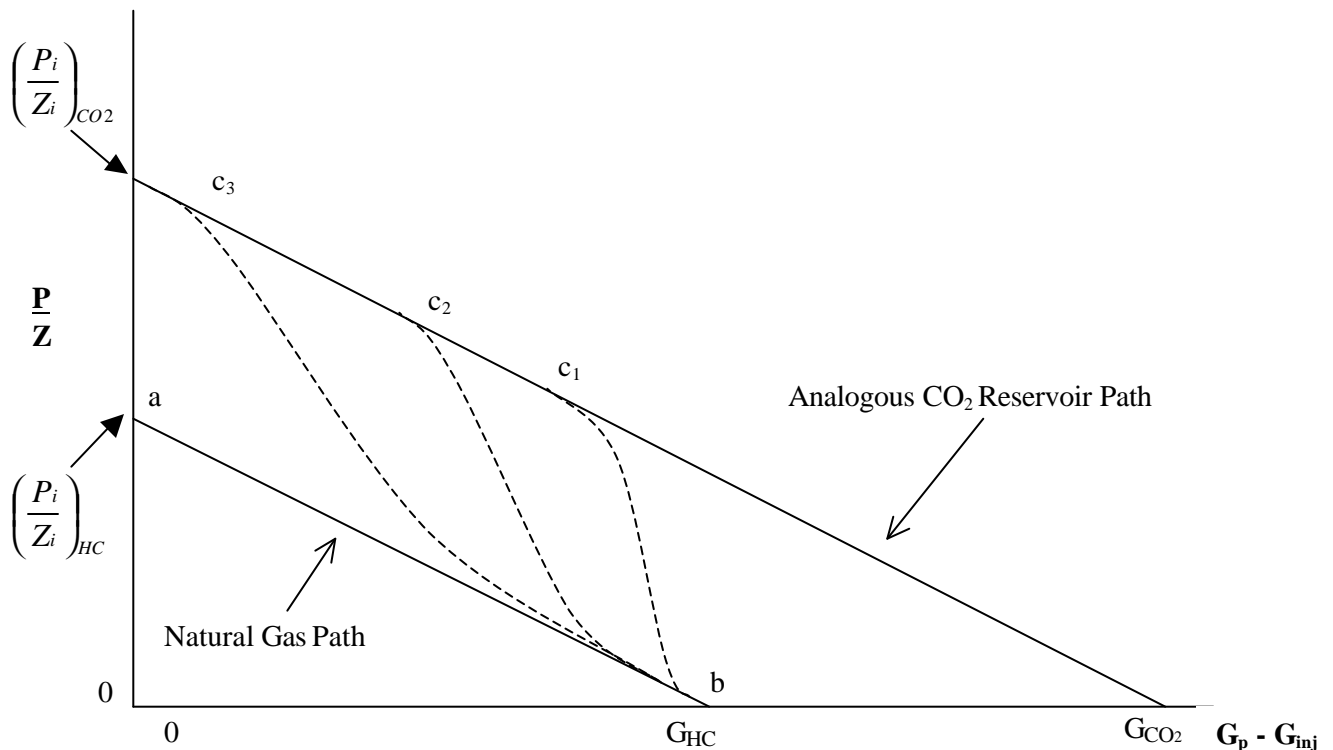


Figure 7.10: Material Balance Schematic for Natural Gas Reservoirs with Sequestration

2.2.1.7.5 Modeling Measured Z-Factor With Cubic Equations

The phase behavior simulation of this research project served two important functions, namely (i) contribution to the design of the laboratory experiments and (ii) estimation of black oil PVT properties for estimating non-compositional benefits of CO₂ storage in depleted gas reservoirs. We have acquired commercial PVT package (Winprop) and compositional model (GEM) from Computer Modeling Group (CMG). Winprop is used for phase behavior modeling of measured PVT data and GEM is used for reservoir compositional simulation of carbon dioxide injection into the gas reservoirs. In addition, the department has Merlin Black Oil simulator, which is used to quantify non-composition aspect of the research project (that is, to estimate black oil properties for CO₂ and hydrocarbon/CO₂ mixtures, which leads into estimating the non-compositional aspects of CO₂ storage). Fluid properties of importance to this research project include Z-factor, density, and viscosity. Z-factor is an important component for CO₂

storage, while density and viscosity are important factors in EGR and ECR. Figures 7.11a to 7.11d show polynomial curve-fit to the laboratory measured Z-factor data. Even though the Z-factor data shown in the figures are not the smooth experimental data (as seen in section of Smooth Measured Z-factor Data in this report), the need arises to acquire better tools to model the Z-factors at low and high pressures because of the wrong trend exhibits by the polynomial functions. Moreover, viscosity measurement is not part of this research project, yet viscosity is an important factor in the establishment of the CSP. With this in mind, a program is set-up to improve existing Z-factor correlations and also to improve parameter characterization of cubic equations-of-state for CO₂-hydrocarbon mixtures.

To provide EOS for modeling the volumetric (Z-factor, density) and transport (viscosity) properties, and phase behavior (vapor-liquid equilibria (VLE) of mixtures of the components identified in the gas reservoirs. That objective is accomplished by selecting *seven* cubic equations-of-state (EOS) that have the greatest appeal to petroleum engineers through their citations in the journals published by the Society of Petroleum Engineers (SPE), Canadian Journal of Petroleum Technology (CJPT), and Journal of Petroleum Science and Engineering (JPSE). The selected equations-of-state are: (i) Redlich-Kwong (RK), (ii) Soave-Redlich-Kwong (SRK), (iii) Peng-Robinson (PR), (iv) Patel and Teja (PT), (v) Schmidt-Wenzel (SW), (vi) Lawal-Lake-Silberberg (LLS), and (vii) Trebble-Bishnoi. By examining the reduced state of the respective EOS in comparison with the experimentally determined Z-factor of CO₂, N₂, and C₁ that are the major species in the gas reservoirs, tuning parameters are established for the various EOS. However, the analysis of results shows that a significant difference exist between the predicted Z-factor from EOS and experimental Z-factor of those components in the vicinity of the critical point. The LLS EOS has been developed to remedy the issue around the critical region. Thus, the critical temperatures and pressures required to establish the reduced properties (P_R , T_R) for Z-factor correlations are established through LLS EOS. The detailed framework of all the EOS is in Appendix A and the framework for Viscosity Equation of State is in Appendix B. The scaling parameter established to make Standing-Katz chart fit acid gases is shown in Appendix C.

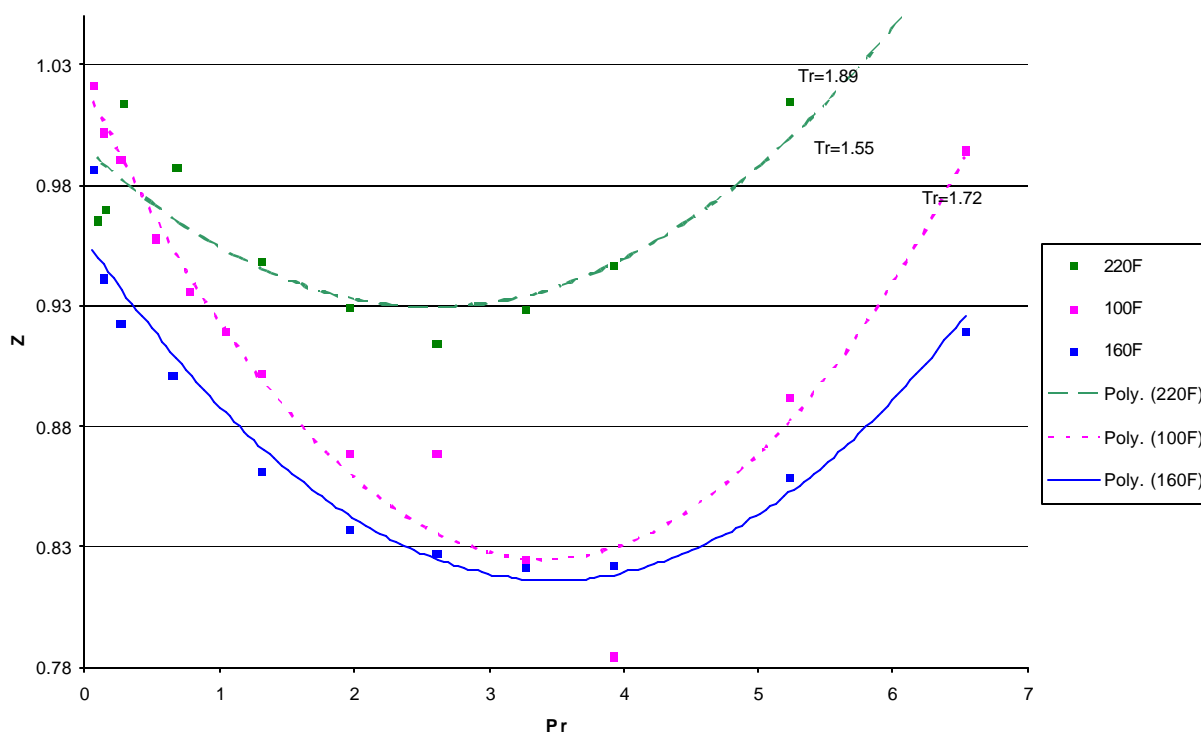


Figure 7.11a– Dry Gas @ 0% CO₂

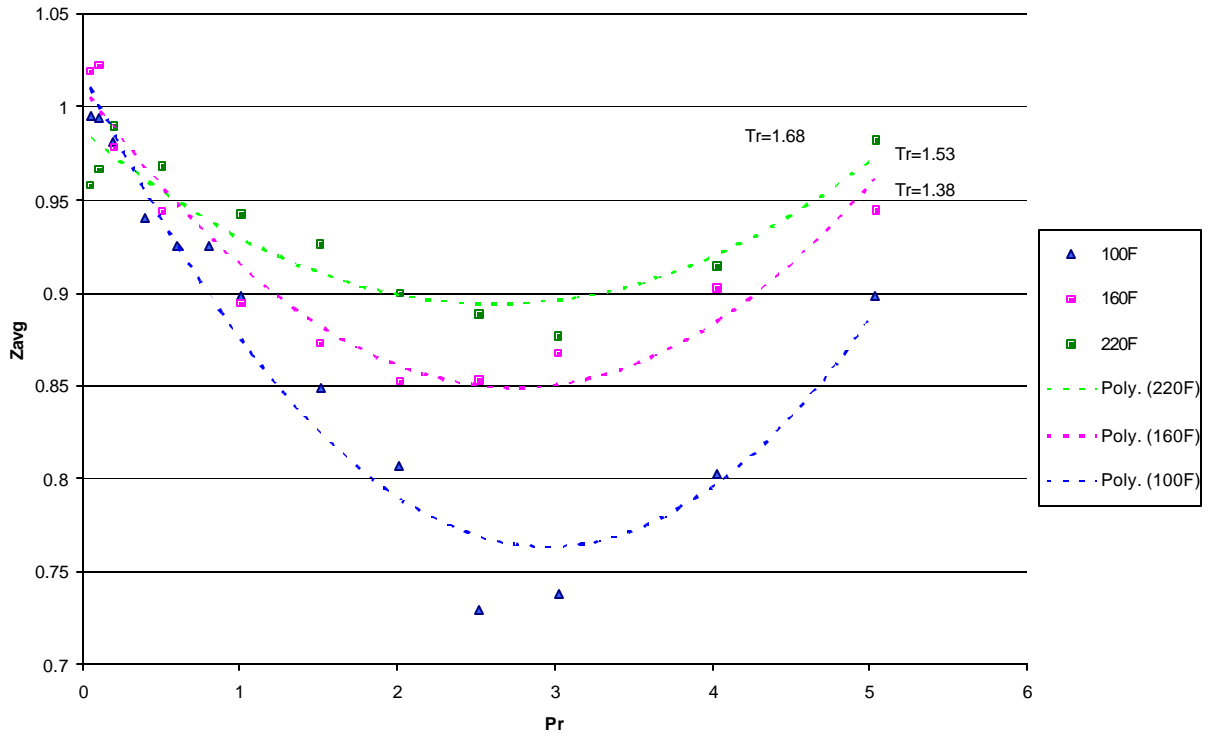


Figure 7.11b – Dry Gas @ 25% CO_2

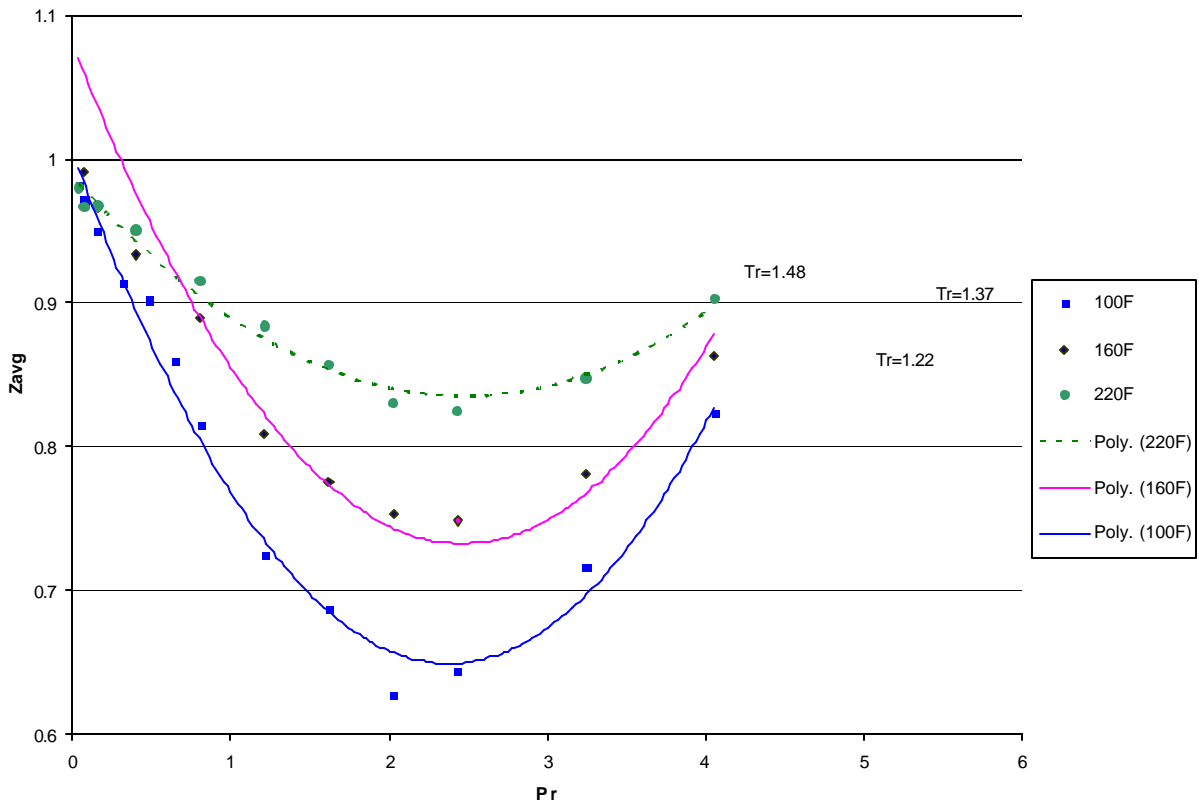


Figure 7.11c – Dry Gas @ 50% CO_2

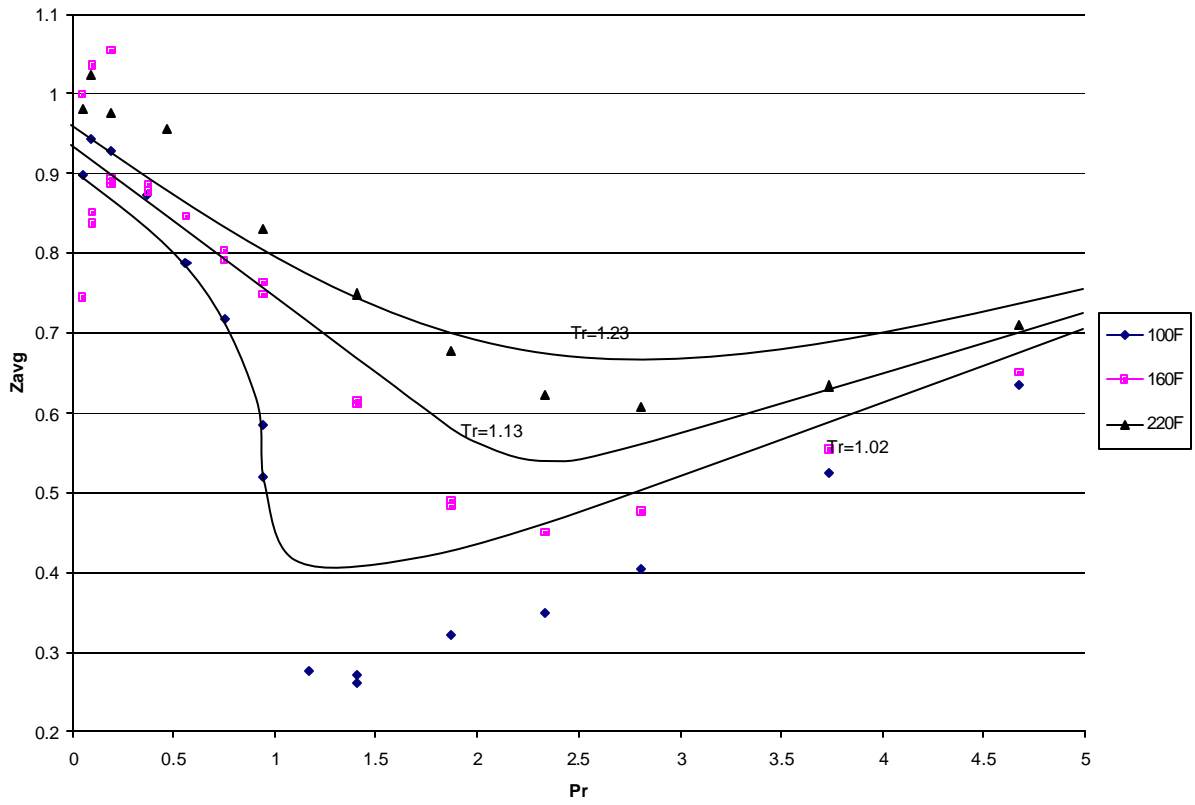


Figure 7.11d – Dry Gas @ 100% CO_2

2.2.1.8 Conclusion

This research focuses on using laboratory investigation and computer simulation to analyze phase behavior and enhanced gas and condensate recovery by CO₂ storage in depleted gas reservoirs. The laboratory measured CO₂ compressibility factor (or Z-factor) is much lower than hydrocarbon gas mixtures at the specified temperatures and pressures. Therefore, that offers the opportunity to store larger surface volumes of CO₂ than hydrocarbon gases. Five times the storage is possible depending on pressure, temperature and hydrocarbon gas composition.

The conceptual view for this research project are two-fold: (1) the effects of natural hydrocarbon gas types and CO₂ on compressibility of the CO₂/HC gas mixtures for CO₂ storage and (2) the potential for increasing gas and condensate recovery as a consequence of CO₂ storage. The conclusions derived on the basis of the conceptual view are briefly stated as:

- **Increasing CO₂ Storage:** Storage of CO₂ increases if the CO₂/HC gas mixture compressibility (Z-factor) is low. Furthermore, if a liquid condensate occupies the reservoir pore space and the addition of CO₂ vaporizes the liquid, then additional pore space is acquired for CO₂ storage. This scenario has been confirmed by our laboratory measurements and analysis of CO₂/HC gas mixture compressibility factor.
- **Decreasing CO₂ Storage:** To the contrary, CO₂ storage decreases if the CO₂ /HC gas mixture compressibility is high. If the phase behavior effects of adding CO₂ to a gas reservoir cause an appearance of liquid phase at reservoir conditions (reservoir temperature and pressure), the pore volume available to for CO₂ storage decreases. This scenario has *not* been confirmed by our laboratory measurements of CO₂/HC gas mixture compressibility factor.
- **Increasing Gas and Condensate Recovery:** Gas and condensate recovery is increased primarily as a result of phase behavior effects. If the addition of CO₂ changes a retrograde gas to a wet gas, by reversing the retrograde phenomena in-situ, additional condensate may be recovered. The qualitative changes in the pressure-temperature (PT) diagram have been used to analyze phase behavior changes in gas reservoir by CO₂ storage. The PT diagrams show a decrease in the relative size of the two-phase region, thereby resulting in retrograde and wet gases becoming dry gases. Thus, CO₂ storage in retrograde reservoirs can results in EOR benefits, as the vaporization action can make the gas reservoirs becoming “drier.” Quantitatively, the degree to which these change the equilibrium vapor/liquids can be converted to volumes of liquid and vapor.
- **Decreasing Gas and Condensate Recovery:** If the CO₂ storage changes a dry gas to a wet or retrograde gas, condensate recovery may be reduced. This situation has not been confirmed by our laboratory measurements because the qualitative changes in the Z-factor plots do not demonstrate this effect; moreover, computational phase behavior simulations of pressure-temperature (PT) diagrams do not show a reduction in condensate recovery. Thus, CO₂ storage in retrograde reservoirs does in result in gas reservoirs becoming “wetter.”

2.2.1.9 References

- Ahmed, U., Crary S. and Coates, G.: "Permeability Estimation: The Various Sources and Their Interrelationships," *Journal of Petroleum Engineers*, May 1991, pp 578-590. SPE 19604.
- Baklid, A., Korbol, R., and Owren, G.: "Sleipner Vest CO₂ Disposal, CO₂ Injection into a Shallow Underground Aquifer," SPE Paper 36600 presented at SPE Annual Technical Conference, Denver, Colorado, U.S.A., 6-9 October 1996.
- Benson, S. et al., Carbon Dioxide Reuse and Sequestration: *The State of the Art Today*, Energy 2000 P.Catania (ed.), 2000.
- Clemens, T., Wit, K.: "CO₂ Enhanced Gas Recovery Studied for an Example Gas Reservoir", SPE Paper 77348 presented at SPE Annual technical Conference, San Antonio, Texas, 29 September – 2 October 2002.
- "First Geologic Sequestration Field Test in US Underway in New Mexico," *Techline*, 03/20/03, http://www.netl.doe.gov/publications/press/2003/tl_sequestration_strata1.html, Retrieved 04/13/03.
- Gomez- Nieto, M. and Robinson, D.B.: Comments on: "A New Two-Constant Equation of State," *Ind. Eng. Chem. Fundamentals*, Vol. 18, No. 2, 1979, 197.
- IEA (International Energy Agency), "Carbon Dioxide Utilization," IEA Greenhouse Gas R&D Programme, 1997; Table 6.
- International Energy Agency Greenhouse Gas Program. Sponsored by European Union Commission, 20 countries and multiple companies. Information on www.ieagreen.org.uk
- Inventory of U.S. Greenhouse Gas Emissions and Sinks: 1990-2000, U.S. Environmental Protection Agency, Office of Atmospheric Programs, EPA 430-R-02-003, April, 2002. www.epa.gov/globalwarming/publications/emissions
- Inventory of U.S. Greenhouse Gas Emissions and Sinks: 1990-2000 U.S. EPA, Office of Atmospheric Programs, EPA 430-R-02-003, April 2002. www.epa.gov/globalwarming/publications/emissions
- Mamora, D.D.: "Enhanced Gas Recovery by Carbon Dioxide Sequestration in Depleted Gas Reservoirs", SPE Paper 77347 presented at SPE Annual technical Conference, San Antonio, Texas, 29 September – 2 October 2002.
- Oldenburg C. and Benson S.: "Carbon Sequestration with Enhanced Gas Recovery: Identifying Candidate Sites for Pilot Study," First National Conference on Carbon Sequestration, U.S. Department of Energy, National Energy Technology Lab, Washington D.C., May 15-17 2001.
- Oldenburg, C. and Benson S.: "CO₂ injection for Enhanced gas and Carbon Sequestration," SPE International Petroleum Conference, Villahermosa, Mexico, February 10-12, 2002.
- Olds, R.H., Reamer, H.H., Sage, B.H. and Lacey, W.N.: "Compressibility factors of Hydrocarbon Gas and Carbon dioxide" *Ind. Eng. Chem.*, 41, 475 (1949).

Olds, R.H., Reamer, H.H., Sage, B.H., and Lacey, W.N.: "Phase Equilibria in Hydrocarbon Systems, Methane-Carbon Dioxide System in the Gaseous Region," *Ind. Eng. Chem.*, Vol. 36, No. 1, Jan. 1944, pp 88-90.

Olds, R.H., Reamer, H.H., Sage, B.H., and Lacey, W.N.: "Phase Equilibria in Hydrocarbon Systems, Volumetric Behavior of Methane," *Ind. Eng. Chem.*, Vol. 35, No. 8, August, 1943, pp 922-924.

Ormerod, W.G., Freund, P. and Smith, A., Ocean Storage of Carbon Dioxide, IEA Greenhouse Gas R&D Programme, 2nd Edition, 2002.

Peng, D.Y. and Robinson, D.B.: "A New Two-Constant Equation of State," *Ind. Eng. Chem. Fundamentals*, Vol. 15, 1976, pp 59-64.

Simon, R., Feshmire, C.J., Dicharry, R.M., and Vorhis, F.H.: "Compressibility Factors for CO₂- Methane Mixtures," *JPT*, January 1977, pp 81-85.

Siregar, S., Hagoort, J., and Ronde, H.: Nitrogen Injection vs. Gas Cycling in Rich Retrograde Condensate Gas Reservoirs, SPE Paper 22360 presented at SPE International Meeting, Beijing, China, 24-27 March, 1992.

Soave, G.: "Equilibrium Constants from a Modified Redlich-Kwong Equation of State," *Chem. Eng. Sci.*, Vol. 27, 1972, pp 1197-1203.

Sobers, L.E.: "Phase Behavior of Carbon Dioxide Sequestration in Depleted Gas Reservoirs", M.S. Thesis, Texas Tech U., Lubbock, TX, 2003.

Standing, M.B. and Katz, D. L.: "*Density of Natural Gases*," *Trans. AIME*, Vol. 146, 1942, pp. 140-149.

Stevens, S.H., J.M. Pearce and Rigg A.A.J.: "Natural Analogs for Geologic Storage of CO₂: An Intergrated Global Research Program," First National Conference on Carbon Sequestration, U.S. Department of Energy, National Energy Technology Lab, Washington D.C., May 15-17 2001.

Stevens, S.H., Kuuskraa, V.A., Spector D. and Riemer P.: "CO₂ Sequestration in Deep Coal Seams: Pilot Results and Worldwide Potential," IEA Greenhouse Gas R&D Programme.
<http://www.ieagreen.org.uk/pwrghgt4.htm>, Retrieved on 4/12/03.

Stewart, W. F., Burkhardt, S.F., and Voo, D.: "Prediction of Pseudocritical Parameters for Mixtures," paper presented at the AIChE Meeting, Kansas City, MO, May 18, 1959.

Sutton, R.P.: "Compressibility Factors for High Molecular Weight Reservoir Gases," SPE Paper 14625 presented at 60th SPE Annual Technical Conference and Exhibition, Las Vegas, Sept 22-25, 1985.

Vogel, J.L. and Yarborough, L.: The Effect of Nitrogen on the Phase Behavior and the Physical Properties of Reservoir Fluids, SPE Paper 8815 presented at First Joint SPE/DOE Symposium on Enhanced Oil Recovery, Tulsa, Oklahoma, April 20-23,1980.

UNFCCC: Protocol adopted by the Third Conference of Parties (COP-3) to the United Nations Framework Convention on Climate Change, Kyoto, Japan, December 1997.

Wichert, E. and Aziz, K.: "Calculation of Z's for Sour Gases," *Hydrocarbon Processing*, Vol. 51, No. 5, 1972 pp. 119-122.

2.2.1.10 Publications

Sobers, L., Frailey, S.M. and Lawal, A. S., "Analysis of Pressure/Z-Factor Plots for Sequestering CO₂ in Depleted Gas and Gas Condensate Reservoirs," *Abstract to be submitted to the SPE/DOE 2004 Symposium.*

Sobers, L., Frailey, S.M. and Lawal, A.S., "Enhanced Retrograde Gas Recovery by Carbon Dioxide Storage in Depleted Gas Reservoirs," *Abstract to be submitted to the SPE/DOE 2004 Symposium.*

Frailey, S.M. and Lawal, A. S., "Development and Analysis of Material Balance-Based Reservoir Model for CO₂ Sequestration in Depleted Gas Reservoirs," *Abstract to be submitted to the SPE/DOE 2004 Symposium.*

Adisoemarta, P., Frailey, S.M. and Lawal, A. S., "Experimental Data of CO₂-DryGas/WetGas/Gas Condensates for Sequestering CO₂ in Depleted Gas Reservoirs," *Abstract to be submitted to the SPE/DOE 2004 Symposium.*

Kumar, N., Frailey, S.M. and Lawal, A. S., "Universal Scaling Parameter for Z-Factor Derived from Standing-Katz Chart for Natural and Sour Reservoir Gases," *Abstract to be submitted to the SPE/DOE 2004 Symposium.*

Zou, K., Frailey, S.M. and Lawal, A. S., "A Component-Based Viscosity Equation-of-State for CO₂ and Gas Condensate Reservoirs," *Abstract to be submitted to the SPE/DOE 2004 Symposium.*

Soefajin, A., Frailey, S.M. and Lawal, A. S., "An Equation-of-State Based-Model for Computing Saturated Densities for Mixtures of CO₂-Hydrocarbon Gases," *Abstract to be submitted to the SPE/DOE 2004 Symposium.*

Adisoemarta, P., Frailey, S.M. and Lawal, A. S., "Laboratory Measurement of Compressibility Factors for Carbon Dioxide and Hydrocarbon Gas Mixture," *Abstract to be submitted for the NIweek2004, Worldwide Measurement and Automation, Austin TX*

Frailey, S.M. and Lawal, A. S., *Use of Depleted Gas and Gas Condensate Reservoirs for the Geologic Storage of CO₂*, CAPRS Report /10/03 (in progress).

Adisoemarta, P., Frailey, S.M. and Lawal, A. S., *Laboratory Measurement of Compressibility Factors for Carbon Dioxide and Hydrocarbon Gas Mixtures*, CAPRS Report /11/03 (in progress).

Sobers, L.E.: "Phase Behavior of Carbon Dioxide Sequestration in Depleted Gas Reservoirs", M.S. Thesis, Texas Tech U., Lubbock, TX, 2003.

2.2.1.11 Bibliography

Sobers, L., Frailey, S.M. and Lawal, A. S., "Analysis of Pressure/Z-Factor Plots for Sequestering CO₂ in Alberta Research Council presentation on CO₂ Sequestration, March 18, 2003:

<http://www.ptac.org/res/dl/rest0201p1.pdf>

Baklid, A., Korbol, R., and Owren, G.: "Sleipner West CO₂ Disposal, CO₂ Injection into a Shallow Underground Aquifer," SPE Paper 36600 presented at SPE Annual Technical Conference, Denver, Colorado, U.S.A., 6-9 October 1996.

Burton Corblin Technical Bulletin (BCTB): <http://www.burtoncorblin.com/BCTB302.pdf>

Dranchuk, P.M. and Abou-Kassem, J.H.: "Calculation of Z-Factors for Natural Gases Using Equations of State," *J. Can. Pet. Tech* (July-Sept. 1975) 14, 34-36.

El-Ahmady, M. H. and Wattenbarger, R. A., "Overestimation of Original Gas in Place in Water-Drive Gas Reservoirs Due to a Misleading Linear P/Z Plot," *Jour. Can. Pet. Tech.*, Nov. 2002, 41(11) 38-43.

"First Geologic Sequestration Field Test in US Underway in New Mexico," *Techline*, 03/20/03, http://www.netl.doe.gov/publications/press/2003/tl_sequestration_strata1.html, Retrieved 04/13/03.

Hitchon, B., Gunter, W.D., and Gentzis, T.: "The Serendipitous Association of Sedimentary Basins and Greenhouse Gases", Proceedings of the *Symposium on Capture, Utilization and Disposal of CO₂* at the ACS National Meeting, Orlando, Vol. 41 #4, p.1428-1432 (1996).

Katz, D. L. and M. Rasin Tek, "Overview of Underground Storage of Natural Gas," SPE Paper 9390 presented at the 59th Annual Fall Technical Conference and Exhibition of the Society of Petroleum Engineers of AIME, held in Dallas, Texas, Sept. 21-24, 1980.

Kay, W.B.: "Density of Hydrocarbons Gases and Vapors at High Temperature and Pressure", *Ind. Eng. Chem.*, 28, 1014(1936).

Lawal, A. S., "Prediction of Vapor and Liquid Viscosities From the Lawal-Lake-Silberberg Equation of State", Presented at the SPE/DOE Fifth Symposium, Tulsa, OK, April 20-23, (1986).

Lawal, A. S., Van derLaan, E. T., and Thambynayagam, R. K. M., "Four-Parameter Modification of the Lawal-Lake-Silberberg Equation of State for Calculating Gas-Condensate Phase Equilibria", SPE 14269, Presented at the 60th Annual Technical Conference, Las Vegas, September 22-25, (1985).

Lawal, A. S. and Van derLaan, E. T., "A Partial Molar Fugacity Coefficient Useful for Changing Mixing Rules of Cubic Equations-of-State," *Fluid Phase Equilibria*, 1994, 95, 109.

McCain, W.D., "Chemical Composition Determines Behavior of Reservoir Fluids." *Petroleum Engineer International* (October 1993) 18-25.

McCain, W.D., "Heavy Components Control Reservoir Fluid Behavior." SPE 28214 (1994).

McCain, W., D., *Properties of Petroleum Fluids 2nd Edition*, PennWell Publishing, 1990.

Monnery, W. D., W. Y. Svrcek and Mehrotra, A. K., "Viscosity: A Critical Review of Practical Predictive and Correlative Methods," *Can. Jour. Chem. Eng.*, Feb. 1995, 73, 3-40.

Moses, P.L., "Engineering Applications of Phase Behavior of Crude Oil and Condensate Systems," SPE paper 15835 (1986).

Patel, N. C. and Teja, A. S., "A New Cubic Equation of State For Fluids and Fluid Mixtures", Chemical Engineering Science, 37 (1982) 463-473.

Peng, Ding-Yu, and Robinson, D. B., "A New Two Constant Equation of State", Ind. Eng. Chem. Fundam., 15 (1976) 59-64.

PVT System Model 2370 User's Manual, Ruska Instrument Corporation, March, 1995.

Redlich, O., and Kwong, J. N. S., "On The Thermodynamics of Solutions," Chemical Reviews, 44 (1948) 233.

Rojas, G. and Requena, O.: "A New Method to Estimate Compressibility Factors for CO₂ Hydrocarbon Mixtures," paper SPE 23661 presented at the Second Latin America Petroleum Engineering Conference, Caracas, Venezuela, March 8-11, 1992.

Schmidt, G. and Wenzel, H.: "A Modified van der Waals Type Equation of State," Chem. Eng. Sci. 1980, 135, 1503-1512.

Shaw, J. and Bachu, S., "Screening, Evaluation, and Ranking of Oil Reservoirs Suitable for CO₂-Flood EOR and Carbon Dioxide Sequestration," Jour. Can. Pet. Tech., Sept. 2002, 41(9) 51-61.

Soave, G.: "Equilibrium Constants from a Modified Redlich-Kwong Equation of State," Chem. Eng. Sci. 1972, 27, 1197-1203.

Sources for NIST Database reference Version 7.0: C:\NIST_Technical Databases - Databases Distributed Standard Reference Data Program.htm

Standing, M.B.: "Volumetric and Phase Behavior of Oil Field Hydrocarbon Systems," Society of Petroleum Engineers of AIME. Dallas, Texas. (1977).

Stevens, S.H., Kuuskraa, V.A., Spector D. and Riemer P.: "CO₂ Sequestration in Deep Coal Seams: Pilot Results and Worldwide Potential," IEA Greenhouse Gas R&D Programme.
<http://www.ieagreen.org.uk/pwrghgt4.htm>, Retrieved on 4/12/03.

Stewart, W.F., Burkhardt, S.F., and Voo, D.: "Prediction of Pseudocritical Parameters for Mixtures," paper presented at the AIChE Meeting, Kansas City, MO, May 18, 1959.

Sutton, R.P.: "Compressibility Factors for High Molecular Weight Reservoir Gases," SPE 14265 presented at SPE 60th Annual Technical Conference and Exhibition, Las Vegas, Sept 22-25, 1985.

Clemens, T., Wit, K.: "CO₂ Enhanced Gas Recovery Studied for an Example Gas Reservoir", SPE Paper 77348 presented at SPE Annual technical Conference, San Antonio, Texas, 29 September – 2 October 2002.

Mamora, D.D.: "Enhanced Gas Recovery by Carbon Dioxide Sequestration in Depleted Gas Reservoirs", SPE Paper 77347 presented at SPE Annual technical Conference, San Antonio, Texas, 29 September – 2 October 2002.

Treble, M. A., and Bishnoi, P. R.: "Development of A New Four-Parameter Cubic Equation of State,"
Fluid Phase Equilibria, 1987, 35, 1.

2.2.1.12 List of Acronyms and Abbreviations

α	parameter of LLS EOS
β	parameter of LLS EOS
γ	Fugacity parameter of LLS EOS
f	Fugacity of a component
ϕ	Porosity
v	Molar volume
μ	Viscosity
ω	Acentric factor
Ω_a	Critical constant specified for each EOS
Ω_b	Critical constant specified for each EOS
Ω_w	Critical constant specified for each EOS
a	van der Waal based EOS critical constant
b	van der Waal based EOS critical constant
c	Denotes critical point
d	Coefficient characteristic constant of EOS
e	Coefficient characteristic constant of EOS
i	Index for specified component
j	Index for specified component
\ln	Natural logarithms
h	Thickness (pay zone)
k	Permeability
m	Mixture parameter
n	Number of moles
p	Average reservoir pressure
psia	Pound-forces per square inch
r	Viscosity Constant (in place of Gas Constant)
scf	Standard cubic feet
x	Mole Fraction of individual component
A	Area
A	Dimensionless parameter in EOS
B	Dimensionless parameter in EOS
Bg	Gas formation volume factor
BCTB	Burton Corblin Technical Bulletin
BRS	Black Oil Reservoir Simulation
CCP JIP	Carbon Capture Project Joint Industry Project
CJPT	Canadian Journal of Petroleum Technology
CMG	Computer Modelling Group
CO ₂	Carbon Dioxide
CSP	CO ₂ Sequestration Parameter
CRS	Compositional Reservoir Simulation
CVD	Constant Volume Depletion
DG	Dry Gas
DGR	Depleted Gas Reservoirs
DOE	Department of Energy
ECR	Enhanced Condensate Recovery
ED	Explosive Decompression
EGR	Enhanced Gas Recovery
EOR	Enhanced Oil Recovery
EOS	Equation of state

FPC	Floating Piston Cell
FSP	Final Sequestration Pressure
G	Original or initial gas in-place at discovery of gas reservoir
G_{inj}	Cumulative gas injected
G_p	Cumulative gas produced
GASIS	Gas Information Systems
GEM	Compositional Simulation Commercially available from CMG
HC	Hydrocarbon
IR	Infrared
ISP	Initial Sequestration Pressure
JPSE	Journal of Petroleum Science & Engineering
K_d	Dispersion
LLS	Lawal-Lake-Silberberg equation of state
MBE	Material Balance Equation
MMscf	Millions of standard cubic feet
Mscf	Thousands of standard cubic feet
Mstb	Thousands of stock tank barrels
NIST	National Instituted of Standards and Testing
P	Pressure
PBS	Phase Behavior Simulation
PC	Pump Cell
PR	Peng-Robinson equation of state
PT	Pressure-Temperature
PT	Patel-Teja equation of state
PVT	Pressure-Volume-Temperature
R	Gas Constant
RG	Retrograde Gas
RK	Redlich-Kwong equation of state
S_w	Water Saturation
SCV	Sequestered Carbon Dioxide Volume
SK	Standing-Katz Z-chart
SMV	Sequestration, Monitoring & Verification Team
SP	Scaling parameter for Standing-Katz Z-chart
SPE	Society of Petroleum Engineers
SRK	Soave-Redlich-Kwong equation of state
SW	Schmidt-Wenzel equation of state
T	Temperature
TB	Treble-Bishnoi equation of state
TTU	Texas Tech University
USCV	Ultimate (final) Sequestration Carbon-dioxide Volume
V	Volume
V_B	Reservoir Bulk Volume
V_p	Pore Volume
VLE	Vapor liquid equilibria
WG	Wet Gas
Z	Compressibility Factor (Z – factor)

2.2.1.13 Report Appendices

Appendix A Form of the Lawal-Lake-Silberberg Equation of State

Pure Substance Parameters

$$P = \frac{RT}{n-b} - \frac{a(T)}{n^2 + abn - bb^2} \quad (6)$$

The following four critical constraints are imposed on Equation 6

$$(i) \left(\frac{\partial P}{\partial n} \right)_{T=T_c, P=P_c, n=n_c} = 0,$$

$$(ii) \left(\frac{\partial^2 P}{\partial n^2} \right)_{T=T_c, P=P_c, n=n_c} = 0 \quad (7)$$

$$(iii) f(P_c, v_c, T_c) = 0,$$

$$(iv) b/v_c = \Omega_w$$

By applying Eq. 7 to Eq. 6, the parameters (a, b, α , β) are established as

$$a = \Omega_a \frac{R^2 T_c^2}{P_c} = [1 + (\Omega_w - 1)Z_c]^3 \frac{R^2 T_c^2}{P_c} \quad (8)$$

$$a(T) = a g(T_R, w)$$

$$b = \Omega_b \frac{RT_c}{P_c} = [\Omega_w Z_c] \frac{RT_c}{P_c} \quad (9)$$

$$a = \frac{1 + (\Omega_w - 3)Z_c}{\Omega_w Z_c} \quad (10)$$

$$b = \frac{Z_c^2 (\Omega_w - 1)^3 + 2\Omega_w^2 Z_c + \Omega_w (1 - 3Z_c)}{\Omega_w^2 Z_c} \quad (11)$$

In Eqs. 8-11, P_c , Z_c , and T_c are pure substance critical constants and Ω_w is the vdW limiting volume. The value of Ω_w has been established for pure substances through the equality.

The **Z-form** of Equation 6 is expressed for pure substances as follows:

$$Z^3 - [1 + (1-a)B]Z^2 + [A - aB - (b+a)B^2]Z - [AB - b(B^2 + B^3)] = 0 \quad (12)$$

Similarly, the v -form of Equation 6 is expressed for pure substances as follows:

$$v^3 - \left(b - ab + \frac{RT}{P} \right) v^2 + \left[\frac{a}{P} - ab \frac{RT}{P} - (a + b)b^2 \right] v - \left[\frac{ab}{P} - \left(b^3 + b^2 \frac{RT}{P} \right) b \right] = 0 \quad (13)$$

Mixture Parameters for the LLS EOS

$$P = \frac{RT}{n - b_m} - \frac{a_m}{n^2 + a_m b_m n - b_m b_m^2} \quad (14)$$

where

$$a_m = \sum_i^n \sum_j^n x_i x_j a_i(T)^{1/2} a_j(T)^{1/2} a_{ij} \quad (15)$$

$$b_m = \left(\sum_i^n x_i b_i^{1/3} \right)^3 \quad (16)$$

$$a_m = \sum_i^n \sum_j^n x_i x_j a_i^{1/2} a_j^{1/2} a_{ij} \quad (17)$$

$$b_m = \sum_i^n \sum_j^n x_i x_j b_i^{1/2} b_j^{1/2} b_{ij} \quad (18)$$

The Z -form of Equation 14 is expressed for mixture as follows:

$$Z^3 - [1 + (1 - a_m)B]Z^2 + [A - a_m B - (b_m + a_m)B^2]Z - [AB - b_m(B^2 + B^3)] = 0$$

Similarly, the v -form of Equation 14 is expressed for mixture as follows:

$$v^3 - \left(b_m - a_m b_m + \frac{RT}{P} \right) v^2 + \left[\frac{a_m}{P} - a_m b_m \frac{RT}{P} - (a_m + b_m)b_m^2 \right] v - \left[\frac{a_m b_m}{P} - \left(b_m^3 + b_m^2 \frac{RT}{P} \right) b_m \right] = 0$$

Fugacity Equation for the Lawal-Lake-Silberberg EOS

Component Fugacity Equation

By applying the thermodynamic relationship to Equation 6,

$$\ln\left(\frac{f}{P}\right) = \int_{P^*}^P (Z-1) \frac{dP}{P}$$

a generalized fugacity coefficient for pure substance is shown for cubic equations-of-state by the following expression for the fugacity coefficient of a pure component:

$$\ln\left(\frac{f_i}{P}\right) = (Z-1) - \ln(Z-B) - Q \quad (\text{A.9})$$

where

$$Q = \left\{ \frac{A}{B(\mathbf{a}^2 + 4\mathbf{b})^{0.5}} \right\} \ln \left[\frac{Z + \left\{ \mathbf{a} + (\mathbf{a}^2 + 4\mathbf{b})^{0.5} \right\} \frac{B}{2}}{Z + \left\{ \mathbf{a} - (\mathbf{a}^2 + 4\mathbf{b})^{0.5} \right\} \frac{B}{2}} \right] \quad (\text{A.10})$$

The fugacity coefficient of component *i* in a mixture can be calculated for Equation 14 from the following relationship (Lawal-van der Laan, FPE, 1994)

$$\ln\left(\frac{f}{x_i P}\right) = \int_{P^*}^P (\bar{Z}-1) \frac{dP}{P}$$

The resulting fugacity coefficient of component *i* in a mixture can be expressed as:

$$\ln\left(\frac{f_i}{x_i P}\right) = (Z-1) \left\{ 3[b_i/b_m]^{1/3} - 2 \right\} - \ln(Z-B) - Q \left\{ 2 \sum_k \frac{x_k a_{ik}}{a_m} - 3[b_i/b_m]^{1/3} + 2 \right\} + \{S(G+1) - WHB\} + 2(SG - WHB) \left\{ \sum_k \frac{x_k \mathbf{a}_{ik}}{\mathbf{a}_m} \right\} - (SK + WHB) \left\{ \sum_k \frac{x_k \mathbf{b}_{ik}}{\mathbf{b}_m} \right\} \quad (\text{A.11})$$

In Equation A.11, $a_{ik} = a_i^{1/2} a_k^{1/2} \mathbf{k}_{ik}$, $\mathbf{a}_{ik} = \mathbf{a}_i^{1/2} \mathbf{a}_k^{1/2} \mathbf{l}_{ik}$, $\mathbf{b}_{ik} = \mathbf{b}_i^{1/2} \mathbf{b}_k^{1/2} \mathbf{x}_{ik}$ and the interaction terms are represented by \mathbf{k}_{ik} , \mathbf{l}_{ik} (or \mathbf{a}_{ij} in Equation A.4), and \mathbf{x}_{ik} (or \mathbf{b}_{ij} in Equation A.5). The mixture parameters used in A.11 are defined by

$$Q = \left\{ \frac{A}{B(\mathbf{a}_m^2 + 4\mathbf{b}_m)^{0.5}} \right\} \ln \left[\frac{Z + \left\{ \mathbf{a}_m + (\mathbf{a}_m^2 + 4\mathbf{b}_m)^{0.5} \right\} \frac{B}{2}}{Z + \left\{ \mathbf{a}_m - (\mathbf{a}_m^2 + 4\mathbf{b}_m)^{0.5} \right\} \frac{B}{2}} \right] \quad (\text{A.12})$$

$$S = \left\{ \frac{Z}{Z-B} - Z - Q \right\} \quad (\text{A.13})$$

$$S(G+1) = \left\{ \frac{Z}{Z-B} - Z - Q \right\} \left[\frac{2(\mathbf{a}_m^2 + 2\mathbf{b}_m)}{\mathbf{a}_m^2 + 4\mathbf{b}_m} \right] \quad (\text{A.14})$$

$$SG = \left\{ \frac{Z}{Z-B} - Z - Q \right\} \left[\frac{\mathbf{a}_m^2}{\mathbf{a}_m^2 + 4\mathbf{b}_m} \right] \quad (\text{A.15})$$

$$SK = \left\{ \frac{Z}{Z-B} - Z - Q \right\} \left[\frac{4\mathbf{b}_m}{\mathbf{a}_m^2 + 4\mathbf{b}_m} \right] \quad (\text{A.16})$$

$$WHB = \left\{ \frac{B}{Z-B} - B \right\} \left[\frac{2\mathbf{a}_m \mathbf{b}_m}{\mathbf{a}_m^2 + 4\mathbf{b}_m} \right] \quad (\text{A.17})$$

The mixture combining rules used in Equations A.11 have been previously defined in Equations 15-18.

Table A.1 - Common Specialization Cubic Equation of State

Authors	Year	Coefficients of the Quadratic		
		α	β	$\alpha + \beta$
Two -Constant Equations :				
van der Waals	1873	0	0	0
Dieterici	1898	0	0	0
Berthelot	1990	0	0	0
Redlich – Kwong	1949	1	0	1
Peng – Robinson	1976	2	- 1	1
Harmens	1977	3	- 2	1
Zakharov	1977	c	0	c
Three -Constant Equations:				
Clausius	1881	$2c/b$	$- c^2/b^2$	1 (c = b)
Martins	1979	2	$- t^2/b^2$	1 (t = b)
Schmidt – Wenzel	1980	$1 + 3\omega$	$- 3\omega$	1
Harmens – Knapp	1980	c	$- (c - 1)$	1
Heyen	1981	$(b + e)/b$	$- e/b$	1
Joffe – Martins	1981	$2c/b$	$- c^2/b^2$	1 (c = b)
Patel – Teja	1982	$(b + c)/b$	$- c/b$	1
Kubic – Martins	1982	$2c/b$	$- c^2/b^2$	1 (c = b)
Yu – Lu	1987	$3 + \omega$	$- \omega$	3
Yu – Lu – Iwai	1987	$(3b + c)/b$	$- c/b$	3 (c = b)
Guo – Du	1989	$2c/b$	$- c/b$	1 (c = b)
Four -Constant Equations:				
Himpan – Danes – Gaena	1979	$2d/b$	$- (d^2 + c)/b^2$	1 (c = 0, d = b)
Lawal – Lake – Silberberg	1983	α	$- \beta$	$\alpha - \beta$
Adachi – Lu	1983	$b_2 (b_2 + b_3)/b^2$	$- b_2 b_3/b^2$	1 (b ₂ = b ₃ = b)
Trebble – Bishnoi	1987	$(b + c)/b$	$- (bc - d^2)/b^2$	1 (c = b, d = 0)

Appendix B
Framework of Viscosity Equation of State

Pure Substance Parameters

$$T = \frac{rP}{\mathbf{m} - b(T)} - \frac{a(T, P)}{\mathbf{m}^2 + ab(T)\mathbf{m} - b[b(T)]^2} \quad (19)$$

The following four critical constraints are imposed on Equation 6

$$\begin{aligned} \text{(i)} \quad & \left(\frac{\partial T}{\partial \mathbf{m}} \right)_{T=T_c, P=P_c} = 0, \\ \text{(ii)} \quad & \left(\frac{\partial^2 T}{\partial \mathbf{m}^2} \right)_{T=T_c, P=P_c} = 0 \quad (20) \\ \text{(iii)} \quad & f(T_c, \mu_c, P_c) = 0, \\ \text{(iv)} \quad & b/\mu_c = \Omega_w \end{aligned}$$

By applying Eq. 19 to Eq. 20, the parameters (a, b, α , β) are established as

$$\begin{aligned} r &= \Omega_r \frac{T_c \mathbf{m}_c}{P_c} = \frac{1}{Z_c} \frac{T_c \mathbf{m}_c}{P_c} \\ a &= \Omega_a \frac{r^2 P_c^2}{T_c} = [1 + (\Omega_w - 1)Z_c]^3 \frac{r^2 P_c^2}{T_c} \quad (21) \end{aligned}$$

$$a(T, P) = \mathbf{a} \mathbf{j} (P_R T_R, \mathbf{w})$$

$$b = \Omega_b \frac{rP_c}{T_c} = [\Omega_w Z_c] \frac{rP_c}{T_c} \quad (22)$$

$$\mathbf{a} = \frac{1 + (\Omega_w - 3)Z_c}{\Omega_w Z_c} \quad (23)$$

$$\mathbf{b} = \frac{Z_c^2 (\Omega_w - 1)^3 + 2\Omega_w^2 Z_c + \Omega_w (1 - 3Z_c)}{\Omega_w^2 Z_c} \quad (24)$$

In Eqs. 8-11, P_c , Z_c , and T_c are pure substance critical constants and Ω_w is the vdW limiting volume. The value of Ω_w is the same as in LLS EOS.

Similarly, the **m-form** of Equation 19 is expressed for pure substances as follows:

$$\begin{aligned} \mathbf{m}^3 - \left(b - \mathbf{a}b + \frac{rP}{T} \right) \mathbf{m}^2 + \left[\frac{a}{T} - \mathbf{a}b \frac{rP}{T} - (\mathbf{a} + \mathbf{b})b^2 \right] \mathbf{m} \\ - \left[\frac{ab}{T} - \left(b^3 + b^2 \frac{rP}{T} \right) \mathbf{b} \right] = 0 \end{aligned} \quad (25)$$

Mixture Parameters for the LLS EOS

$$T = \frac{r_m P}{\mathbf{m} - b_m} - \frac{a_m}{\mathbf{m}^2 + \mathbf{a}_m b_m \mathbf{m} - b_m b_m^2} \quad (26)$$

where

$$r_m = \left(\sum_i^n x_i r_i^{1/3} \right)^3$$

$$a_m = \sum_i^n \sum_j^n x_i x_j a(T)_i^{1/2} a(T)_j^{1/2} a_{ij} \quad (27)$$

$$b_m = \left(\sum_i^n x_i b_i^{1/3} \right)^3 \quad (28)$$

$$\mathbf{a}_m = \sum_i^n \sum_j^n x_i x_j \mathbf{a}_i^{1/2} \mathbf{a}_j^{1/2} \mathbf{a}_{ij} \quad (29)$$

$$\mathbf{b}_m = \sum_i^n \sum_j^n x_i x_j \mathbf{b}_i^{1/2} \mathbf{b}_j^{1/2} \mathbf{b}_{ij} \quad (30)$$

Similarly, the **m-form** of Equation 26 is expressed for mixture as follows:

$$\begin{aligned} \mathbf{m}^3 - \left(b_m - \mathbf{a}_m b_m + \frac{rP}{T} \right) \mathbf{m}^2 + \left[\frac{a_m}{T} - \mathbf{a}_m b_m \frac{rP}{T} - (\mathbf{a}_m + \mathbf{b}_m) b_m^2 \right] \mathbf{m} \\ - \left[\frac{a_m b_m}{T} - \left(b_m^3 + b_m^2 \frac{rP}{T} \right) \mathbf{b}_m \right] = 0 \end{aligned}$$

Appendix C

Universal Scaling Parameter for Z-Factor Derived from Standing-Katz Z-Chart

$$R = \frac{P_c v_c}{Z_c T_c} \quad (1)$$

Real Gas Law states that

$$Pv = ZRT \quad (2)$$

By dividing Eq. 2 by Eq. 1, we have

$$P_R v_R = \frac{Z}{Z_c} T_R \quad (3)$$

At fluid critical point, $P_R = T_R = v_R = 1$, then Eq. 3 becomes

$$\left(\frac{Z}{Z_c} \right) = 1 \quad (4)$$

If we have two Z-charts that can be individually represented by $Z = f(P_R, v_R, T_R)$, then

$$\left(\frac{Z}{Z_c} \right)_1 = \left(\frac{Z}{Z_c} \right)_2 \quad (5)$$

If the left hand side of Eq. 5 is for Standing-Katz Z-factor, the Universal Scaling Parameter can be developed as

$$\left(\frac{Z^{SK}}{Z_{SP}} \right)_{Pr, Tr} = \left(\frac{Z}{Z_c} \right)_{Pr, Tr} \quad (6)$$

where

Z^{SK} = Z-factor derived from Standing-Katz Chart

Z_{SP} = Universal Scaling Parameter for Standing-Katz Chart

Z_c = Critical Compressibility Factor

Z = Compressibility Factor at specified P_R and T_R

The Z-factor derived from Eq. 6 can be expressed as

$$Z = Z_c \left(\frac{Z^{SK}}{Z_{SP}} \right)_{Pr, Tr} \quad (7)$$

Developing of Universal Scaling Parameter, Z_{SP} is detailed elsewhere, but some comment will suffice.

2.2.3 Reservoir Simulation of CO₂ Storage

Report Title

CO₂ Capture Project - An Integrated, Collaborative Technology Development Project for Next Generation CO₂ Separation, Capture and Geologic Sequestration

Reservoir Simulation of CO₂ Storage

Report Reference

2.2.3

Type of Report:	Semi-Annual Report
Reporting Period Start Date:	February 2003
Reporting Period End Date:	July 2003
Principal Author(s):	Gary A. Pope, Kamy Sepehrnoori, Steven L. Bryant, Larry W. Lake
Date Report was issued:	July 2003
DOE Award Number:	DE-FC26-01NT41145
Submitting Organization:	The University of Texas at Austin
Address:	Petroleum and Geosystems Engineering 1 University Station C0300 Austin, TX 78712-0228

Disclaimer

This report was prepared as an account of work sponsored by an agency of the United States Government. Neither the United States Government nor any agency thereof, nor any of their employees, makes any warranty, express or implied, or assumes any legal liability or responsibility for the accuracy, completeness or usefulness of any information, apparatus, product, or process disclosed, or represents that its use would not infringe privately owned rights. Reference herein to any specific commercial product, process, or service by trade name, trademark, manufacturer, or otherwise does not necessarily constitute or imply its endorsement, recommendation, or favoring by the United States Government or any agency thereof. The views and opinions of authors expressed herein do not necessarily state or reflect those of the United States Government or any agency thereof.

2.2.3.1 Abstract

The general goal of this proposed research is to use a compositional reservoir simulator to better understand and quantify the chemical and physical phenomena associated with the sequestration of CO₂ in aquifers. More particularly, we want to quantitatively assess two key features of the process: the effect of brine density increases due to dissolved CO₂, and the effect of geochemical reactions. The former might be exploited to store significant quantities of CO₂ within the aqueous phase, avoiding problems with escape of CO₂ in the gas phase. The latter offers the possibility of an additional sink for CO₂ via mineralization. The storage of CO₂ in residual gas has emerged during the first phase of this project as a potentially very significant issue meriting further study. This is a scoping study intended to improve estimates of the possible magnitudes of these CO₂ sinks by considering the mass transfer under realistic physical conditions. The latter conditions include movement of the CO₂-rich gas phase and dissolved CO₂ plume after injection is halted and the consequent mixing of brines of widely varying CO₂ concentrations. Ultimately we will explore the feasibility of storing *all* of the injected CO₂ in immobile forms.

2.2.3.2 Table of Contents

2.2.3.1 Abstract	868
2.2.3.2 Table of Contents	869
2.2.3.3 List(s) of Graphical Materials	870
2.2.3.4 Introduction	871
2.2.3.5 Executive Summary	872
2.2.3.6 Experimental	873
2.2.3.7 Results and Discussion	873
2.2.3.8 Conclusion	883
2.2.3.9 References	884

2.2.3.3 List(s) of Graphical Materials

- Figure 1. Effect of brine salinity on CO₂ solubility in aqueous phase at 140 °F. 874
- Figure 2. Effect of CO₂ on brine density at 50 C (122 °F) and 5830 psi. 875
- Figure 3. Schematic of aquifer and well locations. 877
- Figure 4. Water-gas relative permeability curves. 877
- Figure 5. Gas saturation at 10 years (vertical slice through the injection well in X-Z direction). 878
- Figure 6. Gas saturation at 1000 years (vertical slice through the injection well in X-Z direction). 878
- Figure 7. Aqueous phase density in lb /cu ft at 1000 years (vertical slice through the injection well in X-Z direction). 879
- Figure 8. Effect of permeability on the distribution of CO₂ between phases at 1000 years.879
- Figure 9. Effect of vertical to horizontal permeability ratio on the distribution of CO₂ between phases at 1000 years. 880
- Figure 10. Effect of residual gas saturation on the distribution of CO₂ between phases at 1000 years. 880
- Figure 11. Effect of salinity on the distribution of CO₂ between phases at 1000 years. 881
- Figure 12. Effect of temperature on the distribution of CO₂ between phases at 1000 years. 881

2.2.3.4 Introduction

This is a scoping study involving modeling and simulation of a prototypic CO_2 sequestration project in a deep saline aquifer. There are three tasks. Task I is to establish a base case against which the potential for additional storage will be measured. This work will build on previous reservoir simulation studies at the University of Texas at Austin (Vikas, 2002). Task II is to quantify the effect of the CO_2 on brine density and its implications for CO_2 storage in the aqueous phase as a function of aquifer geology, heterogeneity, temperature, pressure, salinity, etc. The idea is to explore ways to reduce the risk of CO_2 escape from the aquifer due to highly uncertain geological pathways by storing the CO_2 in a dense phase with little potential for upward migration. Task III will be to determine a representative subset of the possible geochemical reactions. This simplified chemistry will then be coupled to the multiphase flow compositional simulations to estimate the capacity for mineralization as a function of amount and distribution of the minerals in the aquifer.

Both the UTCOMP simulator and CMG's GEM simulator will be used in this study. CO_2 solubility, brine density and brine viscosity models have been calibrated against experimental data as a function of salinity, temperature and pressure. Base case simulations will be conducted for aquifer storage times of 1000 years. Because the goal is to determine feasibility of CO_2 storage in liquid (aqueous phase) and solid (mineralization) forms, we will assume an injection stream of pure CO_2 for the base case. However, both simulators are compositional simulators and mixtures can be studied later as time and interest permit.

The principal geochemical driver accompanying sequestration is the acidification of the brine resulting from dissociation of dissolved CO_2 . Low pH brine in turn induces a wide range of reactions with host minerals in the formation. An obvious example is the dissolution of carbonate cements. Other reactions are analogous to weathering, in which the acid extracts cations from aluminosilicates (feldspars, clays, etc.). On the one hand these reactions buffer the acidification, but on the other the released cations may form relatively insoluble carbonate precipitates such as siderite. The competition between these reactions will determine the potential for additional storage, and the balance is likely to be time dependent as the approach to equilibrium will involve transport time scales (convection, dispersion/diffusion) as well as the kinetics (interphase mass transfer, dissolution, precipitation).

It is imperative to solve the geochemistry simultaneously with the flow and transport equations described above. Brine acidification requires mass transfer from the CO_2 -rich gas phase to the aqueous phase, and contact between these phases has been shown to be a complicated function of time depending on the aquifer heterogeneity, especially after CO_2 injection ceases and buoyancy forces can substantially rearrange the fluid distribution. The latter period will involve the mixing of very different brine compositions, ranging from isolated volumes of residual aqueous phase saturated with CO_2 to original formation brine. We will conduct two- and three-dimensional simulations with fully coupled reactive flow and transport in a wide variety of heterogeneous aquifers both to better understand and predict behavior and to determine whether simpler models (e.g. one-dimensional flow of saturated brine or time evolution of batch chemistry) can adequately represent the net additional CO_2 storage capacity. Some reactive minerals may be distributed in the aquifer in thin layers or otherwise heterogeneous in such a way as to make very fine grid simulations necessary. In extreme cases, some upscaling of the reactive transport may be necessary.

2.2.3.5 Executive Summary

The first phase of a numerical simulation study of geological sequestration of CO₂ in deep, saline aquifers has been completed. A compositional simulator was used for this study after tuning the Peng-Robinson equation-of-state to fit available experimental data on the solubility of CO₂ in brine and the density of brine as a function of CO₂ concentration in the brine, brine salinity, temperature and pressure. The first task of this project was to establish a base case simulation. Because this is a generic study of CO₂ sequestration in deep, saline aquifers rather than the study of a specific aquifer, the goal was to select representative characteristics for the aquifer that would serve our purpose of understanding the potential for CO₂ storage in immobile forms with little or no tendency to escape from the aquifer. There are of course many arbitrary decisions involved setting up such a base case model. However, we are also doing a sensitivity study where many of the most important parameters are being varied over a wide range. Nevertheless, the base case is very important and a great deal of thought and discussion went into it including discussions with geologists with the Bureau of Economic Geology at the University of Texas at Austin. Parameter selection was based in part on our experience with the preliminary study completed by Vikas (2002). As part of task 2 in progress, simulations of CO₂ storage for 1000 years were done to study the impact of several of the most important parameters on the process. The parameters studied to date are mean aquifer permeability, the ratio of vertical to horizontal permeability, residual gas saturation, salinity and temperature. A simple layered permeability model was used for the base case simulation, but future studies will include more complex and realistic heterogeneity descriptions. The most significant conclusion to emerge from the first phase of this study is that the effect of residual gas on CO₂ storage can be very large and has the potential to significantly impact the strategy used to sequester CO₂ in deep, saline aquifers. Therefore, its magnitude and variation merit much more careful study. This form of immobile storage may actually turn out to be more significant than storage in brine and minerals. The concerns about CO₂ escape pathways would certainly be reduced if all or almost all of the CO₂ were to be stored in the form of trapped gas, dense brine and minerals. During the next phase (task 3) of the study, mineralization will be included in the simulations. The goal will be to develop the best strategy for storing all or almost all of the CO₂ in immobile forms so that its escape from the aquifer is unlikely and not as sensitive to possible geological escape pathways as it would be if stored in a mobile gas form. Well placement and completion obviously will play a key role in this strategy and preliminary simulations have already been done that appear very encouraging that this is a viable strategy at least under some conditions.

2.2.3.6 Experimental

Not applicable.

2.2.3.7 Results and Discussion

The first task of this project was to establish a base case simulation. Because this is a generic study of CO₂ sequestration in deep, saline aquifers rather than the study of a specific aquifer, the goal was to select representative characteristics for the aquifer that would serve our purpose of understanding the potential for CO₂ storage in immobile forms with little or no tendency to escape from the aquifer. There are of course many arbitrary decisions involved setting up such a base case model. However, we are also doing a sensitivity study where many of the most important parameters are being varied over a wide range. Nevertheless, the base case is very important and a great deal of thought and discussion went into it including discussions with geologists with the Bureau of Economic Geology at the University of Texas at Austin. Parameter selection was based in part on our experience with the preliminary study completed by Vikas (2002).

The calibration of the fluid property models with experimental data is a very important first step in establishing the input to the simulator. The properties include the solubility of CO₂ in brine, the brine density and the brine viscosity. All of these depend on temperature, pressure and salinity. The brine density and viscosity also depend on the CO₂ concentration. An extensive literature search was made to find the best sources of experimental data. These data were then used to systematically tune the Peng-Robinson equation-of-state for CO₂ solubility and density and the Pedersen correlation for brine viscosity. Flash calculations are done in the compositional simulator each time step to calculate the phase behavior of the CO₂ and H₂O mixtures in each grid block as well as the density of both the gas and aqueous phases. The binary interaction parameter between the CO₂ and H₂O was adjusted to fit the CO₂ solubility data and the volume shift parameter for H₂O was adjusted to fit the aqueous phase density. The computed curves for CO₂ solubility as a function of salinity and pressure are shown in Fig. 1 along with a few experimental data points. Similar plots were made at temperatures ranging from 20 to 100 °C. A linear correlation of the binary interaction coefficient with temperature and salinity was developed based upon the solubility data from 20 to 100 °C and from 0 to 350,000 ppm salinity (NaCl).

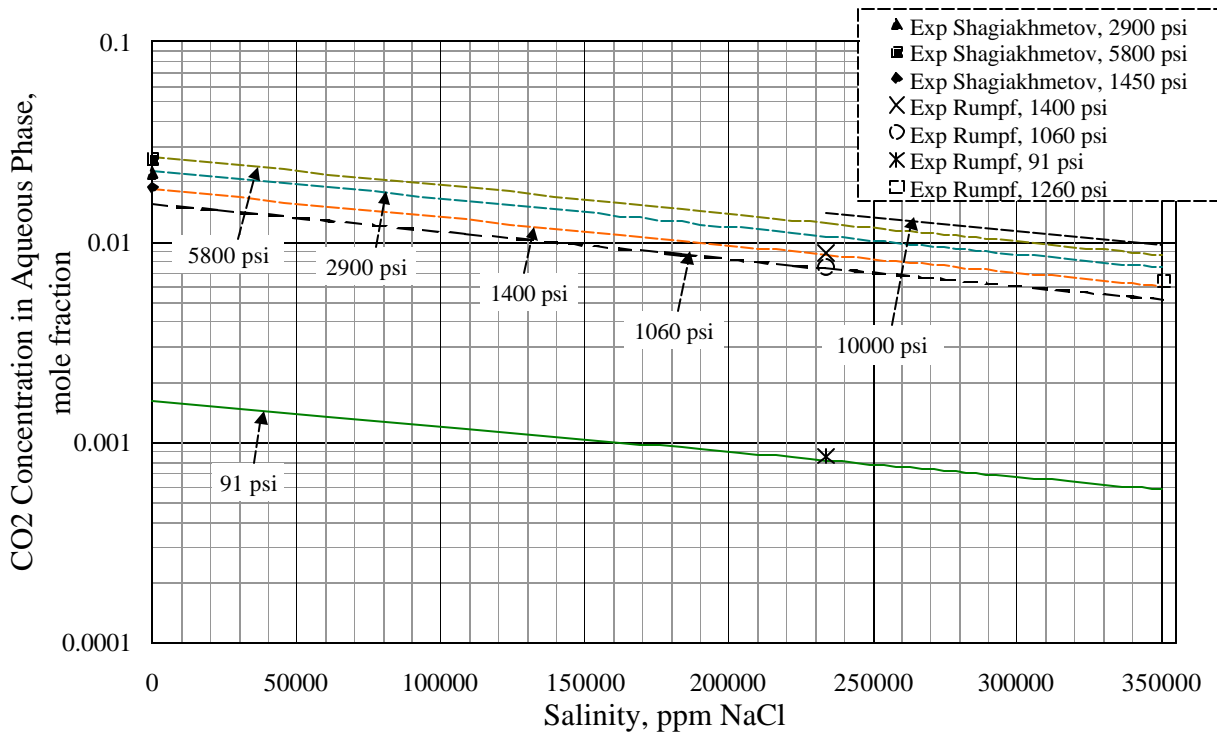


Figure 1. Effect of brine salinity on CO₂ solubility in aqueous phase at 140 °F.

Solubility data for CO₂ in brine are readily available from Rumpf *et al.* (1994), Shagiakhmetov *et al.* (1982) and Teng *et al.* (1998). These sources were preferred over others as they give similar trends over a wide range of temperature and salinity (Table 1).

Table 1. Experimental Data for CO ₂ -Solubility in Brine			
Source	Temperature Range, °F	Pressure Range, psia	Salinity Range, ppm
Rumpf <i>et al.</i>	104-319	100-1400	230,000-350,000
Shagiakhmetov <i>et al.</i>	120-302	1450-5800	0
Teng <i>et al.</i>	40-69	930-4280	0-31,000

Density data for pure water was taken from Wagner *et al.* (2002). This source was preferred over others because it is based on the IAPWS-95 formulation adopted by International Association for the Properties of Water and Steam (IAPWS). Density data for pure brine have been taken from Simonson *et al.* (1994) for a wide range of temperature (77- 477 °F), pressure (1030-5830 psi) and salinity (30,000-300,000 ppm of NaCl). Unfortunately, there are very few experimental data in the temperature and pressure range of interest for the density of brine saturated with CO₂. Parkinson *et al.* (1969) give density values for CO₂-H₂O mixtures for pressures less than 500 psia and temperatures less than 105 °F. Teng *et al.* (1998) give density values of CO₂-brine mixtures for temperatures less than 68 °F. Data from Hnedkovsky *et al.* (1996) was used to verify density trends. Data from Nighswander *et al.* (1989) was not used because it shows a reverse trend for the variation of brine density upon CO₂ dissolution.

Those data that could be found were used to develop a correlation for the volume shift parameter of H₂O used in the Peng-Robinson EOS over the same range of temperature and salinity. Figure 2 shows an example of the predicted density of both brine and brine saturated with CO₂ as a function of salinity at 50 °C (122 °F) and 5830 psia. The density of brine saturated with CO₂ is greater than brine without CO₂ and this is of course favorable for CO₂ sequestration. However, the differences are very small and uncertain and decrease as salinity increases.

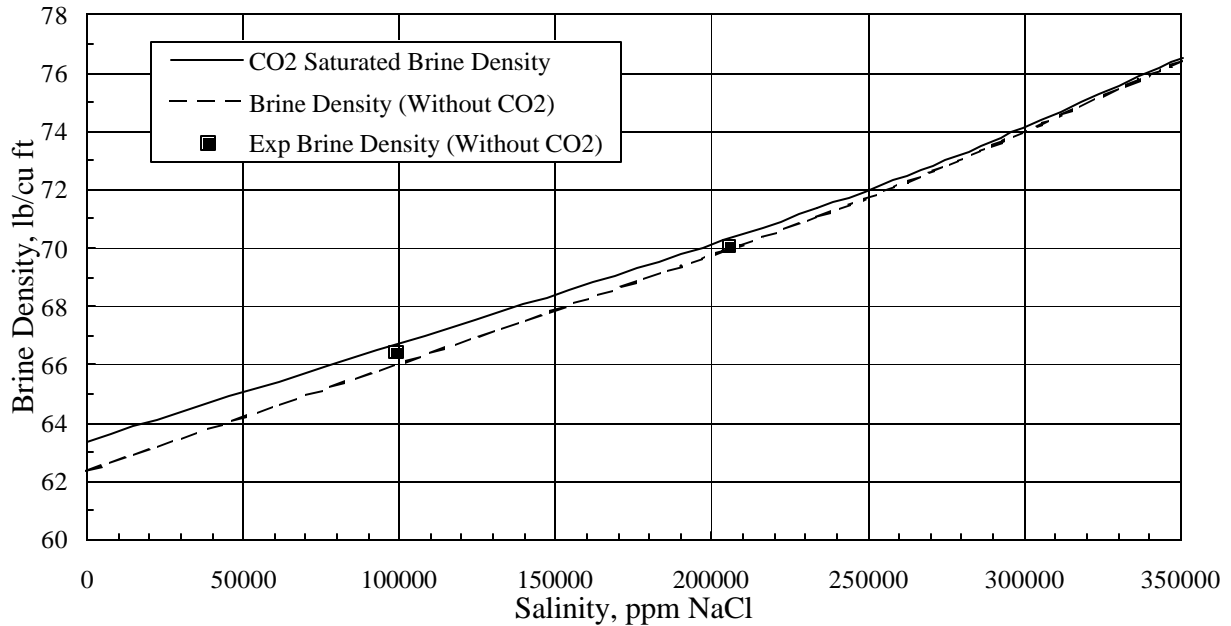


Figure 2. Effect of CO₂ on brine density at 50 C (122 °F) and 5830 psi.

The input parameters for the base case simulation are summarized in Table 2. Pure CO₂ is injected in a well into the aquifer for the first ten years. The total simulation time is 1000 years. The simulation domain is 53,000 ft long, 53,000 wide and 1000 ft thick. Constant pressure wells are used along all boundaries and the injection well is in the center of the aquifer as shown in Fig. 3. The relative permeability curves are shown in Fig. 4. Figure 5 shows the gas injection profile at 10 years for a vertical X-Z cross-section through the injection well and Fig. 6 shows the same profile after 1000 years. These simulations were done with CMG's GEM simulator.

Table 2. Simulation Input for Base Case

<i>Aquifer Properties</i>		
Length, ft	53000	
Width, ft	53000	
Thickness, ft	1000	
Depth at top of formation at injection well, ft	5300	
Temperature, °F	140	
Initial Pressure, psia	2265	
Dip, degree	1	
Salinity, ppm	100000	
Dykstra-Parsons Coefficient	0.7	
Horizontal to vertical permeability ratio	0.001	
Mean Permeability, md	100	
Horizontal Permeabilities of Each Layer*, md		
Layers 1-4	89	
Layers 5-8	65	
Layers 9-12	46	
Layers 13-16	30	
Layers 17-20	15	
Layers 21-24	120	
Layers 25-28	165	
Layers 29-32	235	
Layers 33-36	840	
Layers 37-40	370	
Porosity	0.25	
Residual Water Saturation	0.25	
Residual Gas Saturation	0.25	
Gas End Point Relative Permeability	1.0	
Water End Point Relative Permeability	0.334	
Grid	40×40×40	
Maximum injection pressure (psia)	3300	
Maximum injection rate (MMSCF/D)	50	
<i>Description of Components</i>		
<u>Component</u>	<u>CO₂</u>	<u>H₂O</u>
Critical Press. (psi)	1070.0	3200.11
Critical Temp. (°R)	547.43	1164.77
Critical Vol. (cu ft/lb-mole)	1.5076	0.8962
Molecular Wt. (lb/lb-mole)	44.01	18.015
Accentric Factor	0.22394	0.344
Parachor	78.0	52

*Layer 1 is the top layer.

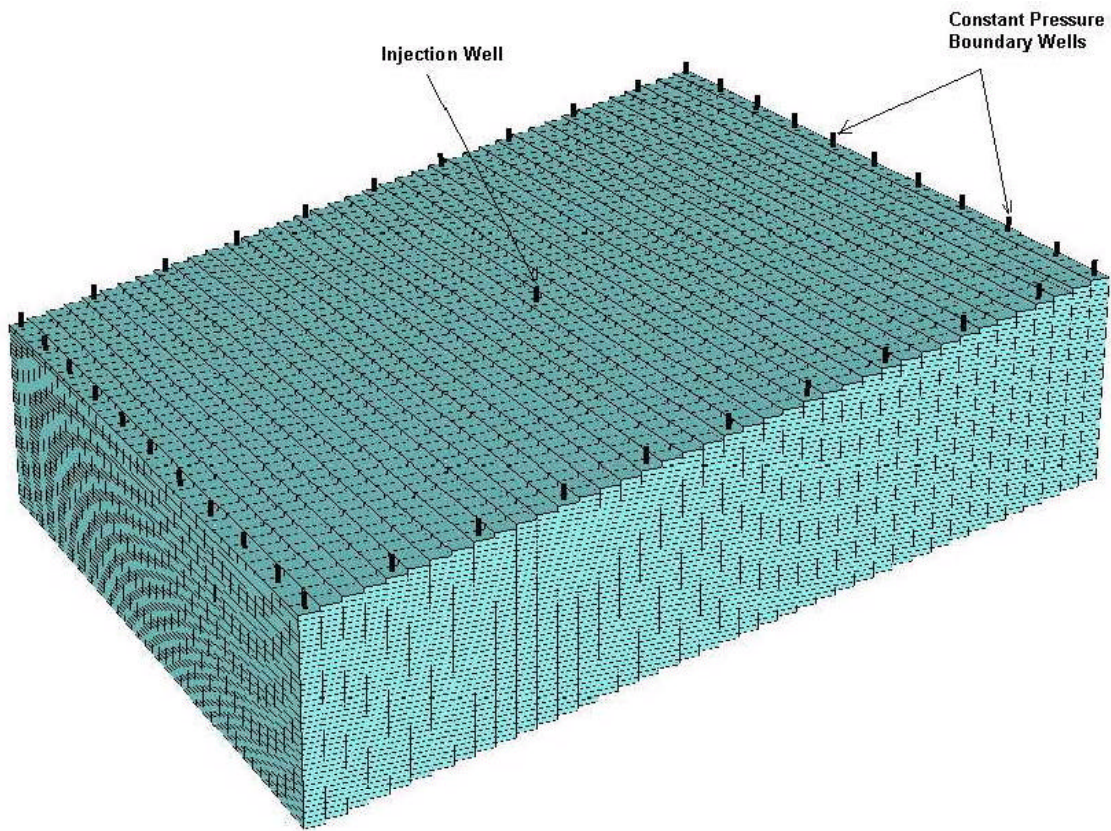


Figure 3. Schematic of aquifer and well locations.

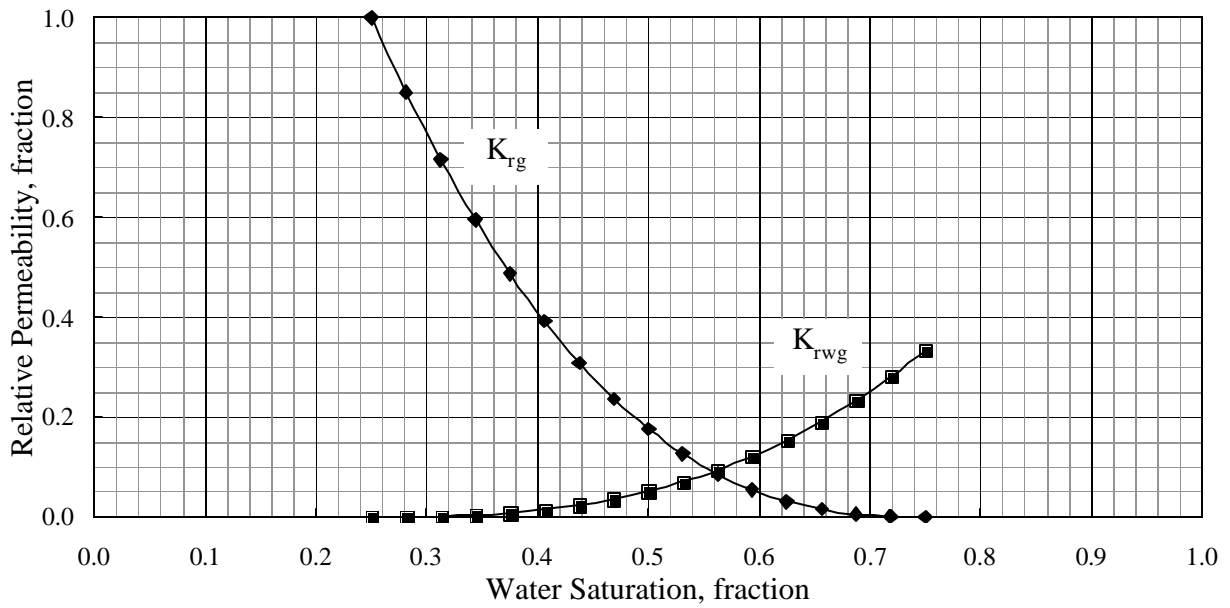


Figure 4. Water-gas relative permeability curves.

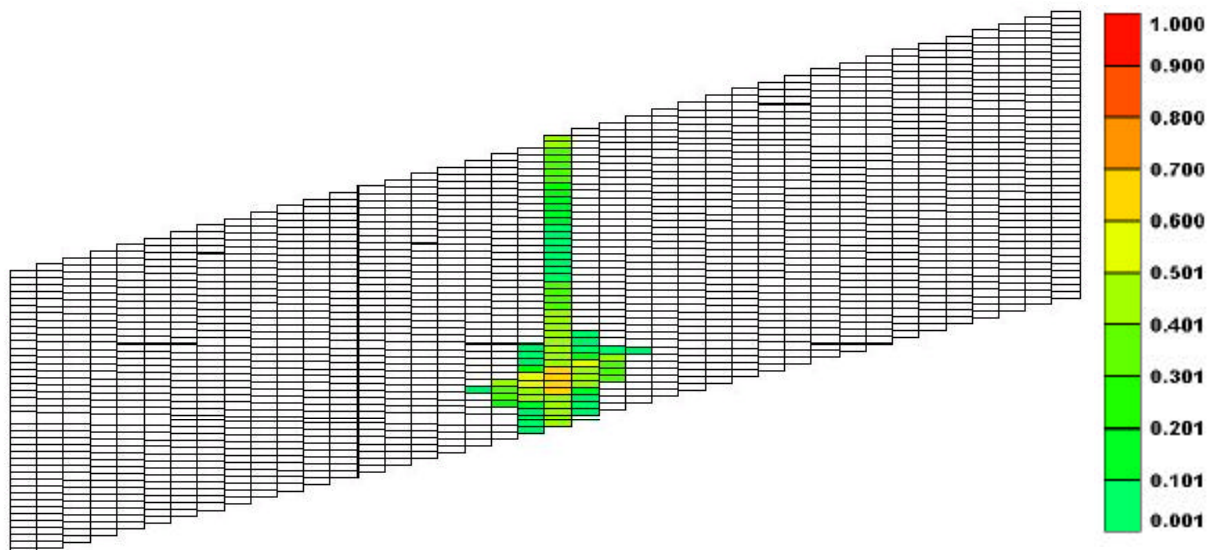


Figure 5. Gas saturation at 10 years (vertical slice through the injection well in X-Z direction).

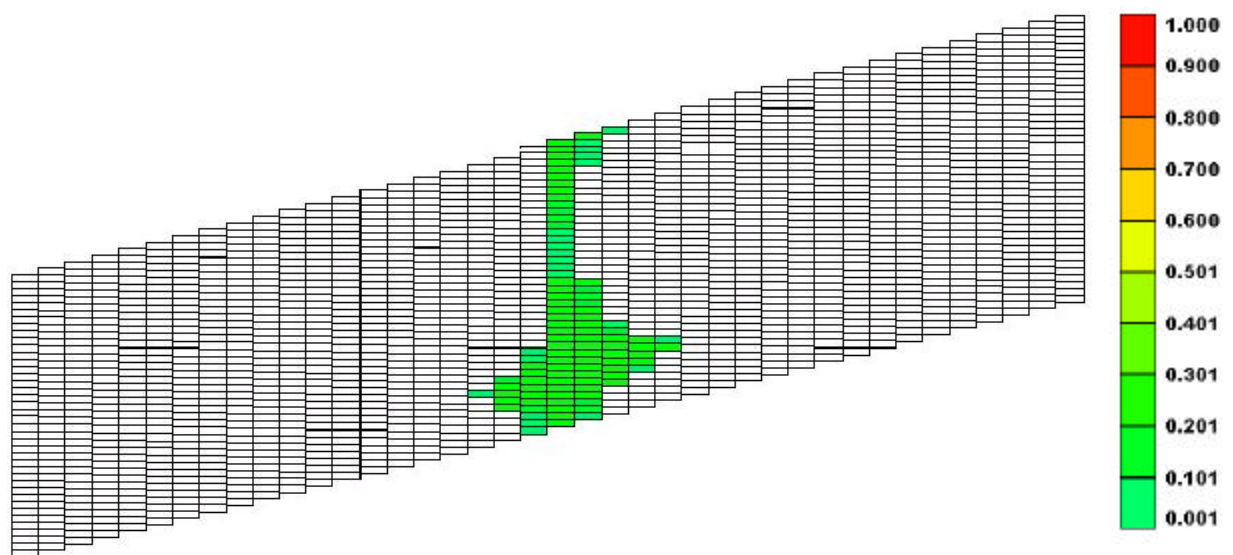


Figure 6. Gas saturation at 1000 years (vertical slice through the injection well in X-Z direction).

Figure 7 shows the aqueous phase density after 1000 years for this same vertical cross-section of the aquifer.

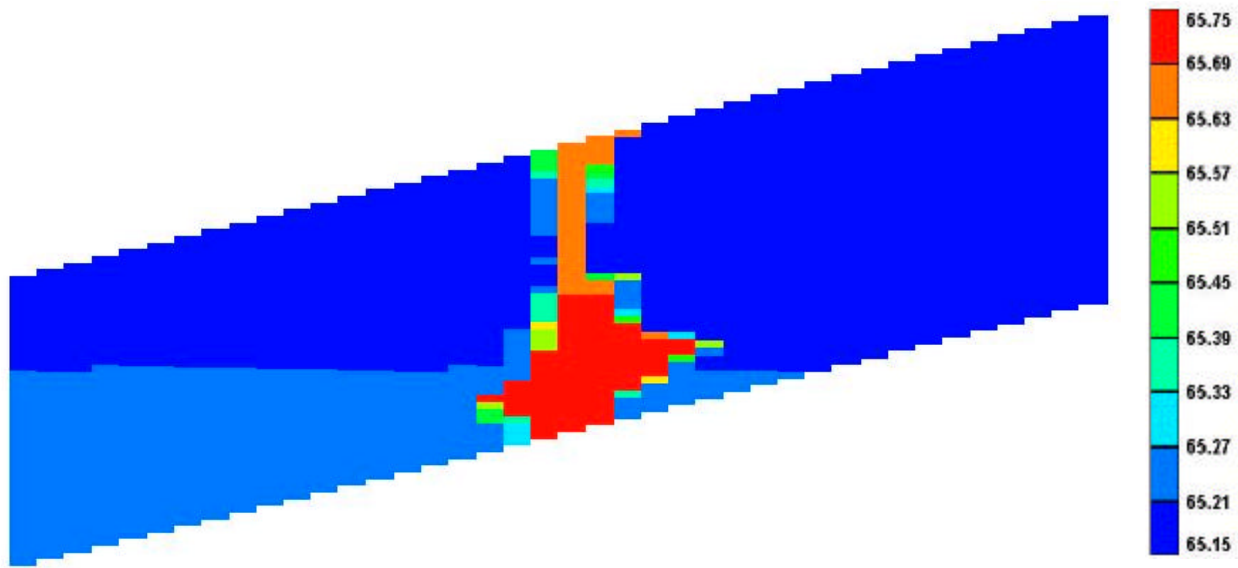


Figure 7. Aqueous phase density in lb/cu ft at 1000 years (vertical slice through the injection well in X-Z direction).

Task 2 of the project is in progress. A large number of simulations to study the effect of the most important parameters affecting CO₂ sequestration in the aquifer have already been completed. These parameters include permeability, the ratio of vertical to horizontal permeability, residual gas saturation, salinity, and temperature. The trends with these parameters are shown in Figs. 8 through 12.

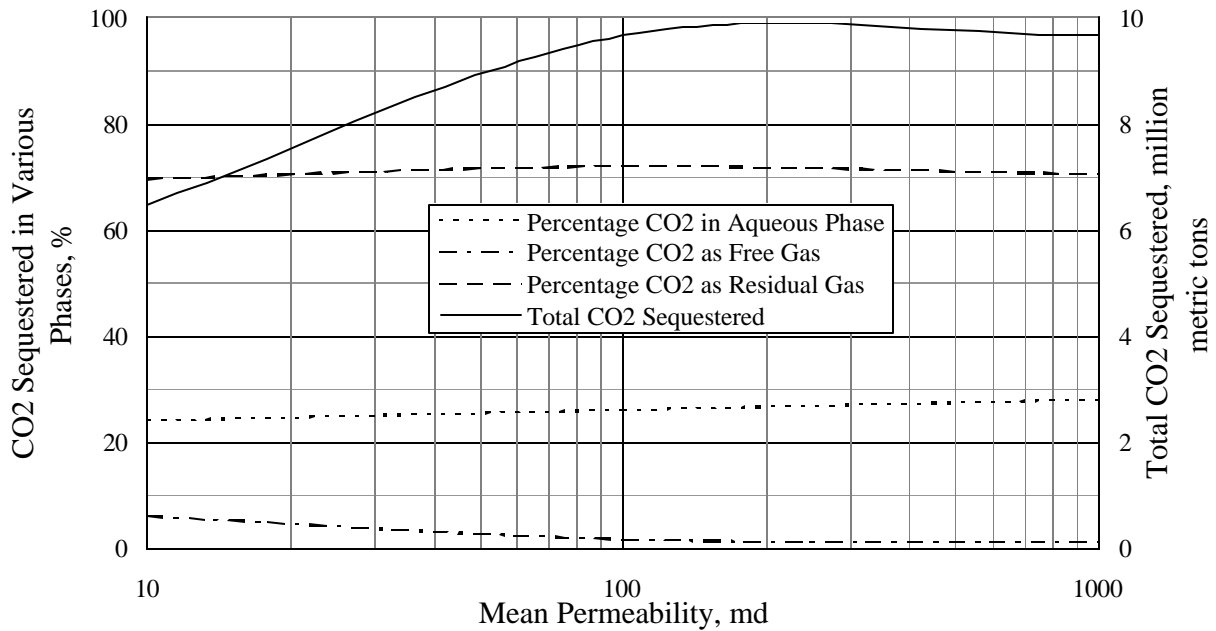


Figure 8. Effect of permeability on the distribution of CO₂ between phases at 1000 years.

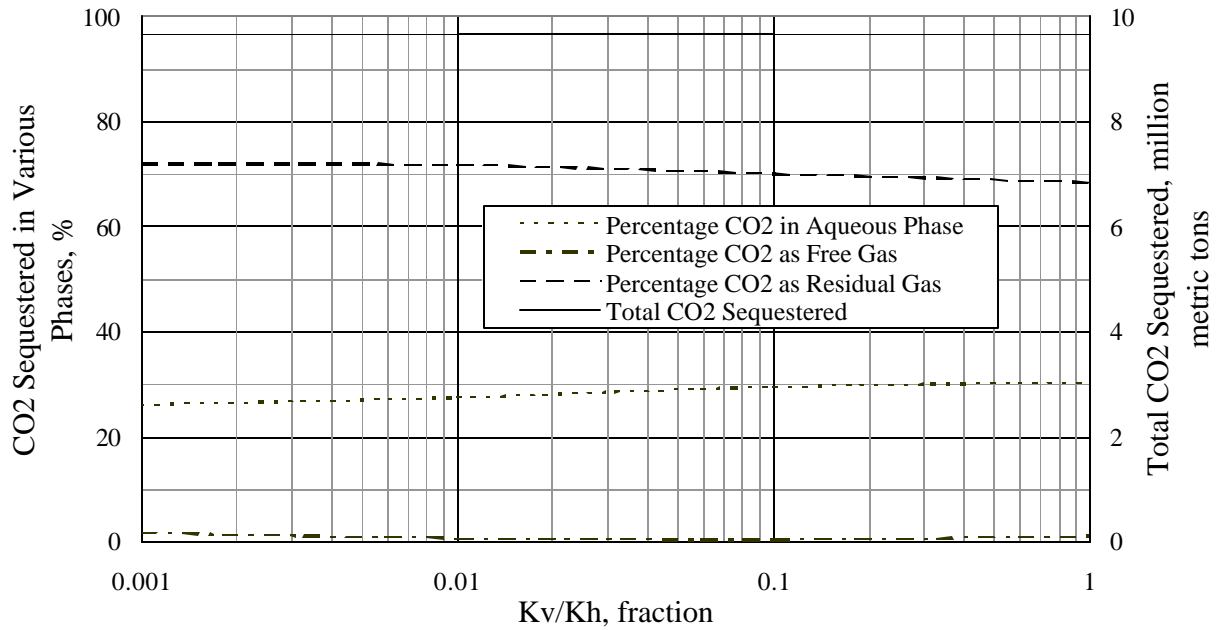


Figure 9. Effect of vertical to horizontal permeability ratio on the distribution of CO₂ between phases at 1000 years.

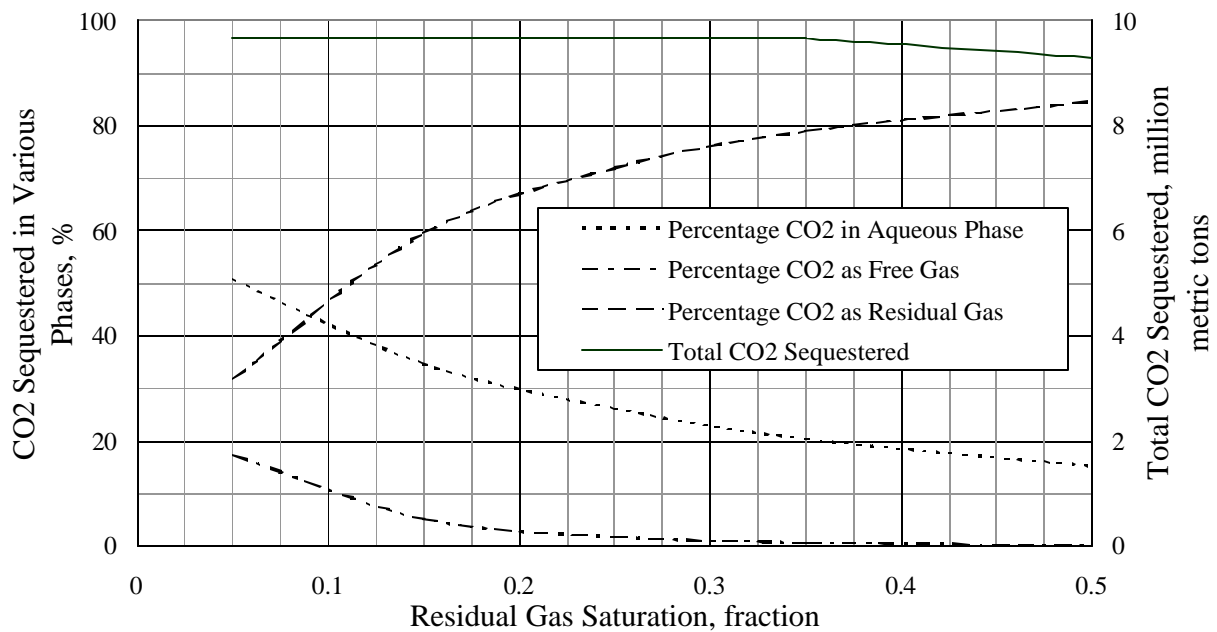


Figure 10. Effect of residual gas saturation on the distribution of CO₂ between phases at 1000 years.

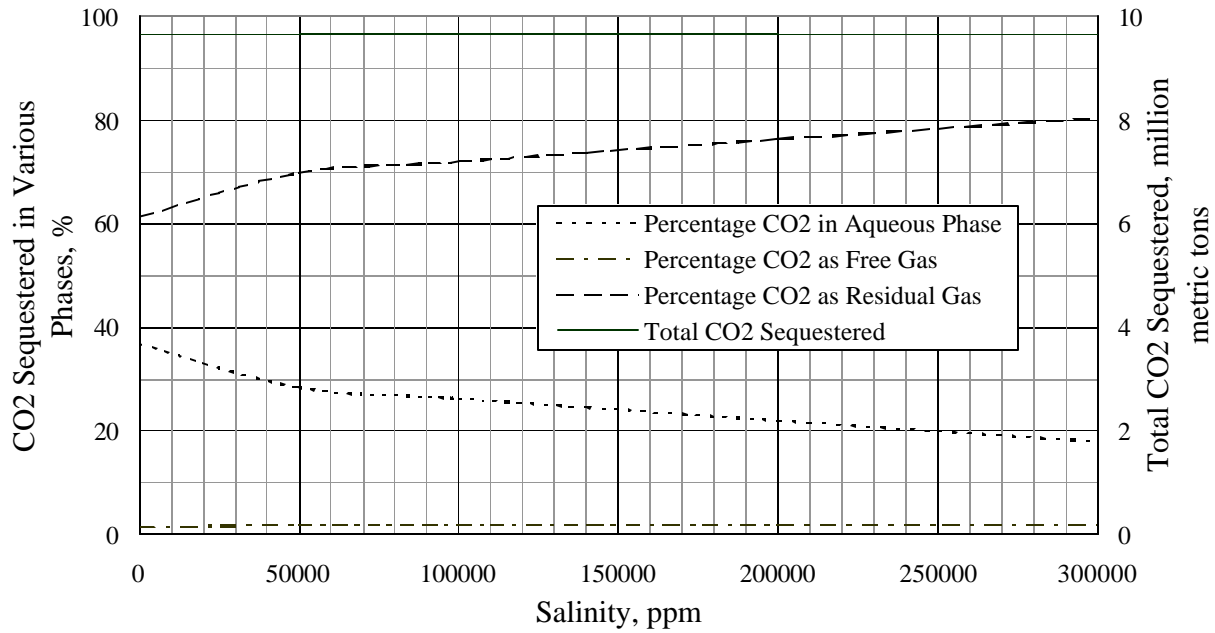


Figure 11. Effect of salinity on the distribution of CO₂ between phases at 1000 years.

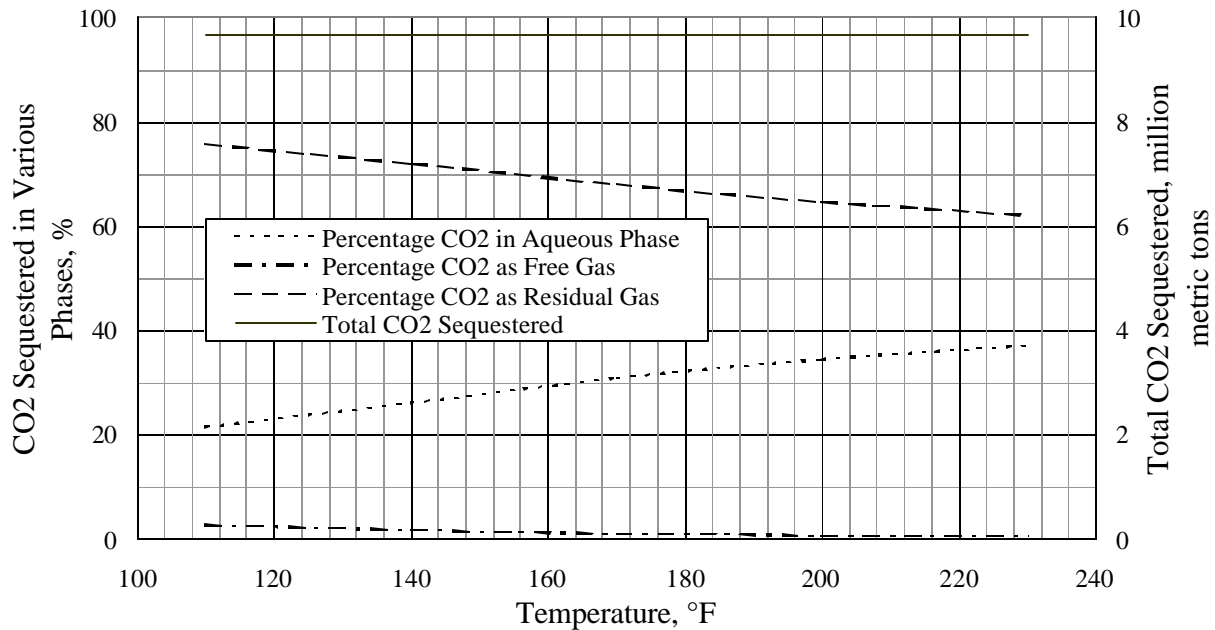


Figure 12. Effect of temperature on the distribution of CO₂ between phases at 1000 years.

Each of these plots show the percentage of the total CO₂ stored as dissolved CO₂ in the brine, stored as free gas and stored as trapped gas. The most interesting observation from these plots is that only a few percent of the total CO₂ is stored in free gas. Almost all of the CO₂ is in residual gas, which means it is immobile. The residual gas saturation for the base case is 0.25. This is a typical value of residual gas saturation for moderate porosity and permeability sandstones under conditions where high gas saturation has been displaced by water. It is close to the trend line shown in Fig. 7 of the recent paper by Holtz (2002). Residual gas saturation is a petrophysical property that depends upon rock type. The fraction of CO₂ sequestered as residual (trapped) gas in Figs. 8-12 clearly illustrates the importance of knowing the value of residual gas saturation. Earlier simulations conducted in this study underline this point. For example, if the value of residual gas saturation is 0.05, the ultimate mode of storage depends strongly

upon the fate of *mobile* CO₂ phase after injection ceases. Because this parameter now appears to be one of the most important parameters affecting CO₂ storage in aquifers, it merits much more careful study. These preliminary simulations did not include hysteresis in the relative permeability curves. We plan to study the effect of hysteresis and make the residual gas saturation a function of the rock properties along the line suggested by Holtz and others.

2.2.3.8 Conclusion

The most significant conclusion to emerge from the first phase of this study is that the effect of residual gas on CO₂ storage can be very large and has the potential to significantly impact the strategy used to sequester CO₂ in deep, saline aquifers. Therefore, its magnitude and variation merit much more careful study. This form of immobile storage may actually turn out to be more significant than storage in brine and minerals. The concerns about CO₂ escape pathways would certainly be reduced if all or almost all of the CO₂ were to be stored in the form of trapped gas, dense brine and minerals. Well placement and completions will obviously play a key role in any strategy focused on immobile storage of the CO₂ and will be included as parameters in the next phase of this study.

2.2.3.9 References

- Firoozabadi, A., Nutakki, R., Wong, T.W., and Aziz, K., "EOS Predictions of Compressibility and Phase Behavior in Systems Containing Water, Hydrocarbons, and CO₂", SPE Reservoir Engineering, SPE 15674, Vol 3, No. 2, May 1988.
- Garcia, J. E., "Density of aqueous solutions of CO₂", Lawrence Berkeley National Laboratory, report LBNL-49023, October 2001.
- Hnedkovský, L., Wood, R. H., and Majer, V., "Volumes of aqueous solutions of CH₄, CO₂, H₂S and NH₃ at temperatures from 298.15 K to 705 K and pressures to 35 Mpa", Journal of Chemical Thermodynamics, Vol 28, pp 125-142, 1996.
- Holtz, H. M., "Residual Gas Saturation to Aquifer Influx: A Calculation Method for 3-D Computer Reservoir Model Construction", paper SPE 75502 presented at SPE Gas Technology Symposium, April–May 2002.
- Nighswander, J. A., Kalogerakis, N. and Mehrotra, A. K., " Solubilities of carbon dioxide in water and 1 wt. % sodium chloride solution at pressures up to 10 MPa and temperatures from 80 to 200 °C", Journal of Chemical & Engineering Data, Vol 34, pp 355-360, 1989.
- Parkinson, W. and Nevers, N. D., "Partial molal volume of carbon dioxide in water solutions", Industrial and Engineering Chemistry Fundamentals, Vol. 8, No. 4, pp 709-713, 1969.
- Rumpf, B., Nicolaisen, H., Ocal, C. and Maurer, G.(1993). "Solubility of Carbon Dioxide in Aqueous Solutions of Sodium Chloride: Experimental Results and Correlation", Journal of Solution Chemistry, Vol. 23, No.3, pp 431-438, 1994.
- Scharlin, P., "Carbon Dioxide in Water and Aqueous Electrolyte Solutions", volume 62 of Solubility Data Series. Oxford University Press, International Union of Pure and Applied Chemistry, Oxford, UK, 1996.
- Shagiakhmetov, R. A., and Tarzimanov, A. A., (1981), SPSTL 200 KHPD 81, 1982.
- Simonson, J. M., Oakes, C. S. and Bodnar, R. J., "Densities of NaCl(aq) to the temperature 523 K at pressures to 40 MPa measured with a new vibrating-tube densitometer", Journal of Chemical Thermodynamics, Vol 26, pp 345-359, 1994.
- Spycher, N., Pruess, K., Ennis-King, J., "CO₂-H₂O Mixtures in the Geological Sequestration of CO₂. I. Assessment and Calculation of Mutual Solubilities from 12 to 100 °C and up to 600 bar", Lawrence Berkeley National Laboratory, report LBNL- 50991, July 2002.
- Steam Tables, Springer-Verlag, Third Edition, 1990.
- Teng, H. and Yamasaki, A., "Solubility of Liquid CO₂ in Synthetic Sea Water at Temperatures from 278 K to 293 K and Pressures from 6.44 MPa to 29.49 MPa, and Densities of the Corresponding Aqueous Solutions", Journal of chemical & engineering data, Vol 43, pp 2-5, 1998.
- Teng, H., Yamasaki, A., Chun, M. K. and Lee, H., "Solubility of liquid CO₂ in water at temperatures from 278 K to 293 K and pressures from 6.44 MPa to 29.49 MPa and densities of the corresponding aqueous", Journal of chemical & engineering data, Vol 29, pp 1301-1310, 1997.
- Vikas, "Simulation of CO₂ sequestration", MS thesis, University of Texas at Austin, 2002.

2.2.4 CO₂ Impurities Tradeoff - Surface

Report Title

CO₂ Capture Project - An Integrated, Collaborative Technology Development Project for Next Generation CO₂ Separation, Capture and Geologic Sequestration

CO₂ Impurities Tradeoff - Surface

Report Reference

2.2.4

Type of Report:	Semi-Annual Report
Reporting Period Start Date:	February 2003
Reporting Period End Date:	July 2003
Principal Author(s):	Bruce Sass and Neeraj Gupta
Date Report was issued:	July 2003
DOE Award Number:	DE-FC26-01NT41145
Submitting Organization:	Battelle Memorial Institute
Address:	505 King Ave Columbus Ohio 43201

Disclaimer

This report was prepared as an account of work sponsored by an agency of the United States Government. Neither the United States Government nor any agency thereof, nor any of their employees, makes any warranty, express or implied, or assumes any legal liability or responsibility for the accuracy, completeness or usefulness of any information, apparatus, product, or process disclosed, or represents that its use would not infringe privately owned rights. Reference herein to any specific commercial product, process, or service by trade name, trademark, manufacturer, or otherwise does not necessarily constitute or imply its endorsement, recommendation, or favoring by the United States Government or any agency thereof. The views and opinions of authors expressed herein do not necessarily state or reflect those of the United States Government or any agency thereof.

2.2.4.1 Abstract

CCP has recently selected Battelle to undertake a preliminary assessment of the effects of impurities in the CO₂ streams on the aboveground processing equipment. The study will focus on SO_x and NO_x impurities and will primarily be based on an assessment of existing literature. The project was awarded in late July and the work is planned to be completed by September 15, 2003. The three main components of the work will include:

- Impact of impurities on the performance of selected amines
- Review the literature on compressed gases to determine the corrosivity of various pipeline and coating materials for various partial pressures of SO_x and NO_x species with moisture present
- Evaluate the phase behavior of multi-component gas mixtures on multi-stage compressors

2.2.4.2 Table of Contents

2.2.4.1 Abstract.....	887
2.2.4.2 Table of Contents	888
2.2.4.4 Introduction	889
2.2.4.5 Executive Summary.....	890
2.2.4.6 Experimental.....	891
2.2.4.7 Results and Discussion.....	892
2.2.4.8 Conclusion	893
2.2.4.9 References.....	893

2.2.4.4 Introduction

Gas impurities, such as SO_x and NO_x, have the potential of interacting unfavorably with aboveground processes. Absorption and regeneration characteristics of amine and other solvents used to separate CO₂ may be affected adversely by acid gas impurities. Aboveground processing equipment is subject to corrosion by acids formed from SO_x and NO_x species in the presence of water. Also, compression of gas mixtures is subject to condensation of the higher boiling constituents, which may limit the ability to achieve adequate interstage cooling and may damage the compressor. These issues will be evaluated under the following three activities:

- Investigate the effects of SO_x and NO_x on a few selected amines that are commonly used by the separation industry. Battelle will make recommendations on the maximum levels of SO_x and NO_x impurities in an amine separation plant. This information may be useful as a guideline for preventing unacceptable levels of heat stable salts from forming during regeneration and thus requiring costly solvent make-up. Also, it will illustrate the potential need for pre-cleaning steps to remove these impurities to minimum levels prior to CO₂ separation.
- Review the literature on compressed gases to determine the corrosivity of various pipeline and coating materials for various partial pressures of SO_x and NO_x species with moisture present. This data collection will result in recommendations for maximum concentrations of impurities to prevent unacceptable rates of corrosion.
- Evaluate the phase behavior of multi-component gas mixtures on multi-stage compressors. This research is needed because large compressors require temperature control for materials safety and to allow removal of condensed water. However, interstage cooling must be controlled to prevent temperature drops that could permit a two-phase region (e.g. liquid + gas). This problem arises, for example, due to the sizable difference in the critical temperature of CO₂ (31 °C) and SO₂ (158 °C).

In keeping with the preliminary nature of this work, most of the research will be limited to compilation of information in existing literature. Preliminary calculations may be performed. However, a detailed technical assessment or predictive modeling is beyond the scope of current task

2.2.4.5 Executive Summary

CCP has recently selected Battelle to undertake a preliminary assessment of the effects of impurities in the CO₂ streams on the aboveground processing equipment. The study will focus on SO_x and NO_x impurities and will primarily be based on an assessment of existing literature. The project was awarded in late July and the work is planned to be completed by September 15, 2003.

Gas impurities, such as SO_x and NO_x, have the potential of interacting unfavorably with aboveground processes. Absorption and regeneration characteristics of amine and other solvents used to separate CO₂ may be affected adversely by acid gas impurities. Aboveground processing equipment is subject to corrosion by acids formed from SO_x and NO_x species in the presence of water. Also, compression of gas mixtures is subject to condensation of the higher boiling constituents, which may limit the ability to achieve adequate interstage cooling and may damage the compressor. These issues will be evaluated under the following three activities:

- Investigate the effects of SO_x and NO_x on a few selected amines that are commonly used by the separation industry. Battelle will make recommendations on the maximum levels of SO_x and NO_x impurities in an amine separation plant. This information may be useful as a guideline for preventing unacceptable levels of heat stable salts from forming during regeneration and thus requiring costly solvent make-up. Also, it will illustrate the potential need for pre-cleaning steps to remove these impurities to minimum levels prior to CO₂ separation.
- Review the literature on compressed gases to determine the corrosivity of various pipeline and coating materials for various partial pressures of SO_x and NO_x species with moisture present. This data collection will result in recommendations for maximum concentrations of impurities to prevent unacceptable rates of corrosion.
- Evaluate the phase behavior of multi-component gas mixtures on multi-stage compressors. This research is needed because large compressors require temperature control for materials safety and to allow removal of condensed water. However, interstage cooling must be controlled to prevent temperature drops that could permit a two-phase region (e.g. liquid + gas). This problem arises, for example, due to the sizable difference in the critical temperature of CO₂ (31 °C) and SO₂ (158 °C).

In keeping with the preliminary nature of this work, most of the research will be limited to compilation of information in existing literature. Preliminary calculations may be performed. However, a detailed technical assessment or predictive modeling is beyond the scope of current task

2.2.4.6 Experimental

No experimental or laboratory studies are planned under this task. All of the work will be based on literature assessment of the potential implications of SO_x/NO_x impurities in the CO₂ streams for the aboveground processing equipment. Only simple calculations will be performed if needed.

Battelle proposes evaluate these issues under the following three activities:

- Battelle will investigate the effects of SO_x and NO_x on a few selected amines that are commonly used by the separation industry. Battelle will make recommendations on the maximum levels of SO_x and NO_x impurities in an amine separation plant. This information may be useful as a guideline for preventing unacceptable levels of heat stable salts from forming during regeneration and thus requiring costly solvent make-up. Also, it will illustrate the potential need for pre-cleaning steps to remove these impurities to minimum levels prior to CO₂ separation.
- Battelle will review the literature on compressed gases to determine the corrosivity of various pipeline and coating materials for various partial pressures of SO_x and NO_x species with moisture present. This data collection will result in recommendations for maximum concentrations of impurities to prevent unacceptable rates of corrosion.
- Battelle will evaluate the phase behavior of multi-component gas mixtures on multi-stage compressors. This research is needed because large compressors require temperature control for materials safety and to allow removal of condensed water. However, interstage cooling must be controlled to prevent temperature drops that could permit a two-phase region (e.g. liquid + gas). This problem arises, for example, due to the sizable difference in the critical temperature of CO₂ (31 °C) and SO₂ (158 °C).

In keeping with the preliminary nature of this work, most of the research will be limited to compilation of information in existing literature. Preliminary calculations may be performed. However, a detailed technical assessment or predictive modeling is beyond the scope of current proposal.

2.2.4.7 Results and Discussion

No results are available at this time. The project is starting at the end of July and the initial results should be available by early September.

2.2.4.8 Conclusion

This task addresses the effects of impurities in CO₂ streams on aboveground processing equipment. Gas impurities, such as SO_x and NO_x, have the potential of interacting unfavorably with aboveground processes. Absorption and regeneration characteristics of amine and other solvents used to separate CO₂ may be affected adversely by acid gas impurities. Aboveground processing equipment is subject to corrosion by acids formed from SO_x and NO_x species in the presence of water. Also, compression of gas mixtures is subject to condensation of the higher boiling constituents, which may limit the ability to achieve adequate interstage cooling and may damage the compressor.

2.2.4.9 References

No references cited.

2.2.5 CO2 Impurities Tradeoff - Sub Surface

Report Title

CO₂ Capture Project - An Integrated, Collaborative Technology Development Project for Next Generation CO₂ Separation, Capture and Geologic Sequestration

CO₂ Impurities Tradeoff - Sub Surface

Report Reference

2.2.5

Type of Report: Semi-Annual Report

Reporting Period Start Date: February 2003

Reporting Period End Date: July 2003

Principal Author(s): Steven L. Bryant and Larry W. Lake

Date Report was issued: August 2003

DOE Award Number: DE-FC26-01NT41145

Submitting Organization: The University of Texas at Austin

Address: Petroleum and Geosystems Engineering
1 University Station C0300
Austin, TX 78712-0228

Disclaimer

This report was prepared as an account of work sponsored by an agency of the United States Government. Neither the United States Government nor any agency thereof, nor any of their employees, makes any warranty, express or implied, or assumes any legal liability or responsibility for the accuracy, completeness or usefulness of any information, apparatus, product, or process disclosed, or represents that its use would not infringe privately owned rights. Reference herein to any specific commercial product, process, or service by trade name, trademark, manufacturer, or otherwise does not necessarily constitute or imply its endorsement, recommendation, or favoring by the United States Government or any agency thereof. The views and opinions of authors expressed herein do not necessarily state or reflect those of the United States Government or any agency thereof.

2.2.5.1 Abstract

This project has two goals, one to examine the potential effect of highly reactive impurities (SO_x, NO_x) on well injectivity during large-scale CO₂ sequestration, and the second to review the literature to determine whether impurities might adversely affect enhanced oil recovery processes. Work to date has focused on the second goal.

Since the early 1970s CO₂ has been used as an enhanced oil recovery agent; research on this technology predates this by nearly 20 years. Since that time, more than 50 CO₂ floods have conducted, primarily in West Texas, with a corresponding accumulation of field experience and production data. There has also grown a large technology base for the process, which we exploit in this work.

Minimum miscibility pressure (MMP) is generally regarded as one of the primary determinants to the success of an oil-recovering CO₂ flood. Miscibility implies the total suppression of capillary forces and excellent oil recovery efficiency on the small scale. However it is important to recall that other factors also contribute to flood efficiency, including WAG (water-alternating-gas) ratio, well productivity, and several reservoir-specific quantities such as heterogeneity and well spacing.

Miscibility develops in most cases because the CO₂ will extract intermediate components from the crude into the CO₂ - rich phase. The extraction depends strongly on the purity of the solvent. CO₂-N₂ mixtures are poorer extractors than CO₂ alone, whereas CO₂-H₂S mixtures are better extractors. MMP should decrease as the solvent becomes more "oil-like." This means that impurities in a CO₂ stream that are more like the oil than CO₂ will decrease the MMP. Impurities that are less like the oil will increase the MMP.

Most of the data on MMP has been captured through correlation, most commonly as statistical correlations. This would be the recommended approach for subsequent estimation of the influence of impurities. The dependency of MMP upon oil composition was addressed most definitively by Holm and Josendal (1982).

Correlations dealing with CO₂ stream impurity also exist. The best of these is by Sebastian et al. (1984). The combination of the Holm and Josendal (1982) and Sebastian et al. correlations accounts for the major influences on MMP. The accuracy is within about 50 psia, which should be sufficient for screening purposes.

2.2.5.2 Table of Contents

2.2.5.1 Abstract.....	896
2.2.5.2 Table of Contents	897
2.2.5.3 Introduction.....	898
2.2.5.4 Executive Summary.....	899
2.2.5.5 Experimental.....	900
2.2.5.6 Results and Discussion.....	900
2.2.5.7 Conclusion.....	903
2.2.5.8 References	904

2.2.5.3 Introduction

One goal of this project is to apply a general purpose simulator of coupled flow, transport, geochemistry and interphase mass transfer to estimate the potential for incremental injectivity reduction caused by geochemical reactions in the brine/SO_x/NO_x/CO₂/rock system. Even small changes in injectivity could have substantial impact on the economics of sequestration projects.

Many paradigms for sequestering CO₂ in subsurface formations (aquifers, hydrocarbon reservoirs) take well injectivity for granted. That is, the pressure gradient required to maintain CO₂ flow at a prescribed rate is assumed to remain constant over the course of the injection operation. The geochemical perturbation arising from the dissolution of CO₂ into subsurface brines is a mechanism for altering rock properties, however. Those alterations in turn have the potential for changing rock permeability and thus injectivity. Even small changes in injectivity could have substantial impact on the economics of sequestration projects, including direct costs associated with drilling and completing new wells, well stimulation treatments, and consequent interruptions in the flue gas pipeline operation, and indirect costs such as longer times to inject the design CO₂ volume.

The rock properties within a few feet of a wellbore largely control injectivity. Because all the CO₂ to be sequestered enters the formation through this small near-wellbore region, the region will be flushed by millions of (local) pore volumes of gas. Thus even slow, incremental geochemical alterations may have a significant cumulative effect over the months or years of the sequestration operation. The presence of impurities such as NO_x and SO_x in the CO₂ stream enhances the possibility of rock alteration, since these components are even more reactive than CO₂ when dissolved into brine.

Yet another feedback loop arises in this application, because in general the injected CO₂ will be undersaturated with water vapor. Thus after displacing water to irreducible saturation in the near-wellbore pore-space, the injected CO₂ will gradually dehydrate or dry the near wellbore region of trapped volumes of water. On one hand this process will concentrate the dissolved species, increasing their reactivity toward the formation minerals. On the other hand, the dehydration will reduce the grain surface area in contact with the irreducible water saturation, limiting the extent of the alteration.

The geochemical changes are likely to change also the surface energies of the water/mineral interface. Feedback therefore exists at the grain scale as well, since the contact between irreducible water and the rock grains is controlled by capillary forces. Investigation of this phenomenon is beyond the scope of the project proposed here; we will assume capillary forces are unaffected by geochemical reactions. It is nevertheless important to note their potential influence. For example, this investigation could find that the deleterious effects of impurities are self-limiting because of dehydration of the near-wellbore water saturation. Such a conclusion would be regarded as tentative until a better understanding of the grain-scale feedback is obtained.

The second goal is to review information in the enhanced oil recovery, petroleum fluids and thermodynamics literature to evaluate whether impurities would significantly affect baseline phase behavior of CO₂/crude oil mixtures. The revenue from oil produced miscibly or near-miscibly by injected CO₂ is an important potential offset to the cost of sequestration. Thus it is of interest to determine whether impurities would adversely or positively move the phase boundaries on a CO₂/crude oil PVT diagram. Experimental work is beyond the scope of this project, but we will survey the enhanced oil recovery, petroleum fluids and thermodynamics literature to determine whether the effect of SO_x/NO_x can be estimated. This survey will be expedited by easy access to more than 25 years of EOR research at the University of Texas at Austin. Advances in methods for first-principles predictions of thermodynamic behavior of a wide range of chemical species in CO₂ could be highly effective for estimating the influence of impurities on the phase behavior of CO₂/crude oil mixtures.

2.2.5.4 Executive Summary

This project has two goals, one to examine the potential effect of highly reactive impurities (SO_x, NO_x) on well injectivity during large-scale CO₂ sequestration, and the second to review the literature to determine whether impurities might adversely affect enhanced oil recovery processes.

Work to date has focused on the second goal. This progress report summarizes the literature on minimum miscibility pressure (MMP), one of the primary determinants to the success of a CO₂ flood intended to recover incremental oil. Particular emphasis is placed on the effect of a diluted or impure CO₂ stream.

Since the early 1970s CO₂ has been used as an enhanced oil recovery agent; research on this technology predates this by nearly 20 years. (Enhanced oil recovery is the recovery of oil by the injection of materials not normally present in a reservoir (Lake, 1989).) Since that time, more than 50 CO₂ floods have conducted, primarily in West Texas, with a corresponding accumulation of field experience and production data. There has also grown a large technology base for the process, which we exploit in this work.

CO₂ is one a family of injectants that recovers oil by mass transfer. Other solvents in this class are miscible gas injection and flue gas injection. Miscible gas injection has been underway at the Prudhoe Bay field for nearly 10 years. Experience with flue gas injection, though significantly less than for CO₂ or miscible gas, is particularly relevant for the possibility of CO₂ sequestration.

Minimum miscibility pressure (MMP) is generally regarded as one of the primary determinants to the success of an oil-recovering CO₂ flood. Miscibility implies the total suppression of capillary forces and excellent oil recovery efficiency on the small scale. MMP is always one of the quantities sought in a screening estimate of oil recovery for CO₂ floods (Paul et al., 1982). However it is important to recall that other factors also contribute to flood efficiency, including WAG (water-alternating-gas) ratio, well productivity as well as several reservoir-specific quantities such as heterogeneity and well spacing. These will be addressed in a subsequent report.

Miscibility develops in most cases because the CO₂ will extract intermediate components from the crude into the CO₂ - rich phase. The extraction depends strongly on the purity of the solvent. CO₂-N₂ mixtures are poorer extractors than CO₂ alone, whereas CO₂-H₂S mixtures are better extractors. MMP should decrease as the solvent becomes more "oil-like." This means that impurities in a CO₂ stream that are more like the oil than CO₂ will decrease the MMP. Impurities that are less like the oil will increase the MMP. Figure 16 in Huang et al. gives a good summary of this effect. See also Johnson and Pollin (1981), Whitehead et al. (1980) and Metcalfe (1981).

Most of the data on MMP has been captured through correlation, most commonly as statistical correlations. This would be the recommended approach for subsequent estimation of the influence of impurities. The dependency of MMP upon oil composition was addressed by Johnson and Pollin (1981) and most significantly by Holm and Josendal (1982). The latter was the culmination of several years of work (Holm and Csaszar, 1982; Holm and Josendal, 1974) on MMP. We regard Holm and Josendal (1982) as the definitive work on MMP because (i) the measure of intermediate content in the crude is quantitative and extensive (it extends to C₃₀), (ii) it makes use of a lumped measure of solvency that should be useful with impure Holm and Josendal (1982) streams, and (iii) the correlations are linear. This method also requires the most information about the crude.

Correlations dealing with CO₂ stream impurity also exist. The best of these is by Sebastian et al. (1984). The combination of the Holm and Josendal (1982) and Sebastian et al. correlations accounts for the major

influences on MMP. The accuracy is within about 50 psia, which should be sufficient for screening purposes.

2.2.5.5 Experimental

Not applicable. This work is a literature survey.

2.2.5.6 Results and Discussion

The objective of this project is to discuss a literature review of the effect of carbon dioxide (CO₂) on oil recovery with particular emphasis on the effect of a diluted or impure CO₂ stream.

Since the early 1970s CO₂ has been used as an enhanced oil recovery agent; research on this technology predates this by nearly 20 years. (Enhanced oil recovery is the recovery of oil by the injection of materials not normally present in a reservoir, Lake, 1989.). Since that time, more than 50 CO₂ floods have conducted, primarily in West Texas, with a corresponding accumulation of field experience and production data. There has also grown a large technology base for the process, which we exploit in this work.

CO₂ is one a family of injectants that recovers oil by mass transfer. Other solvents in this class are miscible gas injection and flue gas injection. Miscible gas injection has been underway at the Prudhoe Bay field for nearly 10 years. Experience with flue gas injection, though significantly less than for CO₂ or miscible gas, is particularly relevant for the possibility of CO₂ sequestration.

This progress report summarizes the literature on minimum miscibility pressure (MMP), thought to be one of the primary determinants to the success of an oil-recovering CO₂ flood. MMP is only one of the factors that determine the efficiency of a CO₂ flood. Other factors include mobility ratio, WAG (water-alternating-gas) ratio, well productivity as well as several reservoir-specific quantities such as heterogeneity and well spacing. These will be addressed in a subsequent report. MMP is always one of the quantities sought in a screening estimate of oil recovery for CO₂ floods (Paul et al., 1982).

As mentioned above, CO₂ recovers oil by mass transfer and if mass transfer is strong enough, the CO₂ will become miscible with resident crude. Miscibility implies the total suppression of capillary forces and excellent oil recovery efficiency on the small scale. In most cases the CO₂ will cause intermediate components from the crude to pass into the CO₂ - rich phase creating, after a few contact, an enriched mixture that is miscible with the crude. In this vaporizing gas drive process, the CO₂, though initially immiscible with the crude is said to have *developed* miscibility through the extraction. The extraction depends strongly on the purity of the solvent; carbon dioxide-nitrogen mixtures are poor extractors than CO₂ alone. On the other hand, carbon dioxide-hydrogen disulfide mixtures are better extractors.

A common way to gauge the approach to miscibility is through slim tube experiments. In these experiments a permeable medium is saturated with a crude and then, at constant temperature, subjected to a succession of CO₂ displacements at successively higher pressures. The ultimate oil recovery in these experiments tends to increase with pressure and, further, the recovery tends to level off at some specific pressure. This threshold pressure is defined as the minimum miscibility pressure or MMP. If attaining miscibility is difficult, the MMP with the high; if easy it will be low. MMP is actually an analogue quantity for minimum miscible enrichment (MME) previously proposed for miscible gas injection (Benhan et al., 1961).

Interestingly, though MMP is defined in term of oil recovery in a flowing medium, it is also intimately associated with the phase behavior of CO₂-crude mixtures. This means that MMP has a thermodynamic basis.

There are three ways to estimate minimum miscibility pressure:

1. Experimental. Within this category are

a. The slim tube experiment discussed above. This is the most common way.

b. The rising bubble apparatus. This technique estimates miscibility as the height in a column of crude at which a bubble of CO₂ disappears under gravity rise. The can be translated into a pressure and thence to MMP. This technique is offered as a commercial service but is much less used than the slim tube experiment.

c. Vanishing interfacial tension. This technique relies on the direct correspondence between miscibility and non-zero interfacial tension (Rao, 1997). The extrapolation of IFT to zero with increasing pressure determines the MMP. This technique, being much newer than the others, is the least used of all (Rao and Lee, 2003).

2. Theoretical. Because of the thermodynamic basis of MMP, it can be estimated by calculation. There are two broad categories of this

a. Mixing cell models. These are calculations in which solvent is mixed with crude in a succession of well-mixed cells. The solvent-crude mixtures comes to equilibrium after each mixing and the equilibrated gaseous phase (solvent plus extracted intermediate components) pass to another cell for further equilibration. There are specialized simulators for this (Walsh, 19xx), but the calculate can be done with any commercial compositional simulator.

b. Method of characteristics (MOC) models. In the limit of zero dispersion--which all mixing cell models posses to some degree--the MOC provides a direct measure of the MMP through quasi-analytic calculation. This procedure has been developed to high sophistication by the Stanford group, as reported on through several publications (for example, Wang and Orr, 1997; Wang and Orr, 2000). The ability of making these calculations exists on desk-top computers within the UT PGE department (Dindoruk et al., 1997) and this method would be a method of choice for future work because it is unrestricted with respect to the identity of components in the solvent.

3. Correlation. Because of the expense of making site-specific MMP measurements, much of the slim tube data has been captured through correlation. There are two types

a. Neural networks. The complexity of the dependencies of MMP has led some to exploit artificial neural networks for correlation (Huang et al., 2003). The success of this has been good but neural network are not easy to use for independent calculation.

b. Statistical correlation. By far the most common type of correlation has been statistical correlation and this, along with the MOC approach above, would be the recommended approach for subsequent estimation. Before reviewing these, we review some of the qualitative trends of MMP with other quantities.

That the composition of crude oils is highly variable accounts for the complexity of MMP correlations. General trends are

i. MMP should increase with temperature. That is, it should be more difficult to develop miscibility at high pressure and at low pressure.

ii. MMP should decrease with intermediate content in the crude. This is a logical consequence of the development of miscibility being predicated on the extraction of intermediates. There is, unfortunately, no simple way of simply characterizing the intermediate content in crudes.

iii. MMP should decrease as the solvent becomes more "oil-like." This means that impurities in a CO₂ stream that are more like the oil than CO₂ will decrease the MMP. Impurities that are less like the oil will increase the MMP. Figure 16 in Huang et al. gives a good summary of this effect. See also Johnson and Pollin (1981), Whitehead et al. (1980) and Metcalfe (1981).

We now turn, in conclusion, to the more significant MMP correlations.

Yellig and Metcalfe (1980) gave one of the earliest (and most controversial) correlations. This correlation was only for West Texas crudes and was light on composition dependence (item ii above) --which accounted for the controversy.

The compositional dependency was addressed by Johnson and Pollin (1981) and, most significantly, by Holm and Josendal (1982). The latter was the culmination of several years of work (Holm and Cszasz, 1965; Holm and Josendal, 1974) on MMP. The earliest of these (Holm, 1961) gives some idea of the maturity of the CO₂ flooding technology.

We regard Holm and Josendal (1982) as the definitive work on MMP because (i) the measure of intermediate content in the crude is quantitative and extensive (it extends to C30), (ii) it makes use of a lumped measure of solvency that should be useful with impure Holm and Josendal (1982) streams, and (iii) the correlations are linear. This method also requires the most information about the crude.

Correlations dealing with CO₂ stream impurity also exist. Perhaps the best of these is by Sebastian et al. (1984) who attempted to combine all of the effects i - iii into the following single correlation of deviations away from the CO₂ critical temperature.

$$\frac{P_{MM}}{(P_{MM})_{CO_2}} = 1.0 - (2.13 \times 10^{-2})(T_{pc} - T_c) + (2.51 \times 10^{-4})(T_{pc} - T_c)^2 - (2.35 \times 10^{-7})(T_{pc} - T_c)^3$$

where

P_{MM} is the MMP of a solvent against a particular crude

$(P_{MM})_{CO_2}$ is the MMP of a pure CO₂ solvent as from, for example, the Holm and Josendal correlation.

T_c is the critical temperature of CO₂, and

T_{pc} is the pseudo-critical temperature of an N-component solvent, where

$$T_{pc} = \sum_{i=1}^{i=N} y_i T_{ci}$$

and y_i is the mole fraction of component i in the solvent. Both temperatures are in degrees Rankine.

The combination of the Holm and Josendal (1982) and Sebastian et al. correlations gives the combined effects i - iii discussed above. The accuracy is within about 50 psia, which should be sufficient for screening purposes. We will report example calculations in future work.

2.2.5.7 Conclusion

The several decades of literature on field and laboratory CO₂ flooding provide a reasonably sound foundation for estimating the effects of impurities in the CO₂ phase on enhanced oil recovery behavior. The minimum miscibility pressure (MMP) is a widely used measure of enhanced recovery performance for CO₂ flooding. Usually miscibility develops during injection as the CO₂ extracts intermediate components from the crude into the CO₂ - rich phase. The solvent composition strongly influences the extraction process. MMP should decrease as the solvent becomes more "oil-like." Thus impurities in a CO₂ stream that are more like the oil than CO₂ will decrease the MMP. CO₂-N₂ mixtures are poorer extractors than CO₂ alone, whereas CO₂-H₂S mixtures are better extractors.

A number of techniques have been developed in the literature for determining MMP. The most common and most convenient are statistical correlations. We have identified correlations of MMP with solvent composition that should allow fairly accurate estimates of the tradeoff between oil recovery vs. the cost of impurity removal. In the next stage of the work we will carry out simple illustrative calculations with these correlations.

2.2.5.8 References

Dindoruk, Birol, Orr, F. M., and Johns, R. T., "Theory of Multicontact Miscible Displacement with Nitrogen," SPE Journal, Vol. 2, pp. 268-279, Sept. 1997.

Holm, L.W., "A Comparison of Propane and CO₂ Solvent Flooding Processes," American Institute of Chemical Engineers Journal pp. 179-184, June 1961

Holm, L.W. and Josendal, V. A., "Effect of Oil Composition on Miscible-Type Displacement by Carbon Dioxide," Society of Petroleum Engineers Journal, Vol. 22, pp. 87-98, (1982)

Holm, L. W. and Csaszar, A. K., "Oil Recovery by Solvents Mutually Soluble in Oil and Water," Society of Petroleum Engineers Reprint Series No. 8, Miscible Processes, pp. 31-38, 1965.

Holm, L.W. and Josendal, V. A., "Mechanisms of Oil Displacement by Carbon Dioxide," Journal of Petroleum Technology, Vol. 26, pp. 1427-1438, December 1974.

Johnson, J.P. and Pollin, J. S., "Measurement and Correlation of CO₂ Miscibility Pressures," SPE/DOE 9790, presented at the 1981 Joint SPE/DOE Symposium on Enhanced Oil Recovery, Tulsa, Oklahoma, 1981.

Lake, Larry W., Enhanced Oil Recovery, Prentice Hall, 1989.

Paul, G. W., Lake, L.W., Pope, G.A., and Young, G.B., "A Simplified Predictive Model for Micellar/Polymer Flooding," SPE 10733, presented at the California Regional Meeting of the Society of Petroleum Engineering, San Francisco, California, 1982.

Rao, Dandina, "A New Technique of Vanishing Interfacial Tension for Miscibility Determination," Fluid Phase Equilibria, 139, pp. 311- 324, 1997.

Rao, Dandina, and Jong I. Lee, "Determination of Gas-oil Miscibility Conditions for Interfacial Tension Measurements," J. of Colloid and Interface Science, 262, pp. 474- 482, 2003.

Sebastian, H.M., Winger, R. S., and Renner, T.A., "Correlation of Minimum Miscibility Pressure for Impure CO₂ Streams," SPE/DOE 12648, presented at the Fourth Joint SPE/DOE Symposium on Enhanced Oil Recovery, Tulsa, Oklahoma, 1984.

Wang, Yun and Franklin M. Orr, Jr., "Analytical Calculation of Minimum Miscibility Pressure," Fluid Phase Equilibrium, 139, pp. 101- 124, 1997.

Wang, Yun and Franklin M. Orr, Jr., "Calculation of Minimum Miscibility Pressure," J. Petroleum Science and Engineering, 27, pp. 151-164, 2000.

2.3 Integrity

2.3.1 Evaluation of Natural CO₂ Charged Systems as Analogues for Geologic Sequestration

Report Title

CO₂ Capture Project - An Integrated, Collaborative Technology Development Project for Next Generation CO₂ Separation, Capture and Geologic Sequestration

Evaluation of Natural CO₂ Charged Systems as Analogs for Geologic Sequestration

Report Reference

2.3.1

Type of Report: Semi-Annual Report / Final Report delete as applicable

Reporting Period Start Date: February 2003

Reporting Period End Date: July 2003

Principal Author(s): James P. Evans, Zoe Shipton

Date Report was issued: August 2003

DOE Award Number: DE-FC26-01NT41145

Submitting Organization: Utah State University

Address: Dept. of Geology
4505 Old Main Hill, Utah State University
Logan, UT 84322-4505

Disclaimer

This report was prepared as an account of work sponsored by an agency of the United States Government. Neither the United States Government nor any agency thereof, nor any of their employees, makes any warranty, express or implied, or assumes any legal liability or responsibility for the accuracy, completeness or usefulness of any information, apparatus, product, or process disclosed, or represents that its use would not infringe privately owned rights. Reference herein to any specific commercial product, process, or service by trade name, trademark, manufacturer, or otherwise does not necessarily constitute or imply its endorsement, recommendation, or favoring by the United States Government or any agency thereof. The views and opinions of authors expressed herein do not necessarily state or reflect those of the United States Government or any agency thereof.

2.3.1.1 Abstract

The study of natural, leaking CO₂-rich groundwater systems provides an opportunity to understand why some geologic systems cannot reliably contain CO₂ for long periods of time, and how the flow of large volumes of CO₂ gas may occur in a natural system. Two fault zones in the central Colorado Plateau of the western United States crosscut sandstones, shales, and siltstones, which would typically create fault seal by the mechanisms of clay-shale smear and cataclasis. However, these faults leak CO₂ to the surface through several low-temperature springs and geysers localized in the fault zones. We characterize the sources, flow paths, and chemical evolution of the emanating gases and waters using their isotopic and compositional chemistries. Six springs and geysers associated with the fault zones are very saline, with total dissolved solid values ranging from 13,848 to 21,228 mg/l, and all fall in the sodium-chloride chemical facies. Solute chemistries indicate that simple calcite and halite dissolution alone are not occurring. Hydrogen and oxygen isotopic compositions of the waters indicate a meteoric source. Values of d¹³C of total dissolved carbon for three locations are 0.0, 0.7 and 1.2‰. The gases emanating from all springs are CO₂ rich (95.66 to 99.41%) with minor amounts of N₂, O₂, and Ar. The latter gases probably originate from entrainment of slight amounts of atmospheric gases as they bubble or erupt. The average d¹³C value of the CO₂ gases is -6.60‰ ± 0.13‰. Helium isotopes for two locations have R/R_a values of 0.302 and 0.310, and CO₂/³He values of 1.75E+11 and 2.92E+11. These values indicate crustal gas with a small amount of air. Comparison of carbon isotopes of gas, water, and calcite carbonate species at the surface indicates that the three phases are in isotopic equilibrium. In this sedimentary basin, processes that can generate large amounts of CO₂ gas with carbon isotope values in the range mentioned above are diagenetic clay-carbonate reactions and/or hydrothermal decarbonation of carbonates. Since intrusives are far from the field area and the CO₂/³He values do not indicate magmatic contribution, clay-carbonate reactions are probably the most likely source of the CO₂ gas. The thermal burial history of the basin indicates impure carbonates have achieved temperatures sufficient to produce CO₂ by clay-carbonate reactions. Our conceptual flow model depicts gas from depth (~>1 km) traveling upwards along the faults and entering shallower formation waters. The waters and gases then both discharge to the surface into zones compromised by faults.

Geologic mapping and cross section analysis, combined with the geochemical data and regional synthesis of water and gas chemistries suggest that CO₂ is sourced from diagenetic clay-carbonate reactions, perhaps occurring at the same time as hydrocarbon catagenesis. The CO₂ flows appears to flow laterally in reservoirs that have a top seal composed of shale-rich rocks. When the CO₂ reaches the faults, it vertically for 1- 1.5 km, and deposition rates appear to be relatively fast, indicated by the size of modern travertine mounds, and the textures of calcite in veins.

These results demonstrate the importance of maintaining seal rock integrity in any designed storage system, and leaking natural systems show that some systems will not be self-sealing.

2.3.2.2 Table of Contents

2.3.1.1 Abstract.....	907
2.3.2.2 Table of Contents	908
2.3.1.3 List(s) of Graphical Materials	909
2.3.1.4 Introduction.....	910
2.3.1.5 Executive Summary.....	912
2.3.1.6 Experimental.....	913
2.3.1.6.1 Introduction.....	913
2.3.1.6.2 Gas-related data collection.....	913
2.3.1.6.2.1 Gas sampling for volumetric compositional percentages and isotopes.....	913
2.3.1.6.2.2 Gas sampling to obtain helium-isotope data	914
2.3.1.6.3 Compositional and isotopic data collection techniques for waters.....	914
2.3.1.6.3.1 Collection of pH data	914
2.3.1.6.3.2 Determining field alkalinity.....	915
2.3.1.6.3.3 Sampling for major ions	915
2.3.1.6.3.4 Sampling to obtain dD and d ¹⁸ O data.....	916
2.3.1.7 Results and Discussion.....	918
2.3.1.7.1 Geological Interpretation.....	918
2.3.1.7.1.1 CO ₂ emissions and springs.....	919
2.3.1.7.1.2 Mineral deposits	919
2.3.1.7.2 Geochemical Results	922
2.3.1.7.2.1 Sampling procedures and analysis	922
2.3.1.7.2.2 Water data.....	922
2.3.1.7.2.3 Carbon isotope analysis	926
2.3.1.7.2.4 Carbon History and the Origin of the CO ₂ gas.....	928
2.3.1.8 Conclusion.....	931
2.3.1.9 References	932
2.3.1.10 Publications.....	936

2.3.1.3 List(s) of Graphical Materials

Figure 2.3.1.4(1) Regional geologic setting of the study area. LGW_ Little Grand Wash fault: SW – Salt Wash fault. These faults cut upper Paleozoic through Cretaceous sedimentary rocks. Carbonate deposits are located along the faults, and active springs, seeps, and geysers are indicated by the red dots.....	911
Figure 2.3.1.7.1(1) Detailed geologic map of the Little Grand Wash fault. Red regions are carbonate deposits.....	919
Figure 2.3.1.7.1(2) Geologic cross section of the study area. CO ₂ sources discussed here lie 1 –1.5 km below the surface, and suggest that CO ₂ flows vertically and as it rises, forms a gas bubble. Periodic eruption of gas at the surface suggests that gas release is followed by a pressure buildup phase, and when P _{CO2} gas > the hydrostatic pressure, another eruption occurs. Near surface, very large veins show this process occurred naturally in the past.....	921
Table 2.3.1.7.2(1): Sample location and the type of data collected at each site. The abbreviation “TDC” stands for “total dissolved carbon”	922
Figure 2.3.1.7.2(2) Solute chemistries of sampled waters presented graphically in a trilinear plot (Piper, 1944). This figure indicates that all of the waters fall in the sodium chloride chemical facies. The close grouping of data points implies a similar chemical evolution history of all the waters.....	923
Table 2.3.1.7.2(3) Temperature, pH, solute chemistry isotope data of total dissolved carbo, and ionic ratios for samples waters. “TDS” stands for “total dissolved solids”.....	924
Table 2.3.1.7.2(4) Saturation indices for sample locations. SI = log IAP/K eq. Saturation occurs when SI = 0.0 + 0.1. A positive number indicates a thermodynamic tendency of a water to precipitate the mineral in question, whereas a negative number represents a tendency for a water to dissolved the mineral.....	924
Table 2.3.1.7.2(5) Gas molecular compositions and ¹³ C _{CO2} values of sampled sites. Emanating gases were collected in glass bottles. To determine whether atmospheric contamination occurred, normalization was performed by equating Ar, O ₂ and N ₂ of the samples to 100%.....	925
Figure 2.3.1.7.2(6) Hydrogen and oxygen isotopic data. Black squares represent data during a previous study from the Green River, at Green River, Utah (Coplen and Kendall, 2000). Blue diamonds represent data collected during this study at various times during 2001 through 2003 for all seven springs and geysers.....	926
Table 2.3.1.7.2(7) Helium isotope data and volumetric gas ratios. R is the ratio of ³ He/ ⁴ He in the collected samples, and Ra is the ³ He/ ⁴ He of the atmosphere.....	926
Table 2.3.1.7.2(8) Comparison of measured and predicted carbon isotopic values of gas and aqueous phases.....	927
Table 2.3.1.7.2(9) Predicted (based on CO ₂ gas samples) and measured 14C of Calcite. Calcite values obtained from Shipton et at. (inpress).....	928

2.3.1.4 Introduction

Effective design and implementation of geologic CO₂ sequestration projects require that we understand the storage capacity of a candidate site, the trapping mechanisms for gas, and the hydrodynamics of the system. The CO₂ must be effectively segregated from the atmosphere for periods of thousands of years (Rochelle et al. 1999). Natural sources of CO₂ include mantle degassing, metamorphism or dissolution of carbonates, oxidation or bacterial degradation of organic matter, and thermal maturation of hydrocarbons (Selley 1998). Numerous naturally occurring gas fields contain large amounts of CO₂, providing analogues for the integrity of stored gas systems (e.g. Allis et al. 2001). In some CO₂ fields, however, gas leaks into the atmosphere, primarily along faults. We can study these active leaks to understand the factors that might control the feasibility and safety of future CO₂ injection projects and guide the design and implementation of such projects.

The hydrology, stratigraphy, structural geology, and geochemistry of naturally degassing CO₂ reservoirs in the Colorado Plateau of East-Central Utah are examined. The CO₂ discharges from the hydrocarbon-rich Paradox Basin along the Little Grand Wash and Salt Wash faults. These faults crosscut sandstones, shales, and siltstones producing zones of clay-rich gouge that should theoretically be a barrier to flow (e.g. Freeman et al. 1998). CO₂-charged springs and geysers, travertines (both active and ancient), and carbonate-filled veins are localised along the fault traces. The faults are presently conducting CO₂-rich fluids and the fault seal has clearly failed numerous times in the past. Abandoned hydrocarbon boreholes are also active conduits for CO₂ to the surface (Doelling 1994).

The Colorado Plateau and Four Corners region of the western United States contains at least nine producing or abandoned CO₂ fields with up to 28 trillion cubic feet of CO₂ gas (Allis et al. 2001). Most of these fields are fault-bounded anticlines with four-way anticlinal closure or fault seal along one margin of the field. We focus on the Little Grand Wash and Salt Wash faults, which are at the northern end of the Paradox Basin. This basin contains a number of actively producing oil and methane fields, as well as CO₂ fields including the Lisbon and McElmo Dome fields. Immediately south of the study area is the abandoned Salt Wash oil field (Peterson 1973). To the north of the Paradox Basin are the active natural gas and CO₂ fields of the San Rafael Swell (e.g. Drunkards Wash, Ferron Dome). Many of the natural gas fields in the area produce significant amounts of CO₂ (Cappa and Rice 1995), much of which is vented to the atmosphere.

The Paradox Basin is defined by the extent of organic-rich Pennsylvanian and Permian marine limestones, shales and evaporites (Fig. 2.3.1.4(1)). Hydrocarbon source rocks occur in the Ismay-Desert Creek and Cane Creek cycles of the Paradox Formation (Nuccio and Condon 1995), a mixed sequence of dolostone, black shales, anhydrite, and halite. These are overlain by Triassic and Jurassic fluvial and aeolian redbeds. The oldest lithologies that crop out in the study area are red-brown fine-grained sandstones of the Middle Jurassic aeolian Entrada and Curtis Formations. The Middle Jurassic Summerville Formation forms characteristic low cliffs with thin bedding and seams of gypsum. The Upper Jurassic Morrison Formation consists of stacked fluvial channels of the Salt Wash Sandstone member, overlain by the bentonite-rich lacustrine shales of the Brushy Basin member. The Lower Cretaceous Cedar Mountain Formation and the Upper Cretaceous Dakota Sandstone are conglomeratic channel sandstones. The youngest formation exposed in the field area is the Upper Cretaceous Mancos Shale, a dark organic-rich marine shale. Approximately 2500 m of Cretaceous and Tertiary rocks have been eroded from the area (Nuccio and Condon 1996).

The Little Grand and Salt Wash faults (Fig. 2.3.1.4(1)) affect the present-day flow of CO₂ gas and water. Carbonate springs, an active CO₂-charged geyser, and actively forming travertine deposits are localized along the Little Grand Wash fault zone (Baer and Rigby 1978; Campbell and Baer 1978; Doelling 1994). Numerous CO₂-charged springs occur in the region of the Salt Wash faults (Doelling 1994). The faults are part of a WNW trending set of 70 to 80° dipping normal faults in the region. Timing of continued movement along these faults is poorly known, though we present arguments below for Early Tertiary and

Quaternary slip. The faults cut the Mancos Shale consistent with substantial fault activity having occurred at least up to the Middle Cretaceous. The faults also cut a north plunging anticline Figure 2.3.1.4(1), which could be related to salt movement in the Paradox Formation at depth. A basin-wide system of salt anticlines initiated when the salt was loaded by the Pennsylvanian/Permian clastics shed off the Uncompagre uplift to the northeast. Reactivation of the salt-related anticlines and faults occurred during Laramide (Eocene) contraction (Chan et al. 2000).

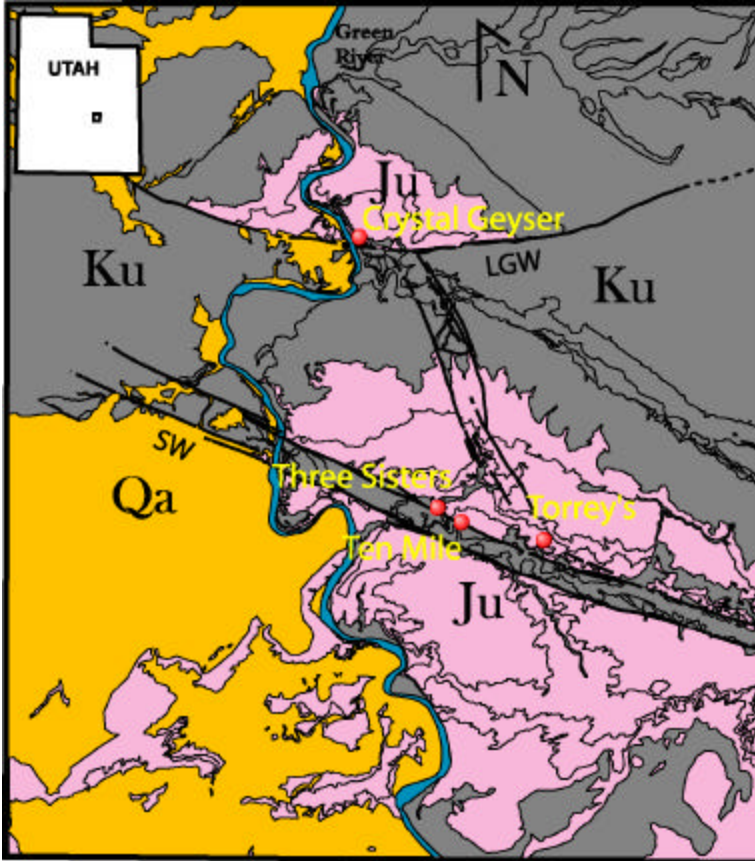


Figure 2.3.1.4(1) Regional geologic setting of the study area. LGW_ Little Grand Wash fault: SW– Salt Wash fault. These faults cut upper Paleozoic through Cretaceous sedimentary rocks. Carbonate deposits are located along the faults, and active springs, seeps, and geysers are indicated by the red dots.

2.3.1.5 Executive Summary

Characterization of the mechanisms and magnitude of CO₂ leakage through the Little Grand Wash and Salt Wash faults requires that the CO₂ sources, pathways, volumes, and rates of flow be determined. The distribution of the fault-associated rocks and related outcrop-scale structures of travertines and carbonate veins are used to characterize the flow paths. The geochemistry of the spring waters, carbonates, and travertines identify the potential sources of the fluids in the system. Integration of these data is used to develop a conceptual model for the groundwater/CO₂ flow system (source, pathways, reservoir and cap rocks).

As our work is approaching the end of its timeframe, we have achieved many of our research objectives. To date we have completed the geologic analyses of the area, which includes geologic mapping, analysis of subsurface data. We show that the faults in the area sole into salt deposits at ~ 1.5 km depth, and have experienced repeated motion over time. The field relationships and textures of veins and travertines associated with the faults indicate repeated and numerous episodes of carbonate charge from some depth, and in some cases, their deposition rates were rapid.

Geochemical studies constrain the source of CO₂ and indicate a likely flow path. Based on water and gas chemistry and isotopic analyses, it is shown that the CO₂ is sourced at depth from a series of clay-carbonate reactions. Upward migration of the CO₂ – charged waters probably resulted in exsolution of the CO₂ into the vapor phase. Further research will examine the rates of flow, rates of carbonate deposition, and explore numerical models of the system.

2.3.1.6 Experimental

2.3.1.6.1 Introduction

Historically, there are diverse reasons for interest in naturally CO₂ - charged systems, the most recent being geologic sequestration of CO₂. A voluminous literature resource is therefore available as a guide to data collection design and sampling techniques. Precision and accuracies of sampling approaches differ in ways that are not always stated. Some papers call for standardization of data presentation or at least a delineation of problems unique to CO₂-rich systems (Lesniak, 1994; Pearson, 1978). Also, typical guidelines for some aspects of the sampling of “average” groundwaters and gases are not suited to particular problems found in the CO₂-rich environment by such phenomena as CO₂ outgassing which can substantially alter the chemical and isotopic properties of groundwater and subsurface gases (Pearson et al., 1978).

Due to the unstable physicochemical nature of subsurface gases and waters, careful planning of data collection procedures is required. Some properties of subsurface fluids change within only a few minutes following sampling and hence require immediate analysis in the field, whereas other properties can be preserved in the field and then determined later in a laboratory (Wood, 1981). Regarding CO₂-rich environments, even further instability of properties is common. CO₂-rich waters typically degas and CO₂ as they travel to and reach the surface. This degassing occurs due to the differences in P_{CO2} of the waters and the atmosphere. Degassing can affect both chemical and isotopic properties of the gases and waters such as δ¹³C values and pH (Pearson et al., 1978). We have developed a detailed description of the sampling methods used in this study, and have identified the sources of errors that might result both as a function of the sampling protocol and of the natural variability of the systems studied.

2.3.1.6.2 Gas -related data collection

As CO₂- or gas-saturated groundwaters travel to the surface, a separate gas phase may develop due to a loss of hydrostatic pressure (Pearson et al., 1978; Lesniak, 1998). The free gas phase can be directly sampled at the surface or a water sample can be collected from which dissolved gases are later collected. The separate gas phase may not reflect accurately the in situ gas conditions; however, it typically provides an approximation of the dissolved gases which is sufficient for isotopic determinations (Clark and Fritz, 1997). The concentrations of the chemical species in subsurface gases can help indicate which reactions may have produced the gas (Hunt, 1996). Gases impact redox, isotopic, and geochemical process in subsurface systems and are important as data inputted into thermodynamic geochemical models (Clark and Fritz, 1997).

2.3.1.6.2.1 Gas sampling for volumetric compositional percentages and isotopes

The same type of sampling can be conducted to provide gas for compositional volumetric ratios and isotopic analysis (¹³C, ¹⁸O, and ²H of CO₂ and CH₄) (Clark and Fritz, 1997). Compositional analysis by gas chromatography determines the percentages of fixed and hydrocarbon gases including: N₂, O₂, Ar, CO₂, CO, H₂, He, H₂S, CH₄, C₂H₆, C₂H₄, C₃H₈, C₃H₆, iC₄H₁₀, nC₄H₁₀, iC₅H₁₂, nC₅H₁₂, and C₆+. Isotopic analysis aids in determining the source of the gases (Clark and Fritz, 1997).

At natural springs or artesian wells, the free gas phased can be sampled simply using a well-rinsed glass or thick-walled polypropylene bottles; soda pop bottles with screw-on caps can also be used (Clark and Fritz, 1997). Shrum (1993) and Heath (in prep.) used glass bottles with resealable rubber-o-ringed porcelain caps (Grolsch Beer bottles). The following technique works best if a small pool of water has formed at the vent of the spring or site being sampled and follows closing instructions given by Clark and Fritz (1997). The bottle is rinsed with the emanating water. The container is filled under water and inverted such that the opening of the bottle is pointing downwards. A funnel is fit into the neck of the

bottle without allowing atmosphere to enter under the upside down bottle. The bottle and funnel are placed in the path of the rising bubbles. Clark and Fritz (1997) recommend that 50% of the water should be displaced by the gases before the bottle is sealed under water. After sealing, the bottle is kept upside down to keep the cap wet in order to minimize diffusion. The bottles are delivered to an analytic laboratory. For the study of CO₂-rich systems, the sampled bottles were sent to Isotech Laboratories, Inc., located at Champaign, IL for both gas chromatographic and isotopic analysis.

Possible error occurs if bottles are not tightly sealed or the improper sampling allows atmospheric gases to enter the bottles. Quality assurance planning should require careful sampling. If N₂/Ar ratios of the sampled gases and atmospheric gases are compared, possible atmospheric contamination can be identified (Shrum, 1993; Heath et al., in prep.).

2.3.1.6.2.2 Gas sampling to obtain helium-isotope data

Helium isotope ratios can be useful in determining if subsurface gases are from crustal or mantle / magmatic sources. The mantle is the largest reservoir of ³He. This primordial helium was incorporated in the mantle when the earth was formed. Radioactive decay processes in the crust have highly enriched the crust in ⁴He relative to ³He (Clark and Fritz, 1997). Helium isotope data is presented as the ratio R/R_{air}, where R is the ³He/⁴He ratio of the sample and R_{air} is ³He/⁴He ratio of air (1.38E-6).

Crustal fluids typically have R/R_{air} values of ~0.02, whereas mantle derived gases typically approach the MORB (mid-oceanic ridge basalt) of ~8 (Kennedy et al., 1997). Typical R/R_{air} values for mantle, crustal, and atmospheric sources along with R/R_{air} values for a sample can be used in a mixing equation to determine what proportions of a sample are made up from these sources. Crustal-sourced He, having R/R_{air} values less than one, makes their distinction from mantle-derived (Dai et al., 1996). It should be noted, however, that the differing physicochemical properties of He and CO₂ and mixing does not guarantee that association of these two gases indicates common origin.

2.3.1.6.3 Compositional and isotopic data collection techniques for waters

2.3.1.6.3.1 Collection of pH data

The pH of groundwaters is a fundamental parameter because it is impacted by and reflective of chemical equilibrium and kinetics of many reactions. The value of pH is related to reactions that consume or produce hydrogen (Hem, 1985) such as acid and base dissociations, and hydrolysis (Wood, 1981). The weak acid geochemistry of carbon in groundwaters, therefore, influences the pH of CO₂-rich groundwaters. Incorrect determination of pH by 0.1 units results in large uncertainties of about 24% in geochemical calculations of mineral saturation indices (Pearson et al., 1978).

A major source of potential error is the outgassing of CO₂ as groundwaters reach the surface. This occurs due to differences of P_{CO2} of the ascending groundwater and the P_{CO2} of the atmospheric. Also, the loss of hydrostatic pressure allows for the formation of a free gas phase (Lesniak, 1998). Significant CO₂ outgassing increases the pH of waters by the following reaction:



where H₂CO₃* consists of both CO₂(aq) and H₂CO₃ (Kehew, 2001). If the sampled waters are exposed to the atmosphere and allowed to outgas during measurement, much outgassing may take place before the electrode system of the pH meter reaches a steady electronic (emf) signal. The measured value may therefore be of higher pH than the actual pH of the sampled waters (Pearson et al., 1978).

Older instructions such as those given by Wood (1981) allow sampled water to be exposed to the atmosphere during measurement. Wood (1981) realized outgassing can occur and recommend using a tightly fitted stopper on the beaker from which the pH reading is made. More recent sampling instructions provided by the U.S. Geological Survey TWRI Book 9 (1998) address the degassing problem. These procedures recommend using downhole or flowthrough-chamber equipment. Emphasis is made that downhole measurements are the most likely to represent actual in situ pH. Thus, whatever sampling method is chosen, the care taken should be commensurate with the data quality needs of the project in question.

For very careful geochemical work on springs, a method to correct pH measurement errors due to any outgassing is suggested by Pearson et al. (1978). This method requires pH measurements to be made, but these during these measurements, outgassing is allowed to occur. Solution composition and temperature data is also collected. During the same collection activity, measurement is also made to determine in situ partial pressure of dissolved CO₂. This procedure involved the use of a pump (peristaltic, submersible, or gravity flow) to supply “uncontaminated, full-column flow of sample water” to a sample flask (Pearson et al., 1978). The sample flask contained a large chamber through which water was allowed to flow to flush the flask. Then the flask was closed and the water was allowed into degas into a previously evacuated sidearm. The gas phases of the sidearm was analyzed by gas chromatography and these, plus the volumes of the main and sidearms, were used to calculate P_{CO₂}. Using the previously measured pH and solution composition, a geochemical model was used to model the composition of the water if the calculated P_{CO₂} of the model were to match that of the in situ value. As this calculation was made, pH was allowed to change and hence a corrected pH value was obtained. The Pearson et al. method, therefore, essentially bypasses outgassing errors. The error associated with the in situ measurement of P_{CO₂} is also very small. A P_{CO₂} error of 5% only results in mineral saturation index error of 0.02 units (Pearson et al., 1978).

In conclusion, careful measurement of pH is important for the interpretation of geochemical data, but the actual sampling procedure should be influenced by the degree of accuracy needed for a specific project.

2.3.1.6.3.2 Determining field alkalinity

Detailed explanation of field alkalinity and sampling procedures is given by the U.S. Geological Survey in the “National Field Manual for the Collection of Water-Quality Data” (1997 to present). Alkalinity is a measure of the acid neutralizing capacity of a filtered water sample (Rounds and Wilde, 2001); or in other words, the amount of titratable bases by a strong acid (Kehew, 2001). The U.S.G.S. provides the qualification that if a titration is performed on an unfiltered sample, then the measured quantity is called acid neutralizing capacity, not alkalinity, which also includes the sum of all titratable bases plus particulate matter by a strong acid (Rounds and Wilde, 2001). Therefore, if water samples do not contain particulate matter, then alkalinity and acid neutralizing capacity values would be the same (Rounds and Wilde, 2001). The importance of alkalinity derives from its buffering capacity of groundwater; or rather, its regulation of pH which in turn impacts chemical and biological processes (McLean, 2002). Alkalinity can also be used to calculate concentration of carbonate species (Rounds and Wilde, 2001).

2.3.1.6.3.3 Sampling for major ions

Solute geochemistry, the chemistry of dissolved constituents, is not generally directly applicable to determine the source of a given groundwater. It basically reflects the “nature and extent of mineral-water exchange reactions” (Sheppard, 1986). Understanding mineral-water reactions can help determine what rocks a body of groundwater has traveled through. For water to have a certain composition, it must have been in contact with certain minerals or gases. Therefore, having a good description of the lithology of potential aquifers is important to chemically link a groundwater to that aquifer.

Solute geochemistry is also very important to aid and complement in the interpretation of isotopic data (Clark and Fritz, 1997). As an example, work by P.I Lesniak will be briefly reviewed. In “d¹³C in low temperature, CO₂-charged waters: a need for consistency with carbonate chemistry” he mentions that some researchers had mistakenly assumed that the d¹³C value of total dissolved carbonates represents the d¹³C value of the aqueous species HCO₃⁻ (Lesniak, 1994). This mistaken assumption has led to erroneous interpretations. Lesniak (1994) determined that the collection of solute chemical data obtained at the same time as d¹³C data of total dissolved carbon allows for the determination of d¹³C_{HCO3-}. This data transformation will be further covered in the next section which covers the synthesis of chemical and isotope data.

Samples are collected to determine major cation (Ca²⁺, Mg²⁺, Na⁺, K⁺, and SiO₂) and anion (Cl⁻, SO₄⁴⁻, and possibly NO₃⁻, F⁻, and Br⁻) concentrations. Collection is straight forward. Directions from “Environmental Isotopes in Hydrogeology” are summarized here (Clark and Fritz, 1997). Use thoroughly rinsed 50 ml polypropylene bottles for both cations and anions. Using a 0.45 μm positive pressure filtering system, filter water into sample bottles and rinse bottles and cap at least two times. Fill anion bottle completely and cap. Fill cation bottle leaving 2-ml head space. Acidify cation bottle with reagent grade HNO₃ to a pH of 2. The acidification keeps cations from precipitating out of solution. Keep samples at 4°C and deliver to laboratory.

Quality control such as trip blanks, field blanks, field duplicates are probably not necessary for the collection of major ions. Trip blanks are typically used if data collection involves volatile organics, gasoline range organics, or petroleum volatile organic compounds. Field blanks are used if contamination from sampling equipment may occur. This may be the case if sampling equipment used is not dedicated for well sampling or not disposed after single use. Field duplicates are also typically used for sensitive data collection such as volatile organics. A simple accuracy check on the quality of major ions is the charge balance error (or cation-anion balance) expressed by the following equation (Hem, 1986):

$$E = \frac{\sum z m_c - \sum z m_a}{\sum z m_c + \sum z m_a} \times 100$$

where z is the ionic valence, m_c is the molality of cation species, and m_a is the molality of anion species (Freeze and Cherry, 1979). If analytical results have already been transformed to milliequivalents per liter, then the valence term in this equation can be omitted. A balance error of five percent or less is typically acceptable (Freeze and Cherry, 1979) and samples of intermediate salinity of 250-1000 mg/L usually do not have errors greater than one or two percent (Hem, 1985). Note, however, that in some cases individual errors of cations and anions can cancel each other out (Freeze and Cherry, 1979) thus charge balance error is not a definitive check on the accuracy of an analysis. This check does include the anion bicarbonate which is determined by field alkalinity tests. Field alkalinity may involve uncertainty which may impact the error of the charge balance. Thus charge balance error may have implications in the analysis of cations, anions, or field alkalinity.

2.3.1.6.3.4 Sampling to obtain dD and d¹⁸O data

In a graph of d²H versus d¹⁸O, the source and history of a groundwater determines where it plots in relation to the mean water line (MWL) as given by Craig’s (1961) equation:

$$dD = 8d^{18}O + 10$$

Most meteoric waters will plot near the MWL (± 1 ‰ d¹⁸O of this line). Shallow groundwaters derived from a meteoric source will reflect the isotopic composition of the meteoric precipitation and plot very near to the MWL, unless the precipitation had undergone excessive evaporation prior to infiltration

(Sheppard, 1986). Waters that have experienced evaporation typically plot away from the MWL on evaporation trajectories with slopes of ~ 5 (Faure, 1986). Hydrothermal groundwaters typically show oxygen isotope values that have been shifted to the right (toward more positive ^{18}O values) of the MWL. In hydrothermal environments, the increased temperature decreases the value of the fractionation factor between the oxygen in the water and the oxygen in the silicate or carbonate rocks, allowing the oxygen isotope values of the water to become closer to the more enriched oxygen isotope values of the rocks. There is no d^2H shift in geothermal waters, because silicate and carbonate rocks have low concentrations of hydrogen compared to the hydrogen content of water (Faure, 1986). Other groundwaters that will plot away from the MWL are waters that have equilibrated with magmas or rocks experiencing metamorphism.

Sampling for δD and $\delta^{18}\text{O}$ is relatively simple since these parameters are not readily affected by chemical or biological processes (Clark and Fritz, 1997). The only equipment needed is the appropriate container. Clark and Fritz (1997) recommended plastic screw cap bottles with a volume of 100 mL (minimum volume 10 mL) made from high-density linear polyethylene, linear polyethylene, or polypropylene. Stephen Nelson of the isotope laboratory at Brigham Young University (BYU), suggests the use of one ounce brown glass bottles with polyseal caps for sampling (personal electronic email, 13 May 2001). The brown glass impedes biota from growing. The sample bottle is simply filled with the emanating water and capped with no head space. The samples do not need to be chilled and storage life for a well sealed bottle is greater than one year (Clark and Fritz, 1997).

Error from sampling will result if sampling bottles do not tightly seal and evaporation occurs. The researcher collecting data should be aware that although field sampling is relatively straightforward, laboratory analysis for $\delta^{18}\text{O}$ may be somewhat more complicated in that typical waters are not enriched in CO_2 gas. At the isotope laboratory at BYU where the Heath (in prep.) analyzed his samples it was found that the high content of CO_2 causes problems when the samples are run by routine continuous flow methods on a Finnigan MAT Delta^{plus} mass spectrometer.

At BYU, $^{18}\text{O}/^{16}\text{O}$ isotopic analysis is completed by placing 0.5 ml of a sample into a 10 mL vial. The water is allowed to equilibrate with a gas mixture that is 99% He and 1% CO_2 . The equilibration is carefully temperature controlled, because the fractionation of oxygen between H_2O and CO_2 is temperature dependent. Samples with high levels of CO_2 , when analyzed in this manner, degas into the headspace of the vial, greatly increasing headspace CO_2 concentrations. When the gas is analyzed in the mass spectrometer, the gas produces too much signal. To overcome this problem, the CO_2 -rich water samples can be prepared offline by conventional means so that they can be run in the dual inlet of the mass spectrometer, which can accommodate much higher levels of CO_2 . This brief digression into the laboratory analysis of oxygen isotopes was made to illustrate a potential analytical problem that is not typically dealt with during the analysis of waters not rich in CO_2 gas. Thus, even if the researcher is not involved with actual laboratory work and only field sampling, he/she should still insure that the laboratory completing the analysis can accommodate this extra complication.

In the case of this work, the degassing problem during laboratory analysis was not overcome by conventional offline preparation, but by degassing the samples of CO_2 before oxygen analysis on the mass spectrometer. This was accomplished by placing 10 mL of sample into 4 ounce bottle with air-tight caps. The bottles were then placed into an oven at 50°C for at least 10 hours. The bottle were then purged for 3 seconds with N_2 gas and then resealed. A laboratory blank of distilled water was subjected in this process and another blank was not degassed. These blanks were made to determine whether this degassing process caused any fractionation of oxygen isotopes. The results of the laboratory analysis and indicates that this process did not cause any more uncertainty than is typically obtained during measurement of oxygen isotopes. Thus, this degassing process can be used in analysis instead of conventional offline preparation.

2.3.1.7 Results and Discussion

2.3.1.7.1 Geological Interpretation

The Little Grand Wash fault is comprised of an anastomosing series of one to several south-dipping arcuate normal faults with a surface trace length of 61 km (Fig. 2.3.1.4(1)). Total vertical separation on the fault near the Green River is 180 to 210 m, most of which is accommodated by the southern fault strand. The two strands of the fault were encountered at depth in an abandoned well (Amerada Hess, Green River no. 2 drilled in 1949, total depth 1798 m) at 805 m and 970 m. Drilling records state that the deeper of the two faults has Cutler Group sediments in the hanging wall and Hermosa Group sediments in the footwall. It is therefore unclear what the offset of the fault is at this depth, or whether the fault cuts the Paradox Formation (Fig. 2.3.1.7.1(1)). The fault is cut by several stream channels that provide excellent cross-sectional exposures of the fault zone and associated host-rock alteration. Between the two main strands of the fault, smaller faults define structural terraces with varying dips. Slickensides on subsidiary fault surfaces indicate mostly dip-slip with some oblique left- and right-lateral movement. The fault zone contains 70 cm to 3 m of foliated clay gouge with occasionally well-defined, sub-planar slip-surfaces. Smaller faults with offsets less than 1 m are decorated with a thin (mm-thick) foliated purple-black, clay-rich fault gouge and occasional thin calcite veins (1-2 mm thick) with sub-horizontal fibers. The normally dark purple-red Summerville Formation is bleached to a pale yellow for up to several meters into the footwall. This alteration is localized along the subsidiary faults and within certain beds.

The Salt Wash faults (sometimes termed the Tenmile Graben) are a set of N 70° W striking normal faults. The map-scale structure of the faults reveals two normal fault systems that form a shallow graben over 15 km long (Fig. 2.3.1.4(1)). The faults offset Jurassic Entrada Sandstone in their footwalls against Cretaceous and Jurassic Cedar Mountain Formation in the centre of the graben. The Salt Wash faults consist of two linked en echelon graben segments (Doelling 2001) and may be structurally linked to the Moab fault system to the southeast (Fig. 2.3.1.4(1)), though Quaternary deposits obscure the area where this linkage potentially occurs. The depth to which these faults extend is uncertain, but they may sole into the Paradox salt sequence, and could be related to salt tectonics in the region. We have studied in detail two areas along the northernmost Salt Wash fault - the Tenmile Geyser and Torrey's spring areas.

The Tenmile Geyser is centred on an abandoned well 200 m into the hanging wall of the northern fault. A drill pipe sits within a low mound of flaky travertine with poorly developed rimstone textures. The Tenmile Geyser has erupted infrequently in the past with 1 to 1.5 m high eruptions (Doelling 1994). A second mineral-charged spring sits on a low mound 100 m into the footwall of the fault. There is anecdotal evidence that a set of travertine terraces with rimstone textures used to exist at this locality. This has since been excavated into a pit about 2 by 3 m in size and 1.5 m deep. The bottom of this pit does not reach the base of the travertine deposit. There is an almost constant stream of CO₂ from three vents in the base of the pool, but this spring has not been documented to have geyser-style eruptions.

There are extensive inactive travertines up to 4 m thick at elevations up to 30 m above the level of the present-day spring, some with well-developed rimstone textures. These travertines are presently being quarried. A 2- to 10-m thick zone of fractures, intense alteration, and veining obliterates primary sedimentary structures beneath portions of the travertine deposits. Two to five cm -thick bedding parallel carbonate veins extend up to 50 m away from the fault zone. In some places mammillated ray-crystal veins change from vertical to horizontal orientation within the outcrop. These occasionally contain open vuggy deposits with rhombohedral calcite crystals, interpreted as forming in subaerial or spelean pools. Fractures up to two metres deep that cut the mounds have been filled with bedded travertine. The travertines tend to form resistant caps to a line of small buttes along the fault trace. All the travertines along the Salt Wash faults are localised either on the northernmost fault trace or in the footwall of this fault. The only activity seen within the graben is the Tenmile Geyser. The fault gouge is locally well-exposed, and consists of a zone up to 5 m thick of slices of lithologies separated by clay-rich foliated gouge. In the footwall north of the Tenmile Geyser, the Entrada Sandstone (usually red) has been

extensively bleached to a light tan to pale yellow. In other places along the fault zone, the Entrada Formation is bleached in zones close to the fault and along fractures. Close to the fault, poikilotopic aragonite cements occur preferentially in certain horizons of the host rock. We have used the detailed geologic mapping and cross sections based on drillhole data to create a geologic model for the area (Fig. 2.3.1.7.1(1)).



Figure 2.3.1.7.1(1) Detailed geologic map of the Little Grand Wash fault. Red regions are carbonate deposits.

2.3.1.7.1.1 CO₂ emissions and springs

Several active CO₂-charged springs are localized along the two strands of the Little Grand Wash fault zone. The Crystal Geyser erupts to heights of up to 25 m at 4 to 12 hour intervals. This is not a geyser in the strict sense of the term; the water in the geyser is cool and the eruptions are powered by CO₂-charged waters rather than a heat source. The geyser began erupting when the Glen Ruby #1-X well was drilled in 1935. This abandoned exploration well was completed to the base of the Triassic section (TD 801 m). Occasionally the geyser water has a strong sulfidicphur odor, and/or a thin film of hydrocarbons coating the water pooled around the drill pipe. The driller's records document that the well was spudded into a travertine mound and that the travertine thickness was 21.5 m before hitting bedrock (Baer and Rigby 1978). The spring system must have been active prior to the well being drilled.

Three other springs are located on the system of travertine mounds around the geyser. To the northeast a water-filled pool and a chocolate-brown, mud-filled pool erupt penecontemporaneously with the geyser. These are located on the back of the travertine mound where it has been badly damaged by vehicle traffic. To the north, another small water-filled pool is located on the active travertine slope. The close correlation of the timing of the geyser and activity of these springs suggest that the latter either reflects some escape of the CO₂-charged waters from the well bore at shallow levels, or that these pools could be the original, pre-well flow paths for the CO₂-charged waters to the surface. It is common for hydrothermal travertine spring sources to switch locations when the flow paths become cemented (Chafetz and Folk 1984). Although in this cool water system, cementation may not be as rapid as in hydrothermal systems, it is still likely that the flow paths switch with time when they become sealed by calcite precipitation. Further to the east, an oil seep is located on the southernmost fault strand. A shallow pit contains fresh oil indicating that there is active flow of petroleum to the surface. The outcrop close to this seep (Salt Wash member of the Morrison Formation) contains patches of oil staining.

2.3.1.7.1.2 Mineral deposits

Modern travertines at the little Grand Wash fault consist of bedded travertine mounds that were deposited from the Crystal Geyser and surrounding springs. The surface of the active geyser mound has a classic rimstone texture and lobes of travertine have built out to form sub-metre scale caves with stalactites. An ochre color indicates a small component of iron oxide. These travertines successively bury the vegetation

that surrounds the geyser. The travertine surface has regions of actively forming and inactive travertines, presumably controlled by switching of the source spring location or by lateral migration of flow across the surface of the mound.

To the southwest of Crystal Geyser, older carbonate deposits are in the process of being covered by the present day mound. These deposits are in the form of two distinct mounds of carbonates and breccias, one at the level of the river cutting an older one to the east. From a distance, it appears as though variably dipping “veins” are visible within these mounds though these are not veins in the usual structural geological sense. They consist of cm-thick to tens of cm-thick sub-horizontal tabular masses of radiating acicular calcite and aragonite crystals 6 to 15 cm long with botryoidal or mammilated top surfaces. Fresh surfaces are bright white, with occasional pale yellow banding. These veins often have paired banding and/or mammilated surfaces, which face toward the centre of the vein. Deposits of this form (described as ray-crystal crusts by Folk et al. 1985) have been interpreted to form underwater, with the apex of the radiating crystals pointing towards the source of fluids (*i.e.*, in the centre of the veins). Occasionally, the centers of these veins contain stalactite-like structures suggesting that sub-horizontal fissures were infilled above the water table. Above these deposits lie travertine-cemented breccias that includes clasts of ray-crystal calcite and sandstone. The surfaces of the inactive mounds have some rimstone textures preserved, though they have been extensively damaged by vehicles. The 1867 Powell expedition documented “satin spar” at this location (Powell, 1895), which we interpret to be either the travertine terraces or the bright white vein-like structures.

Other ancient travertine deposits along the fault are at higher elevations (up to 37 m, Baer and Rigby 1978) than the one presently forming. These deposits tend to form resistant caps to small buttes. The hanging wall of the fault in Figure 4a contains a thick ancient travertine deposit, though it is unclear if this deposit filled in the space left by faulting or if movement on the fault cut a pre-existing deposit. The ancient travertines consist of dense-bedded layers, 1 to 2 mm thick, interbedded with vuggy open carbonate 1 to 3 cm thick. Horizontal and vertical carbonate ray-crystal veins up to 30 cm thick cross cut these deposits. In an outcrop east of the Geyser, an impressive array of mm- to cm-thick veins with a boxwork pattern has completely obliterated the original fabric in the fault gouge (Figure 2.3.1.7.2(2)). The veins in this array are not parallel to the original fault gouge fabric. This boxwork is cross cut and offset by thicker sub-vertical veins with occasional stalactite textures.

The spatial correlation of the ray-crystal calcite/aragonite veins and the travertines is consistent with the latter having been the “plumbing system” to the travertines. The variation in the locations of the inactive deposits shows mounds predominantly form between the two strands of the Little Grand Wash fault, or at structurally complex areas such as stepovers between the fault strands that the loci of active effusion of CO₂-rich waters have changed in the past.

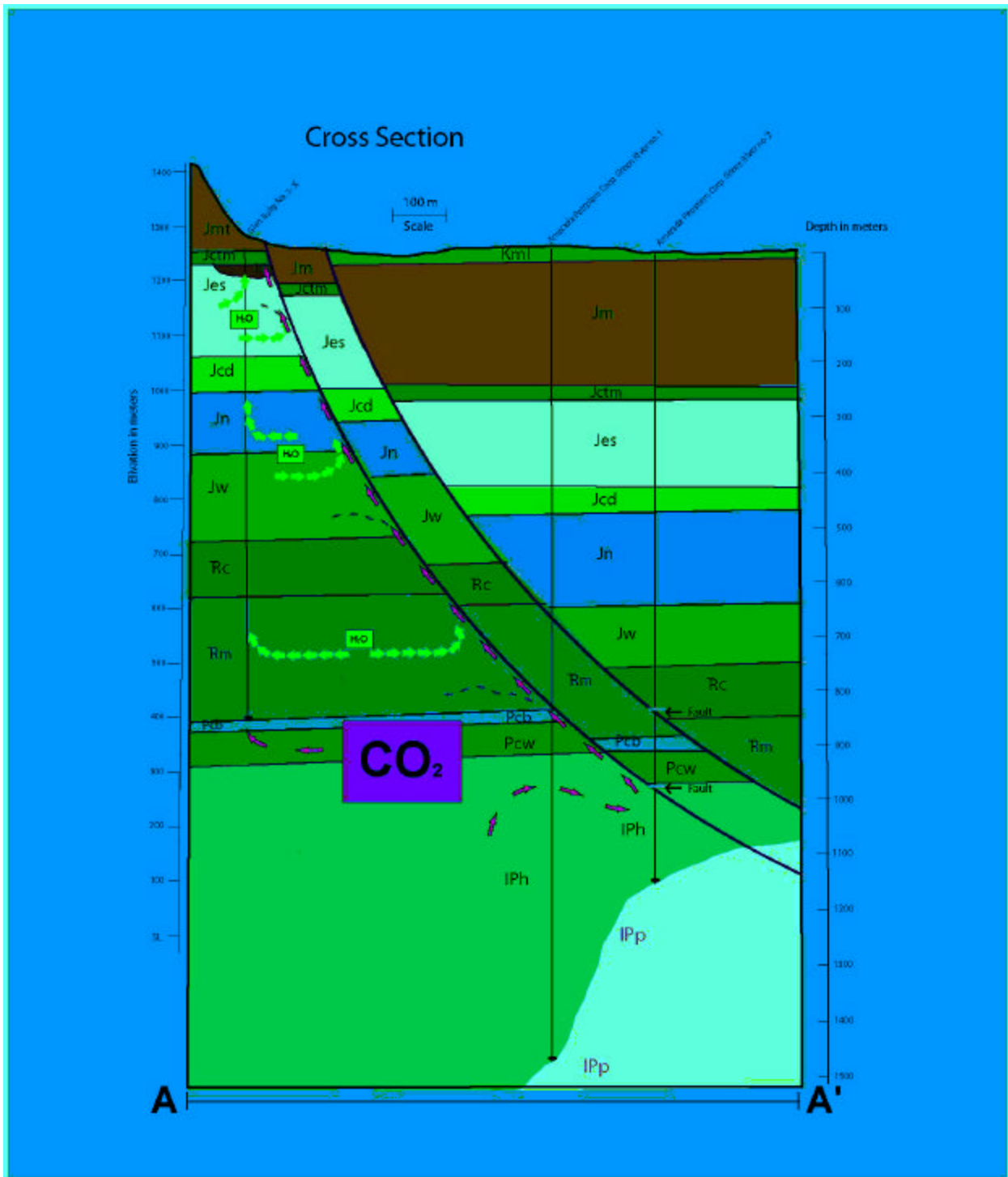


Figure 2.3.1.7.1(2) Geologic cross section of the study area. CO₂ sources discussed here lie 1–1.5 km below the surface, and suggest that CO₂ flows vertically and as it rises, forms a gas bubble. Periodic eruption of gas at the surface suggests that gas release is followed by a pressure buildup phase, and when P_{CO₂} gas > the hydrostatic pressure, another eruption occurs. Near surface, very large veins show this process occurred naturally in the past.

2.3.1.7.2 Geochemical Results

Seven springs and geysers were found through literature searches, a fly-over the field area, and detailed field mapping (Fig. 2.3.1.4(1); Williams, in prep.) of the area encompassing the two fault zones. Three water emanations erupt periodically as geysers. The other four springs continuously discharge low amounts of water (< 1 L/min) and bubble vigorously. Table 2.3.1.7.2(1) details whether the water emanations are springs or geysers, and whether they are natural or flow from abandoned exploration wells.

2.3.1.7.2.1 Sampling procedures and analysis

Water and gas samples were collected at seven locations along or near both fault zones for chemical and isotopic data. Table 2.3.1.7.2(1) lists sample location sites and the type of data collected at each site. Field measurements at the springs included pH, temperature, alkalinity (by titration), redox, and dissolved oxygen. Sample collection for solute chemistries followed procedures detailed by Clark and Fritz (1997) and analysis was completed at Utah State University Analytical Laboratories using Inductively Coupled Plasma spectrometry for cations and total sulfur, and chloride was analyzed using a Lachat QuickChem 8000 Series Flow Injection Analyzer.

Water samples for hydrogen and oxygen isotope analysis were collected with no head-space in glass bottles with air-tight polyseal caps. Samples for $\delta^{13}\text{C}$ of total dissolved carbon were precipitated in the field with BaCl_2 following Clark and Fritz (1997). The isotopic analyses of hydrogen, oxygen, and carbon were performed at the Stable Isotope Laboratory at Brigham Young University, Utah, on a Finnigan MAT Delta^{plus} mass spectrometer. Exsolving gases were collected in glass bottles for molecular compositions and $\delta^{13}\text{C}$ of the CO_2 gas phase. The analysis of the gases was completed at Isotech Laboratories, Inc., in Champaign, IL. Samples for $^3\text{He}/^4\text{He}$ analysis were collected with in situ passive diffusion samplers. The samplers were lowered into the Crystal Geyser and the Big Bubbling spring and left submersed for at least 12 hours. The diffusion samplers consist of copper tubing and a semi-permeable membrane which allowed the gases dissolved in spring or geyser water to equilibrate with the gases in the samplers. The copper tubing was sealed by cold welding. The helium isotopic ratios and the compositional analysis of the gases were completed at the Department of Geology and Geophysics at the University of Utah.

Table 2.3.1.7.2(1): Sample location and the type of data collected at each site. The abbreviation “TDC” stands for “total dissolved carbon”

Fault Zone	Water Emanation	UTM (Zone 12)	Solute Chemistry	D and ^{18}O	^{13}C of TDC	^{13}C of $\text{CO}_2(\text{g})$	$^3\text{He}/^4\text{He}$	Gas Composition
LGW	Crystal Geyser	0575001E 4310087N	x	x	x	x	x	x
SW	Small Bubbling	0576695E 4302816N	x	x		x		x
SW	Big Bubbling	0577141E 4302637N	x	x	x	x	x	x
SW	Ten-mile Geyser	0578040E 4301728N	x	x		x		x
SW	Pseudo Ten-mile	0578105E 4302058N	x	x	x	x		x
SW	Torrey's Spring	0580511E 4301303N	x	x	x	x		x
-	Tumble Weed Geyser	0575817E 4296931N	x	x		x		x

2.3.1.7.2.2 Water data

Table 2.3.1.7.2(3) presents temperature, pH, solute chemistry, and ionic ratio data of representative waters from the sample locations. All water samples have in situ temperatures <18°C, indicating the geysers in the area not geothermal. CO_2 degassing is the mechanism driving the eruptions. The waters are slightly acidic, due to dissolved CO_2 gas, with pH values ranging from 6.07 to 6.55. The waters are very saline,

with total dissolved solids (TDS) values ranging from 13,848 to 21,228 mg/l. Ionic ratios of Cl/Na^+ with values less than one indicate halite dissolution alone is not occurring. Excess sodium input into the waters may result from ion-exchange processes. If only carbonate dissolution were occurring in the system, the $\text{HCO}_3^-/\text{Ca}^{2+}$ ratio would be two. Since the ratios are all greater than two (except for Torrey's Spring), ranging from 2.14 to 4.21, excess HCO_3^- may be due to external CO_2 entering the system and speciating to HCO_3^- , or Ca^{2+} may have been removed from the system by cation-exchange. Figure 4 presents the solute chemistries graphically in a trilinear plot (Piper, 1944), indicating all of the waters fall in the sodium-chloride chemical facies. The close grouping of the data points implies a similar chemical evolution history of all the waters. The d^{13}C values of total dissolved carbon (TDC) from four springs or geysers range from 0.03 to 1.16‰ (Table 2.3.1.7.2(3)).

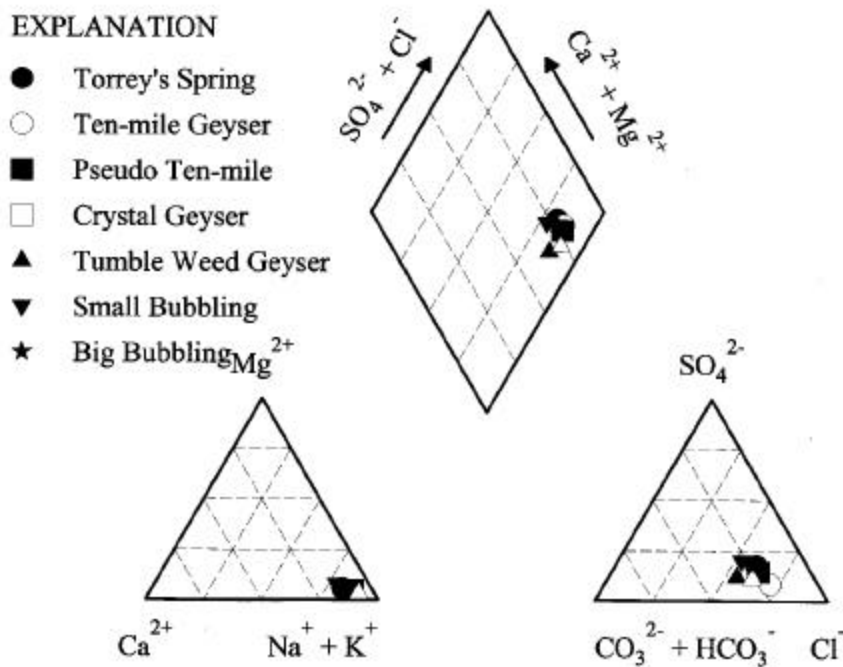


Figure 2.3.1.7.2(2) Solute chemistries of sampled waters presented graphically in a trilinear plot (Piper, 1944). This figure indicates that all of the waters fall in the sodium chloride chemical facies. The close grouping of data points implies a similar chemical evolution history of all the waters.

Table 2.3.1.7.2(3) Temperature, pH, solute chemistry isotope data of total dissolved carbo, and ionic ratios for samples waters. “TDS” stands for “total dissolved solids”.

Location	°C	pH	(meq/l)							(mg/l)		¹⁸ O _{TPC}	¹³ C _{TPC}	(meq/l)	
			Na ⁺	K ⁺	Ca ²⁺	Mg ²⁺	Cl ⁻	HCO ₃ ⁻	SO ₄ ²⁻	Si	TDS			Cl ⁻ /Na ⁺	HCO ₃ ⁻ /Ca ²⁺
Crystal Geyser Small	17.7	6.3	166.0	6.1	17.6	8.8	120.2	72.4	25.9	2.6	14448	22.7	0.0	0.72	4.11
Bubbling Big	15.0	6.1	139.9	5.5	25.9	15.1	114.0	58.4	43.7	3.3	13848	-	-	0.81	2.25
Bubbling Ten Mile	16.4	6.4	196.0	5.8	30.0	13.1	165.0	64.3	49.5	2.8	17662	26.4	0.7	0.84	2.14
Geyser Pseudo Ten Mile	14.4	6.6	201.8	5.6	22.1	11.6	199.5	57.6	23.4	2.4	17173	-	-	0.99	2.60
Torrey's Spring	12.9	6.4	196.0	8.6	19.9	10.9	170.2	60.3	39.2	2.1	16979	25.0	1.2	0.87	3.03
Tumble Weed	16.2	6.5	244.6	13.8	39.3	18.2	195.7	70.8	57.8	3.4	21228	-	-	0.80	1.80
Geyser	16.7	6.4	191.6	5.3	14.4	7.1	139.5	60.7	24.8	1.5	14832	-	-	0.73	4.21

The waters are supersaturated with respect to calcite, aragonite, dolomite, and hematite, and are undersaturated with respect to gypsum and halite (Table 2.3.1.7.2(4)). These saturation indices are confirmed by the carbonate minerals and iron staining (hematite) that are found at the locations of the emanating waters (except iron staining is not found at Pseudo Ten-mile). The carbonate precipitation may be a result of degassing effects that bring the waters to supersaturation with respect to the carbonate phases. These values are much higher than typical soil zone gas values of log P_{CO2} = -3 to -1 (Freeze and Cherry, 1979).

Table 2.3.1.7.2(4) Saturation indices for sample locations. SI = log IAP/K eq. Saturation occurs when SI = 0.0± 0.1. A positive number indicates a thermodynamic tendency of a water to precipitate the mineral in question, whereas a negative number represents a tendency for a water to dissolved the mineral.

Location	Saturation Indices								Log PCO2
	Calcite	Aragonite	Dolomite	Anhydrite	Gypsum	Halite	Hematite	Quartz	
Crystal Geyser Small	0.41	0.26	0.57	-1.36	-1.12	-3.54	4.20	-0.24	
Bubbling Big	0.20	0.05	0.18	-0.97	-0.72	-3.63	3.78	-0.10	
Bubbling Ten Mile	0.65	0.50	0.97	-0.93	-0.69	-3.34	4.41	-0.17	
Geyser Pseudo Ten Mile	0.58	0.43	0.89	-1.35	-1.11	-3.24	4.64	-0.21	
Torrey's Spring	0.35	0.20	0.42	-1.16	-0.92	-3.31	4.35	-0.26	
Tumble Weed	0.84	0.69	1.37	-0.82	-0.58	-3.18	4.53	-0.08	
Geyser	0.29	0.14	0.32	-1.46	-1.22	-3.41	4.30	-0.46	Z

The δD and δ¹⁸O values of the waters are given with reference to the meteoric water line (MWL; Faure, 1986) in Figure 5. The waters are meteoric in origin, as indicated by the close proximity of the data points with the MWL. Most meteoric waters plot within ± 1‰ ¹⁸O of the line (Sheppard, 1986). The waters do not have a major component of Green River water, given that the Green River isotopic values are distinct from this study's data point (Figure 5).

4.2 Gas data

The gases emanating from all the springs are CO₂ rich (95.66% to 99.41%) with minor amounts of Ar, O₂ and N₂ (Table 2.3.1.7.2(5)). Comparing the minor gases with atmospheric gases through N₂/Ar, O₂/Ar, and N₂/O₂ ratios, it is seen that although the emanating gases are almost pure CO₂, some atmospheric contamination has occurred due to the similarity of atmospheric and sample ratios. The process generating the gas therefore produces mainly CO₂. No H₂S gas is present. This correlates with speciation of the waters by PHREEQC (Parkhurst and Appelo, 1999) that indicates the dominant sulfur phase is sulfate. The δ¹³C values of the CO₂ gas phase show little spread, ranging from -6.42 to -6.76‰ with a standard deviation of 0.13‰.

Table 2.3.1.7.2(5) Gas molecular compositions and ¹³C_{CO2} values of sampled sites. Emanating gases were collected in glass bottles. To determine whether atmospheric contamination occurred, normalization was performed by equating Ar, O₂ and N₂ of the samples to 100%.

Location	Sample date	Z (%)									per mil ¹³ C _{CO₂}	Normalized to 100%					
		H ₂ S	He	H ₂	Ar	O ₂	CO ₂	N ₂	CO	C ₁		N ₂	O ₂	Ar	N ₂ /Ar	O ₂ /Ar	N ₂ /O ₂
Crystal Geyser Small	11/29/2002	0.00	0.00	0.00	0.03	0.48	97.85	1.64	0.00	0.00	-6.68	76.5	22.4	1.2	65.6	19.2	3.4
Bubbling Big	11/30/2002	0.00	0.00	0.00	0.05	0.89	95.66	3.41	0.00	0.00	-6.56	78.5	20.5	1.0	75.8	19.8	3.8
Bubbling Pseudo Ten-mile	11/30/2002	0.00	0.00	0.00	0.01	0.13	99.41	0.46	0.00	0.00	-6.76	76.9	21.7	1.3	57.5	16.3	3.5
Torrey's Spring Tumble	11/30/2002	0.00	0.01	0.00	0.01	0.06	99.16	0.76	0.00	0.00	-6.42	91.5	7.2	1.3	69.1	5.5	12.7
Weed Crystal	12/1/2002	0.00	0.00	0.00	0.04	0.66	96.45	2.84	0.00	0.00	-6.47	80.3	18.7	1.0	78.9	18.3	4.3
Crystal Geyser	12/1/2002	0.00	0.00	0.00	0.01	0.21	99.07	0.70	0.00	0.00	-6.72	75.8	22.8	1.4	53.8	16.2	3.3
Atmosphere		-	-	-	0.93	21	-	78	-	-	-	78.2	20.9	0.9	84.0	22.5	3.7

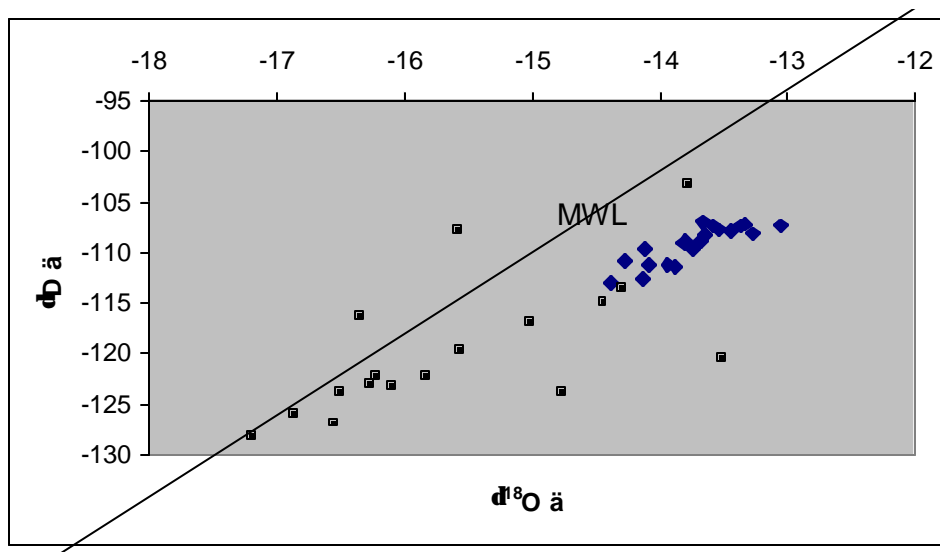


Figure 2.3.1.7.2(6) Hydrogen and oxygen isotopic data. Black squares represent data during a previous study from the Green River, at Green River, Utah (Coplen and Kendall, 2000). Blue diamonds represent data collected during this study at various times during 2001 through 2003 for all seven springs and geysers.

The molecular compositions of gases collected in copper diffusion samplers indicate some atmospheric contamination (Table 2.3.1.7.2(7)). The CO₂ values of 76.6% and 73.9% are much lower than the values of the samples collected in glass bottles (95.66% or greater). At Crystal Geyser, the sampler was submersed in the water in the abandoned exploration well for about 12 hours. Time needed for equilibration of dissolved gases through the semi-permeable membrane of the diffusion samplers is several weeks for typical waters). It was assumed that equilibration would occur more quickly in the geyser waters due to the high P_{CO₂}. The sampler was removed due to an eruption event. At the Big Bubbling spring, the sampler was also left for about 12 hours. The sampler was placed near the center of the pool of the spring under about 2 feet of water. The agitation of the bubbling waters and the lack of submersion for several weeks resulted in contamination. Diffusion of helium is assumed to occur more quickly than larger gas molecules due to the mobility of helium. The R/R_a values, where R = ³He/⁴He ratio of a sample and R_a = ³He/⁴He of the atmosphere, of 0.302 and 0.310 indicate a crustal source for He (< 1.0; Dai et al., 1996) and presumably the associated CO₂. Since atmospheric contamination may have occurred, the actual R/R_a values may be lower than these values. Atmospheric contamination would bring values closer to one.

Table 2.3.1.7.2(7) Helium isotope data and volumetric gas ratios. R is the ratio of ³He/⁴He in the collected samples, and R_a is the ³He/⁴He of the atmosphere.

Sample Location	(%)					
	N ₂	CO ₂	⁴⁰ Ar	O ₂	⁴ He	R/R _a
Crystal Geyser	22.9	76.6	0.058	0.44	1.36E-03	0.302
Big Bubbling	14.3	73.9	0.094	11.6	7.95E-04	0.31

2.3.1.7.2.3 Carbon isotope analysis

To determine whether the waters and gases are in equilibrium with respect to carbon isotopes, calculations can be made to generate predicted δ¹³C_{CO₂(g)} values based on total dissolved carbon isotopes,

which are then compared with actual measured $\delta^{13}\text{C}_{\text{CO}_2(\text{g})}$ values (Lesniak, 1994). This comparison is made to show whether degassing of CO_2 at the surface is causing a non-equilibrium fractionation. Using $\delta^{13}\text{C}_{\text{TDC}}$ of water, pH, emergence temperatures, solute chemistries, and a fractionation factor for HCO_3^- (aq) and $\text{CO}_2(\text{g})$, the predicted values of $\delta^{13}\text{C}_{\text{CO}_2(\text{g})}$ are calculated (Lesniak, 1994). The assumption is made that the emergence temperature is the temperature of last equilibration between the emanating gas and water (Lesniak, 1994). To complete the calculations, it is necessary to determine the molality of dissolved carbon species using a computer program such as PHREEQC (Parkhurst and Appelo, 1999) that determines dissolved species. The mass balance equation for carbon isotopes at a pH below 8.4 is given by:

$$\delta^{13}\text{C}_{\text{TDC}} = X_{\text{CO}_2(\text{aq})} \delta^{13}\text{C}_{\text{CO}_2(\text{aq})} + X_{\text{HCO}_3} \delta^{13}\text{C}_{\text{HCO}_3} \quad (1)$$

where $X_{\text{CO}_2(\text{aq})}$ is ratio of the molality of $\text{CO}_2(\text{aq})$ to the molality of total carbon, and X_{HCO_3} is the ratio of molality of total HCO_3^- to the molality of total carbon. The fractionation factor is related to values for the phases HCO_3^- and $\text{CO}_2(\text{g})$ (Clark and Fritz, 1997) by:

$$a_{\text{HCO}_3-\text{CO}_2(\text{g})} = (d^{13}\text{C}_{\text{HCO}_3} + 1000)/(d^{13}\text{C}_{\text{CO}_2(\text{g})} + 1000) \quad (2)$$

The temperature dependent values of $a_{\text{HCO}_3-\text{CO}_2(\text{g})}$ are determined using:

$$10^3 \ln a^{13}\text{C}_{\text{HCO}_3-\text{CO}_2(\text{g})} = 9.552(10^3\text{T}-1) - 24.10 \quad (3)$$

(Mook et al., 1974). Equations 1 and 2 are solved simultaneously to derive predicted values of $d^{13}\text{C}_{\text{CO}_2(\text{g})}$ (Lesniak, pers. Comm.). Total HCO_3^- includes the following species:

$$\text{HCO}_3^-_{\text{T}} = \text{HCO}_3^- + \text{NaHCO}_3^0 + \text{CaHCO}_3^+ + \text{MgHCO}_3^+ + \text{FeHCO}_3^+ + \text{SrHCO}_3^+ + \text{MnHCO}_3^+ \quad (4)$$

We use the relationships of Equations 1 through 4 to determine if the waters and gases are in equilibrium with respect to carbon isotopes. The theoretical $d^{13}\text{C}_{\text{CO}_2(\text{g})}$ derived values are isotopically-heavier than measured values (Table 2.3.1.7.2(8)) by about 2%. The apparent disequilibrium may be due to uncertainties in pH measurement. An uncertainty of 0.1 pH unit results in a 24% error in calculated molalities of dissolved carbon species (Langmuir, 1971). This uncertainty is likely since degassing can affect pH.

Table 2.3.1.7.2(8) Comparison of measured and predicted carbon isotopic values of gas and aqueous phases

Location	Measured $-^{13}\text{C}_{\text{TDC}}$	Measured $-^{13}\text{C}_{\text{CO}_2(\text{g})}$	$-^{13}\text{C}_{\text{CO}_2(\text{g})/\text{TDC}}$ (Predicted gas-phase carbon isotopic value based on total dissolved carbon)	$-^{13}\text{C}_{\text{HCO}_3-\text{TDC}}$ (Predicted bicarbonate carbon isotopic value based on total dissolved carbon)	$-^{13}\text{C}_{\text{HCO}_3-\text{CO}_2(\text{g})}$ (Predicted bicarbonate carbon isotopic value based on carbon isotopes of gas phase)	Difference between measured and predicted $d^{13}\text{C}$ of $\text{CO}_2(\text{g})$	Difference between $d^{13}\text{C}$ of HCO_3^- based on TDC and CO_2
Crystal Geyser	00.34	-6.72	-4.85	3.89	2.00	-1.87	1.88
Big Bubbling Pseudo Ten-mile	07.02	-6.76	-4.88	4.01	2.11	-1.88	1.90
	11.62	-6.58	-4.17	5.13	2.69	-2.41	2.43

Calculations to determine whether emanating CO_2 gas is in equilibrium with carbonate (calcite) precipitated at the surface used the following equation (Bottinga, 1968):

$$10^3 \ln a^{13}\text{C}_{\text{CO}_2(\text{g})-\text{CaCO}_3} = -2.9880 (10^6\text{T}^{-2}) + 7.6663 (10^3\text{T}^{-1}) - 2.4612 \quad (8)$$

Table 2.3.1.7.2(9) shows that values of $\delta^{13}\text{C}_{\text{CaCO}_3}$ predicted from measured $\delta^{13}\text{C}_{\text{CO}_2}$ values are very similar to measured $\delta^{13}\text{C}_{\text{CaCO}_3}$ values. The average of the predicted and measured $\delta^{13}\text{C}_{\text{CaCO}_3}$ values are 5.1‰ and 5.6‰, respectively. The measured $\delta^{13}\text{C}_{\text{CaCO}_3}$ values have a standard deviation of 1.2‰. The closeness of the predicted and measured values may indicate isotopic equilibrium of carbon isotopes between gases and solid precipitate. This equilibrium will be contrasted in the discussion with the apparent disequilibrium of the gases and waters.

Table 2.3.1.7.2(9) Predicted (based on CO₂ gas samples) and measured 14C of Calcite. Calcite values obtained from Shipton et al. (inpress)

Location	Sampling date	Sample ID	Type of sample	$\delta^{13}\text{C}_{\text{CO}_2(\text{g})}$ (‰)	$\delta^{13}\text{C}_{\text{CaCO}_3\text{-CO}_2(\text{g})}$ (‰)	$\delta^{13}\text{C}_{\text{CaCO}_3}$ (‰)
Crystal Geyser	11/29/2002	CG-1a-g	Gas	-6.68	5.0	
	12/1/2002	CG2-1a-g	Gas	-6.72	4.7	
	11/11/2001	C9-2-99	Vein			5.47
	11/11/2001	C9-3-99A	Travertine			3.67
	11/11/2001	C9-3-99B	Travertine			5.66
	11/11/2001	C9-4-99	Travertine			5.92
	11/11/2001	C9-X-99	Vein			4.79
Small Bubbling	11/30/2002	SB-1a-g	Gas			
Big Bubbling	11/30/2002	BB-1a-g	Gas	-6.76	4.9	
Ten-mile Geyser	11/11/2001	TM100	Vein and travertine			5.6
	11/11/2001	TM500	Vein			5.4
	11/11/2001	TM900 A	White vein material			5.7
Pseudo Ten-mile	11/30/2002	PT-1a-g	Gas	-6.58	5.6	
Torrey's Spring	11/30/2002	TS-1a-g	Gas	-6.42	5.2	
	11/11/2001	TS200	Modern travertine			8.22
Tumble Weed Geyser	12/1/2002	TW-1a-g	Gas	-6.47	5.1	

2.3.1.7.2.4 Carbon History and the Origin of the CO₂ gas

Before possible origin of the gas is established, attention is first given to processes that may overwrite the original carbon isotopic signature imparted to the CO₂ gas at the time of its formation. Processes that may have modified the $\delta^{13}\text{C}_{\text{CO}_2(\text{g})}$ values in the system we examined include degassing of dissolved CO₂ at the surface and advective transport and flow of CO₂ gas to the surface.

The degassing process that may fractionate carbon isotopes is illustrated by the following equations (Poulson et al., 1995; Clark and Fritz, 1997):



These equations describe phase changes of dissolved carbon to CO₂ gas and solid calcite. As the gases reach the surface, these processes take place because the partial pressure of dissolved CO₂ is much higher than P_{CO₂} values at the surface. The equations show that as CO₂ gas exsolves from the water, dissolved carbon concentrations will decrease. No assumption is made that rapid degassing may be an equilibrium process as described by these equations. Removal of carbon and phase changes can both result in isotopic fractionation.

Tables 2.3.1.7.2(8) and 2.3.1.7.2(9) present information on the relationships of carbon isotopes among gas, liquid, and solid carbon (calcite) phases used to determine if the system is in isotopic equilibrium. Isotopic equilibrium would indicate that rapid degassing is not causing a kinetic fractionation or non-equilibrium fractionation that would overwrite isotopic signatures. Measured $\delta^{13}\text{C}_{\text{CO}_2(\text{g})}$ values differ from predicted $\delta^{13}\text{C}_{\text{CO}_2(\text{g})}$ values based on dissolved carbon isotopes and chemical analyses (Table 2.3.1.7.2(8)). Thus, the gas and liquid phases seem to be in disequilibrium by about 2‰ (Table 2.3.1.7.2(8)). This departure from equilibrium must be contrasted with the values in Table 2.3.1.7.2(9) presenting measured and predicted $\delta^{13}\text{C}$ values of $\text{CaCO}_3(\text{s})$. These values are very close to equilibrium with a departure of only 0.5‰. This indicates isotopic equilibrium between CO_2 gas and precipitated CaCO_3 . The departure of the gas and liquid isotopic values is most likely due to inaccuracies in field measurement of pH. The values of pH were used to convert dissolved $\delta^{13}\text{C}$ values to predicted $\delta^{13}\text{C}_{\text{CO}_2(\text{g})}$ values. As noted previously, a 0.1 uncertainty in pH units results in ~ 24% uncertainty in dissolved carbon ion activities (Langmuir, 1971). Inaccuracies in pH measurement are very likely due to degassing that would change pH as shown by Equation 9. To reach a steady electronic signal (emf) by the pH meter, equilibrium of the pH electrode system and the sampled water must be obtained. Degassing, and hence pH changes, can occur before the steady emf value is reached (Pearson et al., 1978). Therefore, isotopic equilibrium has probably been obtained because the comparison of gas and liquid carbon isotopes is within the uncertainty range, and carbon isotopes of gas and calcite are affected less by uncertainties and these values indicate equilibrium. It appears degassing is not causing a kinetic, non-equilibrium fractionation.

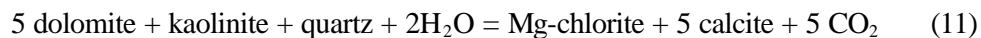
Next, effects of transport of CO_2 on carbon isotopes are considered. Modeling of one-dimensional advective transport and isotope exchange by Lesniak (1998) of CO_2 gas to the surface in the West Carpathians, Poland, indicates that this type of transport can deplete the gas phase in the heavier isotope. Therefore, if advective transport has modified carbon isotopes in the field area, it would have made $\delta^{13}\text{C}_{\text{CO}_2(\text{g})}$ values more negative. Lesniak's (1998) study also mentioned that in low temperature environments, no processes can enrich CO_2 gas in heavy isotopes except for some bacterially-mediated reactions. As will be shown later, bacterially-mediated processes are not significant in the area. Therefore, the $\delta^{13}\text{C}_{\text{CO}_2(\text{g})}$ values of the original source gas are likely the same as or more positive than the gas measured at the surface. Hence, the original source gas may have had values of $\delta^{13}\text{C}_{\text{CO}_2(\text{g})}$ of -6.60 (average values of gases measured at the surface) or higher. Again, it should be noted that degassing and precipitation reactions do not seem to overwrite the carbon isotope values since isotopic equilibrium has been achieved.

Possible processes that have may generated the CO_2 gas in the field area include: 1) mantle or magmatic emanations; 2) the degradation of organic matter; 3) diagenetic reactions involving clay (siliceous) and carbonate rocks; and 4) thermal decarbonation of carbonate rocks by metamorphic processes (Cappa and Rice, 1995; Mayo and Muller, 1996).

Mantle, magmatic, or volcanic degassing is likely not responsible for generating most of the gas in the area. Values of $\delta^{13}\text{C}_{\text{CO}_2(\text{g})}$ for this source is typically -8‰ and such emanations have R/Ra values of helium isotopes of ~ 8. The R/Ra for samples from both fault zones are close to 0.3. Typical crustally-sourced gases have values close of ~0.02 (Kennedy et al., 1997). The somewhat higher value of 0.3 is probably due to some atmospheric contamination, as explained in the Results section.

The generation of CO_2 gas as a result of hydrocarbon formation was investigated because a surface oil seep is located within a kilometer of Crystal Geyser. Carbon isotopes of the oil with respect to saturated and aromatic hydrocarbons are -28.47‰ and -29.26‰, respectively (Lillis et al., 2002). Values of $\delta^{13}\text{C}_{\text{CO}_2(\text{g})}$ generated from oils typically have values close to that of the polar constituents of the source kerogen (Cappa and Rice 1995). Hunt (1996) states that the thermal degradation of organic matter can result in a range of $\delta^{13}\text{C}_{\text{CO}_2(\text{g})}$ from -12 to -8‰. The $\delta^{13}\text{C}$ values from the oil seep are much more depleted than the $\delta^{13}\text{C}$ of the CO_2 gas (~ -6.60‰) emanating at the surface in both fault zones. This difference, therefore, easily disqualifies oil formation reactions as the source of CO_2 in the gas.

A potential candidate for the generation of large amounts of CO₂ gas is clay-carbonate diagenetic reactions that may occur during deep burial of impure carbonate sedimentary rocks. Many of these reactions may take place at temperatures between about 100 and 200°C (Hutcheon and Abercrombie, 1990; Hutcheon et al., 1980; Mayo and Muller, 1996; Hunt 1996). One of the possible reactions is given by the following equation (Mayo and Muller, 1996; Hutcheon et al., 1980):



Another possible reaction pathway to produce CO₂ involves reaction of kaolinite with calcite to form a Ca-smectite with a concomitant dissolution reaction of calcite (Gunter and Bird, 1988). To emphasize the capability of clay-carbonate reactions to produce large amounts of CO₂, at 25°C and 1 atm, 25,800 L of CO₂ could be produced from one cubic meter of a rock, if 10% of it is composed of dolomite, kaolinite, and quartz in the same ratios as given in Equation 11 (Hutcheon et al., 1980). Other studies show that significant amounts of CO₂ are released from impure limestones heated to a temperature of 98°C. The impurities were small amounts of magnesium, iron, manganese, silica and a trace of alumina. There are field examples that indicate large quantities of CO₂ are produced at a subsurface temperature of about 150°C (Farmer, 1965; Hunt, 1979). Although identifying specific reaction pathways for the formation of the CO₂ gas is not possible in this study, it is emphasized that clay-carbonate reactions can produce significant amounts of CO₂.

Studies by Hutcheon and Abercrombie (1989) and Hutcheon et al. (1990) indicate that CO₂ gas produced in basins by clay-carbonate reactions is in equilibrium or close to equilibrium with respect to carbon isotopes of the emanating gases and carbonate material from which the gas is sourced. They used calcite and CO₂ gas fractionation equations to determine equilibrium, and Hutcheon et al. (1990) specifically mentioned that they used the equations of Bottinga (1968) and Mook et al. (1974). Therefore, the clay-carbonate reactions may involve silicate hydrolysis and carbonate dissolution to produce CO₂ gas that is in or is close to being in, equilibrium with respect to carbon isotopes as described by the typically used fractionation equations which describe calcite in equilibrium with CO₂ gas. With this assumption, we can predict the original isotopic value of the carbonate material from which the gas may be sourced.

2.3.1.8 Conclusion

We have integrated geological and geochemical analyses of a naturally-charged CO₂ system in order to examine how CO₂ may flow in a series of low permeability rocks. We have identified the likely source of the CO₂ and infer that it migrates vertically from a subsurface reservoir to the surface, probably at relatively rapid rates. We have compiled a description of sampling strategies and sources of error in sampling and analyzing CO₂ - charged systems, and have also developed a set of relationships that allows use of isotopic systematic to infer the sources and fate of CO₂ in any system.

There are several implications of this work that are relevant to geologic carbon sequestration. We show that careful analysis of seal integrity is critical in designing a geologic sequestration program, as fractures and faults can provide easy pathways for gas migration. In addition, this flow can result in transport of CO₂ in the gas phase for some distance before mineral precipitation occurs, suggesting that such systems may not be “self-sealing”. We have also completed a characterization study that can be used by numerical modelers to benchmark or validate their models. As a three-dimensional geologic model, including flow paths, is being constructed, there will be an opportunity to history match the system with numerical modeling. This will be a valuable tool in predicting future behavior of similar systems.

2.3.1.9 References

- Allis, R., Chidsey, T., Gwynn, J., Morgan, C., White, S., Adams, M., Moore, J., 2000. Natural CO₂ reservoirs on the Colorado Plateau and Southern Rocky Mountains: candidates for CO₂ sequestration. First National Conference on Carbon Sequestration, May 11-14, 2000, U.S. Department of Energy, National Energy Technology Laboratory, compact disk DOE/NETL-2001/1144
- Baer, J.L., Rigby, J.K., 1978. Geology of the Crystal Geyser and environmental implications of its effluent, Grand County, Utah. *Utah Geology* 5 (2): 125–130.
- Bottinga, Y., 1968. Calculation of fractionation factors for carbon and oxygen isotopic exchange in the system calcite–carbon dioxide–water. *Journal of Physical Chemistry*, 72 (3): 800-808.
- Bottinga, Y., 1969. Calculated fractionation factors for carbon and hydrogen isotope exchange in the system calcite–carbon dioxide–graphite–methane–hydrogen–water vapor. *Geochimica et Cosmochimica Acta* 33, 49-64.
- Campbell, J.A., Baer, J.L., 1978. Little Grand Wash fault–Crystal Geyser area. In: Fasset J.E., Thomaidis, N.D. (Eds.), *Oil and Gas Fields of the Four Corners Area*. Four Corners Geological Society, Colorado, pp. 666-669.
- Cappa, J.A., and Rice, D.D., 1995. Carbon dioxide in Mississippian rocks of the Paradox Basin and adjacent areas, Colorado, Utah, New Mexico, and Arizona. *U.S. Geological Survey Bulletin* 2000-H, 21 p.
- Chan, M.A., Parry, W.T., Bowman, J.R., 2000. Diagenetic hematite and manganese oxides and fault-related fluid flow in Jurassic sandstones, southeastern Utah. *AAPG Bulletin* 84 (9), 1281-1310.
- Clark, I.D., Fritz, P., 1997. *Environmental Isotopes in Hydrogeology*. Lewis Publishers, Boca Raton. 328 pp.
- Craig, H., 1961. Isotopic variations in meteoric waters. *Science* 133, 1702-1703.
- Dai, J., Song, Y., Dai, C., and Wang D., 1996, Geochemistry and accumulation of carbon dioxide gases in China: *American Association of Petroleum Geologists Bulletin*, v. 80, p. 1615-1626.
- Doelling, H., 1994, Tufa deposits in western Grand County: *Utah Geological Survey*, v. 26, p. 8-10, 13.
- Doelling, H., 2001, The geologic map of the Moab and the eastern San Rafael Desert 30'x60' quadrangles, *Utah Geological survey Map M-180*.
- Farmer, R.E., 1965. Genesis of subsurface carbon dioxide, In: Young, A., Galley, J. (Editors), *Fluids in subsurface environments, a symposium: American Association of Petroleum Geologists, Tulsa*, pp. 378-385.
- Faure, G., 1986. *Principles of Isotope Geology*. Wiley, New York. 589 pp.
- Folk, R. L., Chavetz, h., and Tiezi, P. A., 1985, Bizzare forms of depositional and diagenetic calcite in hot spring travertines, central Italy: in: *Carbonate Cements, Soc. Sed. Geol. Spec. Pub.* 36, 349-379.

Freeman, B., Yielding, G., Needham, D. T., and Badley, M. E., Fault seal prediction: the gouge ratio method, in: *Structural Geology in Reservoir Characterization*, Geol. Soc. London Spec. Pub. 127, 19-26.

Freeze, R.A., Cherry, J.A., 1979. *Groundwater*: Prentice Hall, Englewood, 604 pp.

Gale, J., 2002. Geological storage of CO₂: what's known, where are the gaps and what more needs to be done. *Proceedings of the 6th International Conference on Greenhouse Gas Control Technologies*, Elsevier, London UK, A1-1.

Hager, D., 1956. The Little Grand Fault and the Green River Nose, Emery and Grand Counties, Utah. *Intermountain Association of Petroleum Geologists*.

Hem, J.D., 1985. *Study and Interpretation of the Chemical Characteristics of Natural Water*. U.S. Geological Survey Water-Supply Paper 2254. 263 pp.

Herzog, H., Drake, E., Adams, E., 1997. CO₂ capture, reuse, and storage technologies for mitigating global climate change. Final Report DOE Order No. DE-AF22- 96PC01257, Energy Laboratory, Massachusetts Institute of Technology, Cambridge, Massachusetts.

Holloway, S., van der Straaten, R., 1995, The Joule II project: the underground disposal of carbon dioxide. *Energy Convers. Mgmt* 36, 519-522.

Hood, J.W., and Patterson, D.J., 1984, Bedrock aquifers in the northern San Rafael Swell area, Utah, with special emphasis on the Navajo Sandstone: State of Utah - Department of Natural Resources Technical Publication, no. 78, 128 p.

Hunt, J.M., 1996. *Petroleum Geochemistry and Geology*. W.H. Freeman and Company, New York, .

Hunt, J.M., 1979, *Petroleum geochemistry and geology*: San Francisco, W.H. Freeman, 617 p.

Hutcheon, I., and Ambercrombie, H., 1990, Carbon dioxide in clastic rocks and silicate hydrolysis: *Geology*, v. 18, p. 541-544.

Hutcheon, I., Abercrombie, H.J., Krouse, H.R., 1990. Inorganic origin of carbon dioxide during low temperature thermal recovery of bitumen: chemical and isotopic evidence. *Geochim. Cosmochim. Acta* 54, 165-171.

Hutcheon, I.E., Abercrombie, H.J., 1989. The role of silicate hydrolysis in the origin of CO₂ in sedimentary basins.

Hutcheon, I., Oldershaw, A., Ghent, E.D., 1980. Diagenesis of Cretaceous sandstones of the Kootenay Formation at Elk Valley (southeastern British Columbia) and Mt Allan (southwestern Alberta). *Geochim. Cosmochim. Acta* 44, 1425-1435.

Kennedy, B.M., Kharaka, Y.K., Evans, W.C., Ellwood, A., DePaolo, D.J., Thordsen, J., Ambats, G., and Mariner, R.H., 1997, Mantle fluids in the San Andreas fault system, California: *Science*, v. 278, p. 1278-1281.

Kehew, A.E., 2001. *Applied Chemical Hydrogeology*. Prentice-Hall, Inc., New Jersey. 368 pp.

Langmuir, D., 1971. The geochemistry of some carbonate ground waters in central Pennsylvania. *Geochim. Cosmochim. Acta* 35, 1023-1045.

- Lesniak, P.M., 1998. Origin of carbon dioxide and evolution of CO₂-rich waters in the West Carpathians, Poland. *Acta Geologica Polonica* 48 (3), 343-366.
- Lesniak, P.M., 1994, d¹³C in low temperature, CO₂-charged waters: a need for consistency with carbonate chemistry: *Mineralogical Magazine*, v. 58A, p. 521-522
- Lillis, P.G., Warden, A., King, J.D., 2003. Petroleum systems of the Uinta and Piceance Basins—Geochemical characteristics of oil types. Chapter 3 or Petroleum systems and geologic assessment of oil and gas in the Uinta-Piceance province, Utah and Colorado. U.S. Geological Survey Digital Data Series DDS-69-B.
- Mayo, A.L., and Muller, A.L., 1996, Low temperature diagenetic -metamorphic and magmatic contributions of external CO₂ gas to a shallow ground water system: *Journal of Hydrology*, v. 194, p. 286-304.
- Mayo, A.L., Shrum, D.B., and Chidsey, T.C., Jr., 1991, Factors contributing to exsolving carbon dioxide in ground-water systems in the Colorado Plateau, Utah, *in* Chidsey, T.C., Jr., ed., *Geology of East-central Utah*: Utah Geological Association Publication 19, p. 335-342.
- Mook, W.G., Bommerson, J.C., and Staverman, W.H., 1974, Carbon isotope fractionation between dissolved bicarbonate and gaseous carbon dioxide: *Earth and Planetary Science Letters*, v. 22, p. 169-176.
- Murray, C., 1990, Observations of Crystal Geyser: *Annual Journal of the Geyser Observation and Study Association*, v. 2, p. 113-138.
- Nuccio, V. F., and Condon, S. M., 1996, Burial and thermal history of the Paradox basin, Utah and Colorado, and the petroleum potential of the Middle Pennsylvanian Paradox formatin, U. S. G. S. Bull. 2000-O.
- Parkhurst, D.L. and Appelo, C.A.J., 1999, User's guide to PHREEQC (Version 2)—A computer program for speciation, batch-reaction, one-dimensional transport, and inverse geochemical calculations: U.S. Geological Survey Water-Resources Investigations Report 99-4259, 310 p.
- Pearson Jr., F.J., Fisher, D.W., Plummer, L.N., 1978. Correction of ground-water chemistry and carbon isotopic composition for effects of CO₂ outgassing. *Geochim. Cosmochim. Acta* 42, 1799-1807.
- Poulson, S.R., Ohmoto, H., Ross, T.P, 1995. Stable isotope geochemistry of waters and gases (CO₂, CH₄) from the overpressured Morganza and Moore-Sams fields, Louisiana Gulf Coast. *Applied Geochemistry* 10, 407-417.
- Peterson, P.R., 1973, Salt Wash Field: *Oil and Gas Field Studies*, no. 4, 3 p.
- Rounds, S.A., Wilde, F.D. (Eds.), 2001. Alkalinity and acid neutralizing capacity. In: *National field manual for the collection of water-quality data*. U.S. Geological Survey Techniques of Water-Resources Investigations, book 9, chap. A1, accessed 14 July 2003 at <http://pubs.water.usgs.gov/twri9A1>
- Sheppard, S.M.F., 1986, Characterization and isotopic variations in natural waters, *in* Valley, J.W., Taylor, J.P., Jr., and O'Neil, J.R., eds., *Stable isotopes in high temperature geological processes: Reviews in Mineralogy*, v. 16, p. 165-183.

Shipton, Z.K., Evans, J.P., Kirschner, D., Kolesar, P.T., Williams, A., Heath, J., in press, Analysis of CO₂ leakage through “low-permeability” faults from natural reservoirs in the Colorado Plateau, east-central Utah: Geological Society of London Special Publication.

Shrum, D.B., 1993, The Origin of High Pressure CO₂ Gas in Selected Ground Water Systems in the Central Cordillera of the Western United States (Masters thesis): Brigham Young University, 65 p.

U.S. Geological Survey, 1997 to present. National field manual for the collection of water-quality data. U.S. Geological Survey Techniques of Water-Resources Investigations, book 9, chaps. A1-A9, 2 v., variously paged. [Also available online at <http://pubs.water.usgs.gov/twri9A>. Chapters originally were published from 1997-1999; updates and revisions are ongoing and are summarized at: <http://water.usgs.gov/owq/FieldManual/mastererrata.html>]

Wood, W.W., 1976. Guidelines for Collection and Field Analysis of Ground-water Samples for Selected Unstable Constituents. Techniques of Water-Resources Investigations of the U.S. Geological Survey, Book 1, Chapter D2. 24 pp.

Yielding, G., Freeman, B., and Needham, D.T., 1997, Quantitative fault seal prediction: American Association of Petroleum Geologists Bulletin, v. 81, p. 897-917.

2.3.1.10 Publications

Heath, J. E., Williams, A. P., and Evans, J. p., Structural and hydrogeochemical characterization of fault zones leaking CO₂-charged fluids: The Salt Wash and Little Grand Wash faults, Utah, in. A. A. PG. Annual Meeting, Salt Lake City, UT, May 11-14, 2003.

Dockrill, B., Shipton, Z. K., and Evans, J. P., Structural controls on leakage from a Carbon Dioxide Reservoir in southeastern Utah, in. A. A. PG. Annual Meeting, Salt Lake City, UT, May 11-14, 2003.

Pasala, S. Forster, C. B., and Deo, M., Simulating the impact of faults on CO₂ sequestration in sandstone aquifers, . A. A. PG. Annual Meeting, Salt Lake City, UT, May 11-14, 2003.

Shipton, Z.K., Evans, J.P., Kirschner, D., Kolesar, P.T., Williams, A., Heath, J., in press, Analysis of CO₂ leakage through “low-permeability” faults from natural reservoirs in the Colorado Plateau, east-central Utah: Geological Society of London Special Publication.

2.3.2 Long Term Sealing Capacity of Cemented Petroleum Well

Report Title

CO₂ Capture Project - An Integrated, Collaborative Technology Development Project for Next Generation CO₂ Separation, Capture and Geologic Sequestration

Long Term Sealing Capacity of Cemented Petroleum Well

Report Reference

2.3.2

Type of Report: Semi-Annual Report

Reporting Period Start Date: February 2003

Reporting Period End Date: July 2003

Principal Author(s): Arild Moen, Torleif Holt

Date Report was issued: August 2003

DOE Award Number: DE-FC26-01NT41145

Submitting Organization: Sintef Petroleum Research AS

Address: N-7465 Trondheim
Norway

Disclaimer

This report was prepared as an account of work sponsored by an agency of the United States Government. Neither the United States Government nor any agency thereof, nor any of their employees, makes any warranty, express or implied, or assumes any legal liability or responsibility for the accuracy, completeness or usefulness of any information, apparatus, product, or process disclosed, or represents that its use would not infringe privately owned rights. Reference herein to any specific commercial product, process, or service by trade name, trademark, manufacturer, or otherwise does not necessarily constitute or imply its endorsement, recommendation, or favoring by the United States Government or any agency thereof. The views and opinions of authors expressed herein do not necessarily state or reflect those of the United States Government or any agency thereof.

Table of Contents

1	Introduction	3
2	A study of possible means of isolating the well construction from stored CO₂ and brine	5
2.1	Objectives	5
2.2	Risk of cement deterioration due to CO ₂ containing brine exposure	5
2.3	Some corrosion tests of cement specimens in the natural gas of the Astrakhan gas-condensate field	6
2.4	Addition of Silica in the Portland cement for an anti-corrosion effect.....	7
2.5	RPC, a Reactive Powders Cement.....	8
2.5.1	Materials	8
2.5.2	Mixing procedure	8
2.5.3	Durability tests.....	8
2.6	<i>ThermaLock</i> cement, an improved CO ₂ resistant cementitious material.....	10
2.6.1	Design criteria	10
2.6.2	Materials	10
2.6.3	Results of the experimentation.....	11
2.6.4	Large scale field testing.....	11
2.7	FCRS, a Flexible Corrosion-Resistant Sealant for acid-gas injection.....	12
2.7.1	Description of the sealant	12
2.7.2	Field application	13
2.8	An Epoxy solution.....	16
2.8.1	Technical data and operating instructions	16
2.9	Conclusion.....	17
2.9.1	Recommendations for further work.....	18
3	Simulations	19
3.1	Objective.....	19
3.2	Model.....	19
3.3	Base case.....	19
3.4	“Worst case scenario”.....	20
3.5	Reduced productivity.....	22
3.6	Constant water rate	23
3.7	Coarsened grid.....	24
3.8	Reduced vertical permeability	24
3.9	Recommendations for future work	25
	References	26

1 Introduction

The advantage of storing CO₂ in abandoned oil and gas reservoirs is that there exists a natural evidence for the formation sealing capacity. When the sealing rock is penetrated by a number of wells the natural seal is broken, however. Despite that the wells are plugged with cement after abandonment there exists a certain risk that reactive carbonic acid may deteriorate steel and cement and that CO₂ eventually will leak out into the atmosphere.

In the oil industry where CO₂ has been used as an injectant for enhanced oil recovery for 30 years, problems related to CO₂ enhanced corrosion due to wet CO₂ have been an important issue. There exist methods to monitor and mitigate the corrosion, e.g. by corrosion inhibitors, coatings, inert liners, and high-grade steels that are less prone to corrosion than standard steel. Such methods have proven quite efficient to control corrosion during the lifetime of the CO₂ injection project. Also special “CO₂ resistant” cements are provided that have twice as good resistance to CO₂ as standard cements.

For CO₂ injection to achieve credits for positive environmental effect, the fields used for CO₂ storage must provide a residence time for CO₂ of hundreds and maybe thousands of years. Hence, before petroleum reservoirs can be qualified for CO₂ storage, plans must be made for well treatments to ensure sufficient sealing integrity.

On the time-scale of hundreds and thousands of years most standard well and plugging materials may corrode or erode in a wet CO₂ rich environment. The influence of these processes on the construction materials must be analysed with respect to long time durability. For static condition it is likely that the cement paste will be carbonated with some densification and strength increase as a result. However for flowing water/CO₂ the cement layer around the casing of an oil well will carbonate and eventually corrode due to dissolution of calcium hydrogen carbonate.

Steel will over time be totally converted to oxides. The permeability of such oxides in a compressed state is not known and should therefore be studied. Correspondingly the long-term stability of cement should be studied.

The possibility for intrusion of CO₂ in the well as a result of degradation of well materials must be analysed with basis in the well construction. The possible escape rates must be evaluated in balance with the secondary storing mechanisms (dissolution of CO₂ in brine) and tertiary mechanism (reaction between dissolved CO₂ and rock minerals).

A possible means to minimise degradation of well construction materials is to inject an inert material into the reservoir that forms a barrier between the reservoir and the well. This will correspond to interventions that are often done in wells in order to prevent undesired flow during petroleum productions. Other injection materials will have to be identified, however.

Figure 1.1 shows schematically a typical well casing from a well in the SACROC field with a cement layer outside.

Typical conditions in geological structures, where CO₂ are captured, are given below:

Temperature: 40-70° C.
Pressure: 150-300 bar
Porosity in the surroundings of the casing: 20 %
95 % of the pore volume is CO₂ and 5 % is water.

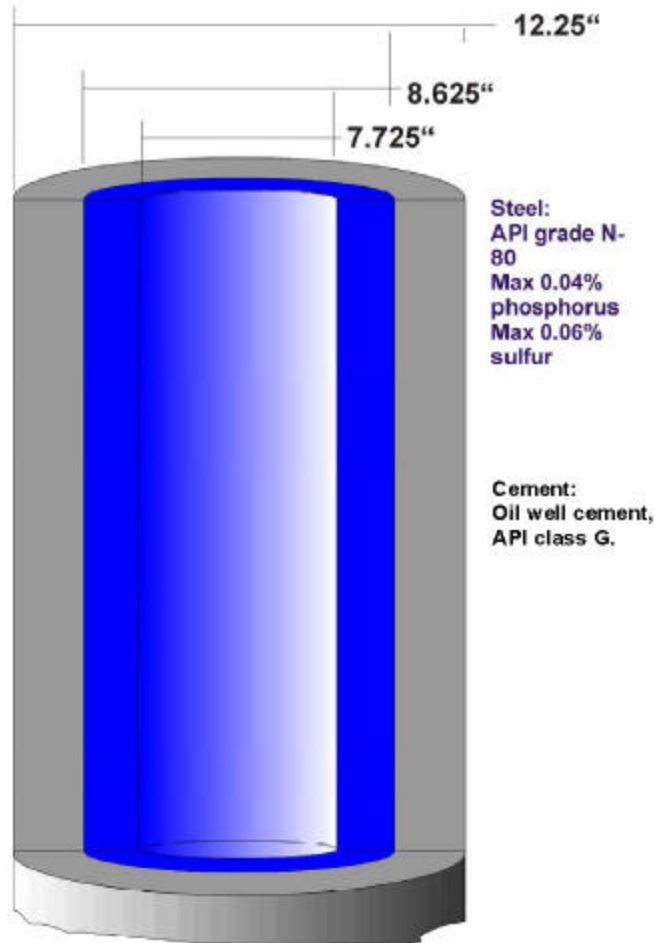


Figure 1.1 A typical well casing with a cement layer outside, shown schematically (Bourgoyne et al.). The surrounding geological structure is not shown.

2 A study of possible means of isolating the well construction from stored CO₂ and brine

2.1 Objectives

The advantage of storing CO₂ in abandoned oil and gas field is that there exists a natural evidence for the formations sealing capacity. If the fields are used for CO₂ storage a residence time of hundreds and maybe thousands of years is desired.

When the carbon dioxide from a CO₂ storage formation has migrated/diffused to the cement layer around the casing of an oil well, the cement will carbonate and eventually corrode due to dissolution of calcium hydrogen carbonate (Lindeberg et. al 2002).

For many years now, laboratories around the world have tried to develop improved CO₂ resistant cementitious materials and additives with more or less success. The objective of this report is to review the techniques and possible benefits of some of these new materials and to suggest recommendation for well plugging.

A computer assisted literature survey has been performed with the key words "carbon dioxide or carbonic acid or carbonation" coupled with "resistant" and "cement" and "well or plugging". Others coupled keywords, like "calcium or magnesium or phosphate", have been used to vary and extend the research. The search was carried out on Dialogu@site, an Internet research tool for bibliographic references and petroleum abstracts. SINTEF Library of Oslo provided the majority of the full-text articles. The US patents were found using the USPTO patent full-text web page. An equivalent research was done using the SPE e-library. More information was found using the Internet pages of the Brookhaven National Laboratory, Halliburton, Norcem and Rescon Mapei, and some contacts.

Another possible means to minimise degradation of well construction materials is to inject an inert material into the reservoir that forms a barrier between the reservoir and the well (Lindeberg 2001). The same computer assisted literature survey has been performed as previously with the key words "carbon dioxide and inert and gas" and "carbon dioxide and protection" without any significant results.

2.2 Risk of cement deterioration due to CO₂ containing brine exposure

A typical chemical composition as oxides of an API class G produced by Norcem is:

- 64.67 % CaO [C]
- 21.95 % SiO₂ [S]
- 5.04 % Fe₂O₃ [F]
- 3.61 % Al₂O₃ [A]
- 1.81 % SO₃ [\bar{S}]
- 1.66 % MgO [M]
- 0.18 % Na₂O [N]
- 0.48 % K₂O

where the letters in brackets are in accordance with the cement chemist's short hand notation.

Due to the presence of carbon dioxide, the cement will carbonate (formation of calcium carbonate) and eventually corrode (loose volume) due to dissolution of calcium hydrogen carbonate since the CO_2 from then on will be in great excess relative to the cement volume. It is difficult to assess the time it takes for a full degradation of 10 mm cement sheet under such conditions since it depends on cement composition, temperature etc, but it is more likely to be months than years. Thus it may be marginal compared to the time for the CO_2 to migrate from the deposit to the cement. Carbon dioxide corrosion of Portland cement is thermodynamically favorable and cannot thus be prevented. The net result is leaching of the cementitious material from the cement matrix, increase of porosity and permeability, and a decrease of compressive strength. Down hole, this translates to a loss of casing protection and zone isolation. By adding pozzolans, the rate of corrosion can be reduced by as much as 50 % (Lindeberg et. al. 2002).

2.3 Some corrosion tests of cement specimens in the natural gas of the Astrakhan gas-condensate field

Corrosion tests of cement specimens (Novokhatskii et. al. 1999) were conducted in the natural gas of the Astrakhan gas-condensate field whose main features were as follows:

- High percentage of H_2S (more than 29%);
- High percentage of CO_2 ;
- Low percentage of water (8 g/m^3);
- Absence of oxygen and oxygen-containing compositions.

Plugging materials of various chemical and mineralogical composition as well as their mixtures recommended to be used for borehole cementation were tested. All samples were kept in testing chamber during 12 months at 100°C and from 20 to 25 MPa in the natural gas. Specimens to be tested were extracted out of the chamber after 3, 6 and 12 months and were analyzed. The gas permeability was measured.

In the materials from the first group, Portland cement or young Portland cement clinker dominate (more than 50%). The following materials are included in this group: plugging Portland cement for moderate temperatures, its mixture with barite, milled quartz sand, dispersed ash of burnable slates, milled zeolite rock (clinoptolite) as well as a weighted plugging cement for "hot" boreholes and its mixture with Portland cement.

The second group was represented by compositions based on crushed metallurgical slags: plugging hydrogen-sulfide resistant cement, slag and sand plugging cement, weighted slag cement and plugging clinkerless corrosion-resistant cement, as well as their mixtures with the above mentioned additives.

The conclusions of these tests are as follow (Novokhatskii et. al. 1999):

- Beam specimens made of the plugging Portland cement and the mixture of Portland cement with barite failed already after 3 months. The reason was the complete deterioration of Ca_2 -hydrosilicate, portlandite and calcium hydroalumoferrites under the action of H_2S and CO_2 .